THESIS FOR THE DEGREE OF DOCTOR OF PHILOSOPHY

Transport theory and finite element methods for mesoscopic superconducting devices

KEVIN MARC SEJA

Department of Microtechnology and Nanoscience (MC2)

Applied Quantum Physics Laboratory

CHALMERS UNIVERSITY OF TECHNOLOGY

Göteborg, Sweden 2022

Transport theory and finite element methods
for mesoscopic superconducting devices
KEVIN MARC SEJA
Göteborg, Sweden 2022
ISBN 978-91-7905-670-4

Doktorsavhandlingar vid Chalmers tekniska högskola
Ny serie Nr 5136
ISSN 0346-718X

Applied Quantum Physics Laboratory
Department of Microtechnology and Nanoscience (MC2)
Chalmers University of Technology
SE-412 96 Göteborg, Sweden
Telephone: +46 (0)31-772 1000

Printed by Chalmers Reproservice
Göteborg, Sweden 2022

Transport theory and finite element methods
for mesoscopic superconducting devices
KEVIN MARC SEJA
Applied Quantum Physics Laboratory
Department of Microtechnology and Nanoscience (MC2)
Chalmers University of Technology

Abstract

At low temperatures, electrons in a superconductor exhibit pairing correlations that result in a macroscopic, phase-coherent ground state. This leads to peculiar electromagnetic properties such as the flow of dissipationless charge currents and expelling of external magnetic fields. This thesis investigates superconductors that are brought out of equilibrium through injection of charge and heat from normal-metal reservoirs. In particular for unconventional superconductors, where the pairing correlations have a non-trivial orbital symmetry, the resulting non-equilibrium is thus far only partially explored. A better understanding is desirable both from a fundamental point of view as well as for applications in superconducting devices.

As a step in this direction, we study transport in mesoscopic superconducting hybrid structures with arbitrary mean free path using the quasiclassical theory of superconductivity. In order for fundamental conservation laws to be satisfied, a description of the non-equilibrium state requires a fully self-consistent solution of the underlying equations. We present strategies on how such a self-consistent solution can be achieved. Using these techniques, we investigate the non-linear steady-state response of both conventional and unconventional superconductors to an external voltage- or temperature-bias. Specifically, we study charge transport in a conventional s-wave and an unconventional d-wave superconductor under voltage bias, the thermoelectric effect due to elastic impurity scattering in both systems, and the influence of spectral rearrangements on a suggested subdominant s-wave order-parameter component in d-wave superconductors. Lastly, we introduce a finite element method for the quasiclassical theory. It can be used to study transport in two or more dimensions where geometric effects such as current focussing and dilution can occur. We present exemplary results based on this method for equilibrium transport in two dimensions.

Keywords: unconventional superconductors, transport theory, nonequilibrium superconductivity, quasiclassical theory, finite element methods

Acknowledgements

First of all, I would like to thank my supervisor Tomas Löfwander for taking me on as a PhD student and his supervision during the last years. Feels like I started just yesterday! I certainly have learned a lot about complicated physics and life in general. I am grateful for the experience and enjoyed our discussions about physics and politics. Secondly, Louhane Jacob deserves a big thanks for her work during her summer project, it was fun and rewarding to work with you. The daily life at AQP has been fun mostly because of all the nice people I get to meet (almost) every day. I've enjoyed the lunches, ice cream and coffee breaks, and discussions a lot. All of you have made the last years much more pleasant. A special thank you goes to Janine Splettstoesser whose open-door policy has been immensely helpful on many occasions. Lastly, I would like to thank all of my friends, local and abroad, and my family for their support and not loosing their mind about my permanent absent-mindedness.

In the beginning of my (undergraduate) studies our math professor recommended an article with the beautiful title "The importance of stupidity in scientific research"[1]. At the time it made for a good laugh and made us feel better about ourselves. Years later and having spend some additional years as a researcher-in-training now, I'm still not sure whether or not I agree. I sure hope my share of stupidity will turn out to have been helpful.

List of publications

This thesis presents an introduction, summary and extension to the following appended papers:

[I] K. M. Seja and T. Löfwander, "Quasiclassical theory of charge transport across mesoscopic normal-metal–superconducting heterostructures with current conservation", Phys. Rev. B **104**, 104502 (2021).

[II] K. M. Seja, L. Jacob, and T. Löfwander, "Thermopower and thermophase in a d-wave superconductor", Phys. Rev. B **105**, 104506 (2022).

[III] K. M. Seja and T. Löfwander, "Self-consistent theory of current injection into d and $d + is$ superconductors", arXiv (2022) 10.48550/arXiv.2203.06532, eprint: 2203.06532.

[IV] K. M. Seja and T. Lofwander, "A finite element method for the quasiclassical theory of superconductivity", arXiv (2022) 10.48550/arXiv.2205.09001, eprint: 2205.09001.

We always refer to these publications as paper I, II, ..., according to the labelling in the list above.

Specification of my contributions to the appended papers

I The project developed over time out of a suggestion from my supervisor. I wrote the code, performed the simulations, analysed the results, and wrote the paper with the help of my co-author.

II The project was decided on in a joint discussion. I wrote the code and performed around half of the simulations and analysed the results. Louhane Jacob performed the other half of the simulations and analysed the results as part of her three-month summer internship. The paper was written in collaboration with my co-authors.

III The project was natural continuation of paper I. I wrote the code, performed the simulations, analysed the results, and wrote the paper with the help of my co-author.

IV The project was decided on in a joint discussion. I adapted the finite-element method to Eilenberger quasiclassical theory, wrote the code, performed and analysed the simulations, and wrote the paper with the help of my co-author. One of the example problems was a suggestion by my co-author.

List of figures

1.1 Sketch of the unit cell in YBCO. 2
1.2 Comparison of s- and d-dwave order parameters. 2

2.1 The quasiclassical Green's function as an envelope 9
2.2 Sketch of connected trajectories for specular interface scattering . . . 18

3.1 Sketch of a piecewise constant self-energy profile 26
3.2 Example for basis functions in a continuous FEM method 31
3.3 Comparison of the exact and weak solutions for an example problem. 32
3.4 Difference between a continuous and discontinuous Galerkin method. 33
3.5 Sketch of the flow boundaries and internal edges of a triangulation. . 33

4.1 Bulk DOS and self-energies at an interface in an s-wave SC. 40
4.2 Density of states for the bulk of a clean d-wave superconductor. . . . 41
4.3 Influence of scalar impurites on the d-wave order-parameter. 42
4.4 Effects of impurity scattering on the bulk properties of a d-wave SC. . 42
4.5 Illustration of the misalignment angle α. 43
4.6 Midgap states in the density of states for d-wave SC 45
4.7 s-wave pairing close to a pair-breaking surface in a d-wave SC 46

5.1 General setup considered in a mesoscopic transport setup 47
5.2 Energy-like and charge-like modes in a reservoir at finite voltage . . . 48
5.3 Energy-like modes in the normal state 49
5.4 Charge-like modes in the normal state 49
5.5 Left-mover and right-mover potentials in the normal state 50
5.6 Sketch of a Sharvin-type tunnel contact 51
5.7 BTK conductance for an s-wave superconductor 53
5.8 A superconducting nanowire coupled to two reservoirs. 55
5.9 Current conversion in an s-wave SC. 56
5.10 Spatial dependence of the superflow in an s-wave superconductor. . . 56
5.11 Effect of superflow on the density of states in an s-wave superconductor. 57
5.12 Spectral current density in an s-wave superconductor. 58
5.13 Effect of superflow on the density of states in an s-wave superconductor. 58
5.14 Nonequilibrium current flow in a d-wave SC in the Born limit. 60
5.15 Nonequilibrium current flow in a d-wave SC in the unitary limit. . . . 60
5.16 Density of states in a d wave SC in the presence of current flow. . . . 61
5.17 Scattering-approach interface conductance in the presence of an ABS. 61
5.18 Suppression of the surface Andreev bound state with applied bias. . . 62
5.19 Interface conductance compared to fully self-consistent conductance. . 63

5.20 Influence of the different contributions to the interface conductance. . 64
5.21 Thermoeletric currents in a d-wave superconductor. 65
5.22 Example for T_{eff} in a d-wave SC under thermal bias. 66
5.23 Non-linear thermopower due to scattering in a d-wave superconductor. 67
5.24 Impurity-induced thermopower for an s-wave superconductor 67
5.25 Example for a phase crystal 68
5.26 Grooved Dayem bridge: Sketch and mesh. 69

Nomenclature

Abbreviations

ABS	Andreev bound state
CG	Continuous Galerkin
DG	Discontinuous Galerkin
DoS	Density of states
FEM	Finite Element method
FS	Fermi surface
HTCS	High-temperature superconductor
MF	Mean field
MGS	Midgap states
SC	Superconductor
SQUID	superconducting quantum interference device
YBCO	Yttrium Barium Copper Oxide

Symbols

$\mathbf{p}_\mathrm{F}$	Fermi momentum
$\mathbf{v}_\mathrm{F}$	Fermi velocity
E_F	Fermi energy
ℓ	elastic mean free path
ξ_0	(clean-limit) superconducting coherence length
T_c	critical temperature
Δ	order parameter
k_B	Boltzmann constant
e	elementary charge
h	Planck constant
$\hbar = h/(2\pi)$	reduced Planck constant
ϕ	quasiparticle potential
$\phi_{\leftrightarrows}$	quasiparticle potential for right-/left-movers
x	superconducting distribution function

Contents

Abstract iii

Acknowledgements v

List of publications vii

List of figures ix

Nomenclature xi

Contents xiii

1 Introduction 1
- 1.1 Conventional superconductivity . . . 1
- 1.2 Unconventional superconductivity & cuprates . . . 2
- 1.3 Nonequilibrium in (mesoscopic) superconductors . . . 3
- 1.4 Thesis overview . . . 4

2 Quasiclassical theory 5
- 2.1 Green's functions & the Gor'kov equation . . . 5
- 2.2 Quasiclassical approxiation & Eilenberger equation . . . 8
- 2.3 Ricatti parametrization & distribution functions . . . 10
  - 2.3.1 Modes of the nonequilibrium distribution . . . 12
  - 2.3.2 Splitting of the distribution function . . . 15
  - 2.3.3 Boundary Conditions . . . 16
- 2.4 Self-energies . . . 19
- 2.5 Observables . . . 21

3 Solution strategies 25
- 3.1 Self-consistency of solutions . . . 25
- 3.2 1D: Stepping method . . . 26
  - 3.2.1 Propagating functions . . . 26
- 3.3 2D: Finite Element Method . . . 29
  - 3.3.1 Key concepts in short examples . . . 29
  - 3.3.2 Discontinuous Galerkin method for Eilenberger quasiclassical theory . . . 32
  - 3.3.3 Coherence function . . . 34
  - 3.3.4 Distribution function . . . 36

3.3.5 Boundary conditions and coupling to reservoirs 37
3.3.6 Generalization to the spin-dependent problems 38

4 Superconductors in equilibrium **39**
4.1 Influence of impurities 39
4.1.1 Impurity scattering in a s-wave superconductor 39
4.1.2 Impurity scattering in a d-wave superconductor 41
4.2 Surface physics in a d-wave superconductor 43
4.3 mixed $d + is$ order parameter 45

5 Transport in superconductors **47**
5.1 Nonequilibrium in the normal state 47
5.2 Voltage bias in the superconducting state 51
5.2.1 Interface conductance 51
5.2.2 Beyond the interface 54
5.2.3 s-swave order parameter 55
5.2.4 d-wave order parameter 59
5.2.5 mixed $d + is$ order parameter 62
5.3 Temperature bias 65
5.3.1 d-wave order parameter 65
5.3.2 s-wave order parameter 67
5.4 Transport in two dimensions 68
5.4.1 Effect of impurities on phase crystals 68
5.4.2 Current flow in a Dayem bridge 69

6 Paper overview **71**
6.1 Paper I 71
6.2 Paper II 72
6.3 Paper III 72
6.4 Paper IV 73

7 Conclusion & Outlook **75**

Appendices **77**

A Self-consistency & charge conservation **79**

References **83**

Appended papers **93**

Paper I **95**

Paper II **113**

Paper III 125

Paper IV 141

1 Introduction

The aim of this chapter is to give some background to the work in this thesis. What is a superconductor, and how can they be unconventional? What are mesoscopic superconductors in non-equilibrium interesting? We will try to answer these questions in the following.

1.1 Conventional superconductivity

At temperatures below a critical temperature T_c a range of metals can undergo a phase transition and become superconducting. The defining experimental consequences of this new phase of matter are the ability to carry dissipationless currents, as first discovered by Kamerlingh-Onnes[2, 3], and the expelling of external magnetic fields, also known as the Meissner effect[4]. The theoretical explanation for these observations was developed in the form of the **B**ardeen-**C**ooper-**S**chrieffer, or BCS, theory[5, 6]. The key ingredient of the theory is the appearance of non-vanishing pairing correlations for electrons around the Fermi surface as consequence of an effectively attractive interaction. In the original theory this attractive interaction was the result of electron-phonon interaction. Within the pairing theory of BCS, the interaction is assumed to be uniform in momentum space and between electrons of opposite spin. As a result a complex scalar order parameter is formed at T_c:

$$\Delta = |\Delta| e^{i\chi} = V \sum_{\mathbf{k}} \langle c_{\mathbf{k},\uparrow} c_{-\mathbf{k},\downarrow} \rangle, \tag{1.1}$$

where V measures the strength of the net attractive interaction. The BCS ground state of the system is then a condensate of correlated electron pairs, with a coherent phase on the scale of the so-called coherence length ξ_0. While the underlying equations describing the system are invariant under transformations of the form $c_{\mathbf{k},\uparrow(\downarrow)} \rightarrow c_{\mathbf{k},\uparrow(\downarrow)} e^{i\alpha}$ the order parameter is evidently altered by such a transformation. A superconductor is thus said to spontaneously break the $U(1)$ gauge symmetry[7]. Superconductors that break this only symmetry are referred to as *conventional* superconductors.

1.2 Unconventional superconductivity & cuprates

By definition, *unconventional* superconductors spontaneously break $U(1)$ gauge symmetry and *additional* symmetries after the phase transition[7, 8]. The order parameter and the pairing correlations will typically show traces of this broken symmetry, so we generalize Eq. (1.1) to allow for a non-trivial dependence on the momentum $\mathbf{k}$,

$$\Delta_{\mathbf{k}} = |\Delta_0|\eta(\mathbf{k})e^{i\chi}, \tag{1.2}$$

where $\eta(\mathbf{k})$ is the orbital basis function characterizing the broken symmetry of the unconventional superconductor. Signs of such unconventional pairing were first discovered in He^3[9, 10], heavy-fermion superconductors[11–13] and organic superconductors[14].

More relevant for this thesis, however, are the so-called high-temperature superconductors (HTSC) that can exhibit much higher values of T_c at ambient pressure than all known conventional superconductors. After the initial discovery of an HTSC by Bednorz and Müller in 1986[15, 16], a range of superconducting materials containing copper oxides, such YBCO[17] and BSSCO[18], were discovered. The common denominator of such *cuprates* is the presence of copper oxide planes. A sketch of the unit cell of YBCO is shown in Fig. 1.1 as an example for the crystal structure in such materials.

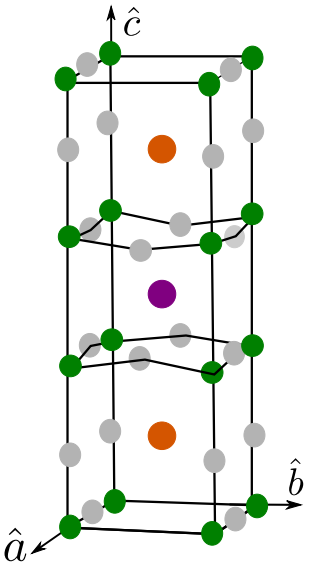

Figure 1.1:
Unit cell in YBCO with copper in green, oxygen in grey, barium in orange and ytrium in purple.

A large body of experimental evidence points towards a non-trivial d-wave symmetry, or $d_{x^2-y^2}$ form of the pairing, in such materials, possibly in combination with so-called sub-dominant pairing with a lower T_c[19–22]. The momentum dependence of the $d_{x^2-y^2}$ basis function is shown in comparison to the conventional s-wave case in Fig. 1.2. In this case, the additional broken symmetry is that of an (approximate) four-fold rotational symmetry of the crystal lattice in such materials.

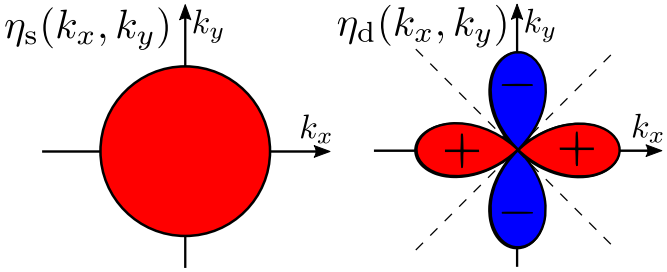

Figure 1.2:
Comparison of the momentum-dependence of the orbital basis function η for the s-wave [left] and d-wave [right] case.

It is an important open question within condensed-matter physics what underlying mechanism causes superconductivity in this class of materials. An exact determination of the symmetry of the order parameter in Eq. (1.2), or equivalently of the pairing correlations, is an important step on the way toward determining the underlying mechanism of the pairing. One possible way to investigate it is to probe the response of an SC to external perturbations. Investigating the non-equilibrium effects in an SC can thus be used a tool to answer questions of fundamental physical interest, such as that of the symmetry of the pairing in unconventional superconductors.

1.3 Nonequilibrium in (mesoscopic) superconductors

A superconductor can be driven out of thermal equilibrium into a non-equilbrium state by, for example, electro-magnetic radiation or injection of charge or heat from other materials. This non-equilibrium can be an essential part of the operating principle of a device, such as in superconducting bolometers that are used for Terahertz radiation detection[23] or in superconducting caloritronics[24]. In other instances an induced non-equilibrium might be an due to unwanted environmental influences that should be actively suppressed, for example quasiparticle poisoning in superconducting qubits[25, 26]. In either case it is desirable to be able to have some degree of control over the non-equilibrium state in a superconducting device. Inherently this requires an understanding of the physics at play. In conventional superconductors, this non-equilibrium state has largely been investigated for temperatures close to T_c[27] or in the limit of effectively diffusive transport, where approximations can simplify the theoretical description[28, 29]. The non-equilibrium regime in conventional superconductors is less well-studied at very low temperatures $T \ll T_c$ and in mesoscopic systems, despite its relevance for current-day superconducting devices[30], Even less is known about the non-equilibrium state in unconventional superconductors such as the d-wave cuprates.

The term mesoscopic refers to a length scale that is somewhere "in the middle", in this case in between the scale of atoms, and hence quantum mechanics, and that of bulk materials that we might describe more in terms of classical physics. For a condensed-matter system this means that it has to be large compared to the Fermi wavelength λ_F of the given material in at least one spatial dimension. Typical values of λ_F are on the order of tens of nanometers. At the same time, the system should be smaller than the phase coherence length l_ϕ that is on the order of several hundred nanometers at sub-Kelvin temperatures[32]. The physics in systems on this intermediate length scale can then be described in terms of individual particles that still exhibit quantum-mechanical effects such as superconducting coherence. In the absence of inelastic scattering transport on such lengthscales strongly depends on the ratio of the mean free path ℓ to the system size L. The main interest of this thesis was in mesoscopic devices in the regime

of $\ell \approx L$, where transport is neither fully ballistic nor fully diffusive.

As we will see later in this thesis, a d-wave superconductor is strongly affected by impurities. As a result approximations made to study the non-equilibrium state in conventional superconductors, such as that of fully diffusive transport, cannot be made. Studying the non-equilibrium in unconventional superconductors thus requires considerable conceptual and numerical effort. The work presented in this thesis is trying to face that challenge and develop solution strategies and an understanding of the behaviour of unconventional superconductors out of equilibrium. Our investigations are restricted to systems consisting of a single superconducting region. In this case a stationary solution can be established[31]. Time-dependent non-equilibrium phenomena are beyond the scope of this thesis, although this is not a restriction of the quasiclassical theory.

1.4 Thesis overview

The remainder of this thesis is structured as follows.

In Chapter 2, we give an overview over the quasiclassical theory of superconductivity. Since we are interested in studying non-equilibrium phenomena, we introduce concepts such as modes of the non-equilibrium distribution that are useful to study non-diffusive superconductors out of equilibrium .

This is followed, in Chapter 3, by a presentation of solution strategies in one and two dimension that were used to obtain the results in the appended papers. Specifically, we introduce a stepping method that is natural to use in one-dimensional systems. As an alternative approach to such a stepping method in higher dimensions, we introduce a finite element method for the underlying transport equations of quasiclassical theory.

In Chapter 4, we briefly discuss the different effects of non-magnetic impurities on conventional s-wave and unconventional d-wave superconductors, as well as the surface physics in d-wave superconductors, in equilibrium.

In the following Chapter 5, an introduction to the results of the appended papers on non-equilibrium and equilibrium transport in superconductors is given. Specifically, we study the self-consistent response of both s-wave and d-wave SCs to an external voltage bias or an external temperature bias. Additionally, we investigate the effect of a voltage bias on a proposed sub-dominant order parameter near pair-breaking interfaces in d-wave SCs. Lastly, we briefly discuss two samples problems for equilibrium flow in two dimensions.

The thesis concludes with a concise paper overview in Chapter 6, and a conclusion and outlook in Chapter 7.

2 Quasiclassical theory

In this chapter, we introduce the concept of Green's functions and how they can be used to describe superconducting systems, both in equilibrium and non-equilibrium, by the Gor'kov equation. We proceed to describe the quasiclassical approximation which leads to the *quasiclassical theory of superconductivity*. This theory forms the "toolbox" for the work in this thesis and we summarize the underlying equations and definitions.

2.1 Green's functions & the Gor'kov equation

In condensed-matter theory and statistical physics, we often try to describe many-body systems with a macroscopically large number of particles $N \approx 10^{23}$. As a quantum-mechanical starting point such a system can be described in terms of its Hamiltonian $\mathcal{H}$. To obtain any physical quantity of interest – say the spectrum, charge conductances, or response to a magnetic field – we "only" have to solve the Schrödinger equation for the N-particle wave function Ψ. Since N is typically too large for many-body systems there are intractably many degrees of freedom and a solution of the Schrödinger equation itself is impossible. To solve this problem alternative mathematical descriptions of many-body systems have been derived. They rely on "appropriate" approximations to discard some of information contained in Ψ in order to make the problem tractable. The theory used in this thesis uses so-called Green's functions that contain less information than Ψ but still allow for the calculation of observables within the accuracy of the approximation[34]. We briefly outline the underlying theory, more details can be found in [35–37]. For fermions, the retarded (R), advanced (A), and Keldysh (K) single-particle Green's functions are defined as

$$G^{\mathrm{R}}(\mathbf{r}t;\mathbf{r}'t') \equiv -i\theta(t-t')\left\langle\left\{\Psi(\mathbf{r},t),\Psi^{\dagger}(\mathbf{r}',t')\right\}\right\rangle, \tag{2.1}$$

$$G^{\mathrm{A}}(\mathbf{r}t;\mathbf{r}'t') \equiv i\theta(t'-t)\left\langle\left\{\Psi(\mathbf{r},t),\Psi^{\dagger}(\mathbf{r}',t')\right\}\right\rangle. \tag{2.2}$$

$$G^{\mathrm{K}}(\mathbf{r}t;\mathbf{r}'t') \equiv -i\left\langle\left\{\Psi(\mathbf{r},t),\Psi^{\dagger}(\mathbf{r}',t')\right\}\right\rangle, \tag{2.3}$$

with two positions $\mathbf{r},\mathbf{r}'$ and times t,t', and $\{A,B\}$ denoting the anticommutator. In the Heisenberg picture the quantum-mechanical field operators $\Psi(\mathbf{r},t)$ and

$\Psi^\dagger(\mathbf{r},t)$ are, for example,

$$\Psi(\mathbf{r},t) \equiv e^{-i\mathcal{H}t}\psi(\mathbf{r})e^{i\mathcal{H}t}, \tag{2.4}$$

and similarly for $\Psi^\dagger(\mathbf{r},t)$. In equilibrium at finite-temperature T, the $\langle \dots \rangle$ in Eq. (2.3) is a statistical average, with $\beta = 1/k_\mathrm{B}T$ and Tr a sum over states, given by $\langle \hat{A} \rangle \equiv \mathrm{Tr}\; e^{-\beta\mathcal{H}}A/(\mathrm{Tr}\; e^{-\beta\mathcal{H}})$. We interpret G^R and G^A in Eqs. (2.1)–(2.2) as propagation probabilities. What is the likelihood of finding a particle at position $\mathbf{r}$ at time t if it was inserted at $\mathbf{r}'$ at time t'? From the above definitions the retarded (advanced) function is only non-zero if $t > t'$ ($t < t'$) holds. The retarded (advanced) function thus describes propagation forward-in-time (backward-in-time), G^K in Eq. (2.3) describes how the occupation of states propagates. The above functions are "single-particle" Green's functions. The time evolution of $\Psi(\mathbf{r},t)$ and hence $G^{\mathrm{R,A,K}}$ is determined by the full Hamiltonian, including all many-body effects by Eq. (2.4). In practice this is just as intractable as solving the Schrödinger equation. The advantage of Green's function methods is that we can start from a solvable problem, for example non-interacting free electrons with a Hamiltonian $\mathcal{H}_0$ which gives a "free" Green's function G_0^R. To include the interaction V we split the full Hamiltonian into $\mathcal{H} = \mathcal{H}_0 + V$, this leads to a Dyson equation for the full Green's function G^R,

$$G^\mathrm{R}(\mathbf{r}t;\mathbf{r}'t') = G_0^\mathrm{R}(\mathbf{r}t;\mathbf{r}'t') + \int d\mathbf{r}'' G_0^\mathrm{R}(\mathbf{r}t;\mathbf{r}''t'')V(\mathbf{r}'',t'')G^\mathrm{R}(\mathbf{r}''t'';\mathbf{r}'t'). \tag{2.5}$$

Solving this equation gives then a Green's function G^R that includes the effects of the interaction V. By inserting G^R on the right-hand side, Eq. (2.5) gives an infinite series that might be impossible to sum up. By representing the series in the form of Feynman diagrams, it is often possible to gain some intuition for the approximations that are physically appropriate. If a summation is possible, the effects of the a given interaction can be expressed through a self-energy Σ that alters G^R. Once they are obtained single-particle Green's functions can be used to obtain single-particle physical observables. The charge current, for example, is given by an integral over the spectral current density,[36]

$$e\mathbf{j}(\varepsilon) \equiv -\frac{e}{2m}\left(\vec{\nabla} - \vec{\nabla}'\right)\left[G^\mathrm{K}(\mathbf{r};\mathbf{r}') - \left(G^\mathrm{R}(\mathbf{r};\mathbf{r}') - G^\mathrm{A}(\mathbf{r};\mathbf{r}')\right)\right]\Big|_{\mathbf{r}=\mathbf{r}'}. \tag{2.6}$$

The time argument t in Eqs. (2.1) - (2.4) can, in equilibrium, be replaced by an "imaginary time" $\tau = it$. The equilibrium, imaginary-time Green's functions is then

$$G_{\sigma,\sigma'}(\mathbf{r}\tau;\mathbf{r}'\tau') \equiv -\left\langle \mathcal{T}_\tau \Psi_\sigma(\mathbf{r},\tau), \Psi^\dagger_{\sigma'}(\mathbf{r}',\tau')\right\rangle, \tag{2.7}$$

where σ, σ' label the spin orientation and $\mathcal{T}_\tau$ is the "time"-ordering operator. Gor'kov first introduced two additional Green's functions[38], referred to as anomalous Green's functions or Gor'kov functions.

They are defined, analogously to Eq. (2.7), as

$$F^{\dagger}_{\sigma\sigma'}(\mathbf{r}\tau;\mathbf{r}'\tau') \equiv \left\langle \mathcal{T}_\tau \Psi^{\dagger}_{\sigma}(\mathbf{r},\tau), \Psi^{\dagger}_{\sigma'}(\mathbf{r}',\tau') \right\rangle , \tag{2.8}$$

$$F_{\sigma\sigma'}(\mathbf{r}\tau;\mathbf{r}'\tau') \equiv \left\langle \mathcal{T}_\tau \Psi_{\sigma}(\mathbf{r},\tau), \Psi_{\sigma'}(\mathbf{r}',\tau') \right\rangle . \tag{2.9}$$

The label anomalous indicates that they are zero in the normal state, but non-zero in superconductors. The two functions F and $F^{\dagger}$ are thus referred to as superconducting correlations. From the additional definition

$$\Delta_{\sigma\sigma'}(\mathbf{r}) \equiv |\lambda| F_{\sigma\sigma'}(\mathbf{r},\mathbf{r}), \tag{2.10}$$

it is clear that a non-zero superconducting order parameter Δ is indicates the presence of such superconducting correlations. We now define a Nambu, or particle-hole, space matrix $\hat{G}$

$$\hat{G}(\mathbf{r}\tau;\mathbf{r}'\tau') \equiv \begin{pmatrix} G(\mathbf{r}\tau;\mathbf{r}'\tau') & F(\mathbf{r}\tau;\mathbf{r}\ '\tau') \\ -F^{\dagger}(\mathbf{r}\tau;\mathbf{r}'\tau') & \overline{G}(\mathbf{r}\tau;\mathbf{r}'\tau') \end{pmatrix}, \tag{2.11}$$

where $\overline{G}$ is the particle-hole conjugate of G. The equation of motion for this matrix is the Gor'kov equation[38],

$$\left(\hat{\tau}_3 \frac{\partial}{\partial \tau} + \hat{\mathcal{H}} - \hat{\Sigma} \right) \hat{G}(\mathbf{r}\tau;\mathbf{r}'\tau') = \hat{1}\delta(\mathbf{r}-\mathbf{r}')\delta(\tau-\tau'), \tag{2.12}$$

where

$$\hat{\mathcal{H}} = \begin{pmatrix} \mathbf{p}^2/(2m) - \mu & -\Delta \\ -\Delta^* & \mathbf{p}^2/(2m) - \mu \end{pmatrix}, \tag{2.13}$$

$\mathbf{p} = -i\hbar\nabla$ is the momentum operator, $\hat{\tau}_3$ is the third Pauli matrix in Nambu space, and $\hat{\Sigma}$ is a self-energy matrix that describes the effects of interactions, as discussed above. In the conjugate equation, all derivatives instead act on the primed coordinates and time, it reads

$$\hat{G}(\mathbf{r}\tau;\mathbf{r}'\tau') \left(-\hat{\tau}_3 \frac{\partial}{\partial \tau'} + \hat{\mathcal{H}}' - \Sigma' \right) = \check{1}\delta(\mathbf{r}-\mathbf{r}')\delta(\tau-\tau'), \tag{2.14}$$

where $\hat{\mathcal{H}}'$ and Σ' are obtained by replacing $\mathbf{r} \to \mathbf{r}'$ and $\mathbf{p} \to \mathbf{p}'$ in Eq. (2.13). A solution of the Gor'kov equation would give the full Green's function for a superconductor and allow the calculation of observables. In practice the Gor'kov function contains still "too much" information which lead to the development of the quasiclassical approximation.

2.2 Quasiclassical approxiation & Eilenberger equation

Eilenberger[39], and separately Larkin and Ovchinnikov[40], argued that most relevant excitations in a superconductor happen in a small energy shell around the Fermi surface. This is effectively an expansion in a small parameter, namely

$$\frac{\Delta}{E_{\mathrm{F}}} \ll 1. \tag{2.15}$$

For conventional superconductors this ratio is on the order of 10^{-3}, for unconventional ones it usually on the order of $10^{-2}-10^{-1}$. Physical observables, such as the charge current in Eq. (2.6), involve taking the limit of $\vec{r} \to \vec{r}\,'$ after differentiation in real space representation. This corresponds to a momentum integration in the momentum-space representation. The quasiclassical approximation then consists in replacing such momentum integrations in the spirit of

$$\frac{d^3p}{(2\pi\hbar)^3} \approx d\xi_p \frac{d\Omega_{\vec{p}}}{(2\pi\hbar)^3 v_F}, \tag{2.16}$$

where ξ_p is the dispersion relation in the normal state and v_F is the Fermi velocity. The quasiclassical Green's functions are then obtained by integrating the full Green's function G over ξ_p,

$$g(\hat{p}) \equiv \int \frac{d\xi_p}{\pi i} \hat{G}(\vec{p}), \tag{2.17}$$

implicitly assuming that $\hat{G}$ is peaked at $|\mathbf{p}| = p_{\mathrm{F}}$, such that the resulting function $\hat{g}$ only depends on the *orientation* of the momentum vector on the Fermi sphere, $\hat{p}$, while the magnitude of the momentum is assumed to be equal to the Fermi momentum p_F. This procedure then gives an equation of motion for the (retarded) quasiclassical Green's function, in the steady state it reads

$$i\hbar \mathbf{v}_{\mathrm{F}} \cdot \nabla \hat{g}^{\mathrm{R}} = \left[\varepsilon \hat{\tau}_3 - \hat{h}^{\mathrm{R}}, \hat{g}^{\mathrm{R}}\right] = 0. \tag{2.18}$$

The missing normalization, due to the trivial right-hand side, was found by Eilenberger, and Larkin and Ovchinnikov, to be

$$(\hat{g}^{\mathrm{R}}) = -\pi^2. \tag{2.19}$$

The condition Eq. (2.15) is equivalent to assuming the superconducting coherence length, the natural lengthscale of superconducting phenomena,

$$\xi_0 \equiv \frac{\hbar v_F}{2\pi k_B T_c}, \tag{2.20}$$

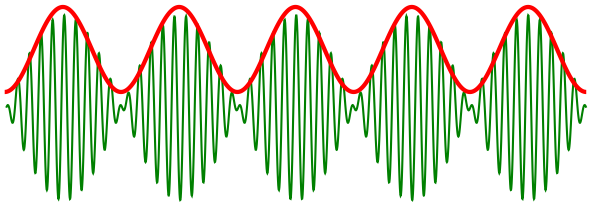

Figure 2.1: *The quasiclassical Green's function (red) describes the envelope of the atomic-scale oscillations of the Gor'kov Green's function (green).*

is much larger than the Fermi wave length λ_F of a given material, $\xi_0 \gg \lambda_F$[41]. Pictorially, we can imagine that the quasiclassical Green's function neglects fast oscillations on the atomic scale and instead describes the envelope of the oscillations, as seen in Fig. 2.1. As a result, the quasiclassical theory is not valid on atomic scales, resulting in mismatches at atomically sharp surfaces that have to be treated in separate boundary conditions, see Sec. 2.3.3.

In the generalization of Eq. (2.18) to the non-equilibrium case, due to Eliashberg[43] and Larkin and Ovchinnikov[44], the full quasiclassical Green's function $\check{g}$ becomes a two-by-two matrix in the so-called Keldysh space. It can be written as

$$\check{g}(\mathbf{p}_F, \mathbf{R}, \varepsilon) = \begin{pmatrix} \hat{g}^R(\mathbf{p}_F, \mathbf{R}, \varepsilon) & \hat{g}^K(\mathbf{p}_F, \mathbf{R}, \varepsilon) \\ 0 & \hat{g}^A(\mathbf{p}_F, \mathbf{R}, \varepsilon) \end{pmatrix}. \tag{2.21}$$

The retarded and advanced components, $\hat{g}^R$ and $\hat{g}^A$, fully determine the spectrum of the system. The remaining Keldysh component $\hat{g}^K$ then contains all information about the occupation of states. Throughout this thesis, we will consider systems in the time-independent steady state and note that the more general expressions for time-dependent phenomena can be found in, e.g., Refs. [42, 45]. In the time-independent case $\check{g}$ satisfies the equation of motion

$$i\hbar \mathbf{v}_F \cdot \nabla \check{g} + \left[\varepsilon \hat{\tau}_3 \check{1} - \check{h}, \check{g}\right] = 0, \tag{2.22}$$

where $[\check{A}, \check{B}]$ is commutator between matrices $\check{A}$ and $\check{B}$, ε is an energy, $\mathbf{v}_F$ is a Fermi-velocity vector, and $\check{h}$ is a self-energy matrix in Keldysh space. It has a structure correspdonding to that of $\check{g}$,

$$\check{h}(\mathbf{p}_F, \mathbf{R}, \varepsilon) = \begin{pmatrix} \hat{h}^R(\mathbf{p}_F, \mathbf{R}, \varepsilon) & \hat{h}^K(\mathbf{p}_F, \mathbf{R}, \varepsilon) \\ 0 & \hat{h}^A(\mathbf{p}_F, \mathbf{R}, \varepsilon) \end{pmatrix}. \tag{2.23}$$

Eq. (2.22) has be combined with the normalization condition

$$\check{g}\check{g} = -\pi^2 \check{1}, \tag{2.24}$$

which gives two independent conditions

$$\hat{g}^R \hat{g}^R = \hat{g}^A \hat{g}^A = -\pi^2, \qquad \hat{g}^R \hat{g}^K + \hat{g}^K \hat{g}^A = 0 \tag{2.25}$$

The components of $\check{g}$ and $\check{h}$ are in turn matrices in Nambu, or particle-hole, space. Their elements are labelled as

$$\hat{g}^{\mathrm{R,A}} = \begin{pmatrix} g & f \\ \tilde{f} & \tilde{g} \end{pmatrix}^{\mathrm{R,A}} \qquad \hat{g}^{\mathrm{K}} = \begin{pmatrix} g & f \\ -\tilde{f} & -\tilde{g} \end{pmatrix}^{\mathrm{K}}. \tag{2.26}$$

The diagonal elements g^X and $\tilde{g}^X$ are the propagators for electron-like and hole-like quasiparticles, while the off-diagonal elements f^X and $\tilde{f}^X$ describe superconducting electron-hole correlations. The self-energy matrix $\check{h}$ has the elements

$$\hat{h}^{\mathrm{R,A}} = \begin{pmatrix} \Sigma & \Delta \\ \tilde{\Delta} & \tilde{\Sigma} \end{pmatrix}^{\mathrm{R,A}} \qquad \hat{h}^{\mathrm{K}} = \begin{pmatrix} \Sigma & \Delta \\ -\tilde{\Delta} & -\tilde{\Sigma} \end{pmatrix}^{\mathrm{K}}. \tag{2.27}$$

Self-energies describe effects such as (in)elastic impurity scattering, electron-electron interaction, or spin-orbit coupling. For the retarded and advanced components, the diagonal elements Σ and $\tilde{\Sigma}$ are quasipartice self-energies that shift and broaden quasiparticle states, while the off-diagonal elements Δ and $\tilde{\Delta}$ affect the superconducting coherence. The Keldysh selfenergies, in contrast, describes the effects on the occupation of interaction with quasiparticle states (Σ^{K}) or the condensate (Δ^{K}).

All elements of $\hat{g}^X$ and $\hat{h}^X$ are, generally, two-by-two matrices in spin space. We use σ_0 and $\sigma_{1/2/3}$ to denote the unit matrix and the three Pauli matrices in spin space, respectively, and define a vector $\boldsymbol{\sigma} \equiv (\sigma_1, \sigma_2, \sigma_3)$. The spin structure for the retarded and advanced functions can then written as

$$\hat{g}^{\mathrm{R,A}} = \begin{pmatrix} g_0\sigma_0 + \boldsymbol{g}\cdot\boldsymbol{\sigma} & (f_0\sigma_0 + \boldsymbol{f}\cdot\boldsymbol{\sigma})i\sigma_2 \\ i\sigma_2(\tilde{f}_0\sigma_0 - \tilde{\boldsymbol{f}}\cdot\boldsymbol{\sigma}) & \tilde{g}_0\sigma_0 - \sigma_2\tilde{\boldsymbol{g}}\cdot\boldsymbol{\sigma}\sigma_2 \end{pmatrix}^{\mathrm{R,A}}, \tag{2.28}$$

see also Ref. [46]. We will return to the spin structure of the Keldysh component in Sect. 2.5.

Lastly, we note that a central symmetry within quasiclassical theory is particle-hole conjugation that can be expressed as the "tilde"-symmetry

$$A(\varepsilon, \mathbf{p}_{\mathrm{F}}, \mathbf{R}) = A^*(-\varepsilon^*, -\mathbf{p}_{\mathrm{F}}, \mathbf{R}). \tag{2.29}$$

2.3 Ricatti parametrization & distribution functions

Any solution to Eq. (2.22) has to satisfy the normalization condition, Eq. (2.24). This can be guaranteed by the usage of appropriate parametrizing functions for the elements of $\check{g}$. For the retarded and advanced elements $\hat{g}^{\mathrm{R}}$ and $\hat{g}^{\mathrm{A}}$, one such parametrization uses the so-called coherence amplitudes γ and $\tilde{\gamma}$[47–49]. Their physical interpretation is that of a local probability of conversion from hole to electron (γ) or electron to hole ($\tilde{\gamma}$)[50].

The retarded component in Eq. (2.26) can be written as

$$\hat{g}^{\mathrm{R}} = -2\pi i \begin{pmatrix} \mathcal{G} & \mathcal{F} \\ -\tilde{\mathcal{F}} & -\tilde{\mathcal{G}} \end{pmatrix}^{\mathrm{R}} + i\pi\hat{\tau}_3, \tag{2.30}$$

where

$$\mathcal{G}^{\mathrm{R}} \equiv (1-\gamma^{\mathrm{R}}\tilde{\gamma}^{\mathrm{R}})^{-1}, \qquad \mathcal{F}^{\mathrm{R}} \equiv \mathcal{G}^{\mathrm{R}}\gamma^{\mathrm{R}} = \left(1-\gamma^{\mathrm{R}}\tilde{\gamma}^{\mathrm{R}}\right)^{-1}\gamma^{\mathrm{R}}. \tag{2.31}$$

Note that the latter two functions are fully determined by the γ and $\tilde{\gamma}$. An analagous expression exists for the advanced element $\hat{g}^{\mathrm{A}}$. Starting from Eq. (2.22) one can derive transport equations for γ and $\tilde{\gamma}$, they read

$$(i\hbar\mathbf{v}_{\mathrm{F}}\cdot\nabla + 2\varepsilon)\,\gamma^{\mathrm{R,A}} = \left(\gamma\tilde{\Delta}\gamma + \Sigma\gamma - \gamma\tilde{\Sigma} - \Delta\right)^{\mathrm{R,A}}. \tag{2.32}$$

$$(i\hbar\mathbf{v}_{\mathrm{F}}\cdot\nabla - 2\varepsilon)\,\tilde{\gamma}^{\mathrm{R,A}} = \left(\tilde{\gamma}\Delta\tilde{\gamma} + \tilde{\Sigma}\tilde{\gamma} - \tilde{\gamma}\Sigma - \tilde{\Delta}\right)^{\mathrm{R,A}}. \tag{2.33}$$

For a spin-degenerate, spin-singlet superconductor, where $\Delta = \Delta_0 i\sigma_2$, the bulk solution is

$$\gamma^{\mathrm{R}} = \gamma^{\mathrm{R}}_{\mathrm{bulk}} i\sigma_2 = \frac{-\Delta_0 i\sigma_2}{\varepsilon - (\Sigma-\tilde{\Sigma})/2 + i\sqrt{\Delta_0\tilde{\Delta}_0 - (\varepsilon - (\Sigma-\tilde{\Sigma})/2\,)^2}}, \tag{2.34}$$

where ε has a small positive imaginary part for the retarded function. Eqs. (2.32) – (2.33) are so-called Ricatti equations and well-studied in literature[59]. An important property of Ricatti equations is that knowledge of a single particular solution – for example the above bulk solution – allows the construction of a general solution, we will return to this in Sec. 3.2.1.

The Keldysh component $\hat{g}^{\mathrm{K}}$ is similarly parametrized in terms of the coherence functions γ and $\tilde{\gamma}$ and two distribution-like functions x and $\tilde{x}$,

$$\hat{g}^{\mathrm{K}} = -2\pi i \begin{pmatrix} \mathcal{X} & \mathcal{Y} \\ \tilde{\mathcal{Y}} & \tilde{\mathcal{X}} \end{pmatrix} \equiv -2\pi i \begin{pmatrix} \mathcal{G} & \mathcal{F} \\ -\tilde{\mathcal{F}} & -\tilde{\mathcal{G}} \end{pmatrix}^{\mathrm{R}} \begin{pmatrix} x & 0 \\ 0 & \tilde{x} \end{pmatrix} \begin{pmatrix} \mathcal{G} & \mathcal{F} \\ -\tilde{\mathcal{F}} & -\tilde{\mathcal{G}} \end{pmatrix}^{\mathrm{A}}, \tag{2.35}$$

where $\mathcal{G}^{\mathrm{A}}, \mathcal{F}^{\mathrm{A}}$ etc. are obtained by replacing the retarded functions with advanced ones in Eq. (2.31). The distribution function x itself then satisfies a variant of the Boltzmann equation that includes the effects of superconducting coherence. In the time-independent steady state it reads

$$\begin{aligned} i\hbar\mathbf{v}_{\mathrm{F}}\cdot\nabla x - \left(\gamma\tilde{\Delta} + \Sigma\right)^{\mathrm{R}} x - x\left(\Delta\tilde{\gamma} - \Sigma\right)^{\mathrm{A}} \\ = -\gamma^{\mathrm{R}}\tilde{\Sigma}^{\mathrm{K}}\tilde{\gamma}^{\mathrm{A}} + \Delta^{\mathrm{K}}\tilde{\gamma}^{\mathrm{A}} + \gamma^{\mathrm{R}}\tilde{\Delta}^{\mathrm{K}} - \Sigma^{\mathrm{K}}. \end{aligned} \tag{2.36}$$

The directional derivative $\mathbf{v}_{\mathrm{F}}\cdot\nabla$ in the equations for both γ and x indicates that they are transport equations. They thus have to be solved along trajectories

parallel to the given direction $\mathbf{v}_\mathrm{F}$. For a trajectory starting at $\mathbf{r}_0$, the spatial coordinate $\mathbf{r}$ of solutions can then be parametrized by a scalar parameter ρ as $\mathbf{r} = \mathbf{r}_0 + \rho\hat{\mathbf{v}}_F$. In order to obtain stable solutions, it is important for the equation is solved from the start point to the end point of a given trajectory for $\gamma^\mathrm{R}, \tilde{\gamma}^\mathrm{A}$, and x. The remaining functions $\tilde{\gamma}^\mathrm{R}, \gamma^\mathrm{A}$, and $\tilde{x}$ have to be integrated in the opposite direction.

In this thesis, only systems with a cylindrical Fermi surface in at most two dimensions are considered, the Fermi surface is then effectively a circle with radius k_F. For transport along a unique spatial direction x, we then parametrize the Fermi velocity vector $\mathbf{v}_\mathrm{F}$ using a single parameter φ_F via

$$\mathbf{v}_\mathrm{F} = \begin{pmatrix} v_\mathrm{F}^x \\ v_\mathrm{F}^y \end{pmatrix} = v_\mathrm{F} \begin{pmatrix} \cos\varphi_\mathrm{F} \\ \sin\varphi_\mathrm{F} \end{pmatrix} \tag{2.37}$$

For later usage, we then define the Fermi surface average of a function A as

$$\langle A \rangle_\mathrm{FS} (\dots) \equiv \int_0^{2\pi} \frac{\mathrm{d}\varphi_\mathrm{F}}{2\pi}\, A(\varphi_\mathrm{F}, \dots), \tag{2.38}$$

where the $\dots$ indicate dependencies on other variables such as position or energy. In addition, we define partial Fermi-surface averages

$$\langle A \rangle_\pm (\dots) \equiv \int_0^{2\pi} \frac{d\varphi_\mathrm{F}}{\pi}\, A(\varphi_\mathrm{F}, \dots)\Theta(\pm\cos\varphi_\mathrm{F}). \tag{2.39}$$

The Heaviside step function $\Theta(\pm\cos\varphi_\mathrm{F})$ equals unity if the x component of $\mathbf{v}_\mathrm{F}$, see Eq. (2.37), is positive (+) or negative (-), and zero otherwise. Clearly,

$$\langle A \rangle_\mathrm{FS} = \frac{\langle A \rangle_+ + \langle A \rangle_-}{2}, \tag{2.40}$$

by the choice of normalization in Eq. (2.39) in comparison to (2.38).

2.3.1 Modes of the nonequilibrium distribution

The parametrization of $\hat{g}^\mathrm{K}$ by means of the distribution x, as in Eq. (2.35), is not the only possible choice. Another option is that in terms of a distribution matrix $\hat{f}$ with elements

$$\begin{aligned} \hat{f}(\varepsilon, \mathbf{p}_\mathrm{F}, \mathbf{R}) &\equiv f_1(\varepsilon, \mathbf{p}_\mathrm{F}, \mathbf{R})\hat{1} + f_3(\varepsilon, \mathbf{p}_\mathrm{F}, \mathbf{R})\hat{\tau}_3 \\ &= \begin{pmatrix} h(\varepsilon, \mathbf{p}_\mathrm{F}, \mathbf{R}) & 0 \\ 0 & -\tilde{h}(\varepsilon, \mathbf{p}_\mathrm{F}, \mathbf{R}) \end{pmatrix}, \end{aligned} \tag{2.41}$$

where h and $\tilde{h}$ are real functions. We will, for now, assume spin degeneracy which gives the elements of $\hat{f}$ a trivial spin structure. In terms of $\hat{f}$, the matrix $\hat{g}^{\mathrm{K}}$ is written as

$$\hat{g}^{\mathrm{K}} = \hat{g}^{\mathrm{R}}\hat{f} - \hat{f}\hat{g}^{\mathrm{A}}. \tag{2.42}$$

This parametrization was originally introduced by Larkin and Ovchinnikov[40]. We refer to the two functions

$$f_1(\varepsilon, \mathbf{p}_{\mathrm{F}}, \mathbf{R}) \equiv \frac{h(\varepsilon, \mathbf{p}_{\mathrm{F}}, \mathbf{R}) - \tilde{h}(\varepsilon, \mathbf{p}_{\mathrm{F}}, \mathbf{R})}{2}, \tag{2.43}$$

$$f_3(\varepsilon, \mathbf{p}_{\mathrm{F}}, \mathbf{R}) \equiv \frac{h(\varepsilon, \mathbf{p}_{\mathrm{F}}, \mathbf{R}) + \tilde{h}(\varepsilon, \mathbf{p}_{\mathrm{F}}, \mathbf{R})}{2}. \tag{2.44}$$

as energy-like (f_1) and charge-like (f_3) modes. They can be used to describe different types of non-equilibrium imbalances that can be induced in a system. The charge-like mode is related to a *charge imbalance* caused by a difference in occupation of electron and holes. The energy mode, in contrast, captures an excess population of equally many electrons and holes that can be related to a higher effective temperature. By using the tilde symmetry, Eq. (2.29), we find

$$f_1(\varepsilon, \mathbf{p}_{\mathrm{F}}, \mathbf{R}) = -f_1(-\varepsilon, -\mathbf{p}_{\mathrm{F}}, \mathbf{R}), \qquad f_3(\varepsilon, \mathbf{p}_{\mathrm{F}}, \mathbf{R}) = f_3(-\varepsilon, -\mathbf{p}_{\mathrm{F}}, \mathbf{R}). \tag{2.45}$$

The functions can can be seen as momentum-resolved generalizations of the so-called energy and charge modes used in the theory of diffusive superconductors[27]. In the following we suppress the explicit arguments $(\varepsilon, \mathbf{p}_{\mathrm{F}}, \mathbf{R})$ for brevity.

One benefit of the reformulation in terms of $\hat{f}$ is that it allows for easier interpretation of the results. For example, the non-equilibrium distribution of electron-like quasiparticles is simply given by

$$f_e \equiv \frac{1-h}{2} = \frac{1}{2}\left(1 - f_1 - f_3\right). \tag{2.46}$$

The hole-like quasiparticle distribution is similarly related to $\tilde{h}$. In equilibrium, h is simply given by

$$h^{\mathrm{eq}}(\varepsilon, \phi, T) = \tanh\frac{\varepsilon - e\phi}{2k_{\mathrm{B}}T}, \tag{2.47}$$

so that f_e reduces to a Fermi-Dirac distribution at temperature T and electrochemical potential $\mu = e\phi$.

Since $\hat{g}^{\mathrm{R,A}}$ are traceless[50], Eq. (2.41) implies that most non-equilibrium observables are fully determined by one of the two modes alone, see also Sec. 2.5. It can thus also be illuminating to study the modes themselves or (partial) Fermi-surface averages. The full Fermi-surface averages are simply given by

$$f_{\mathrm{L}}(\varepsilon, \mathbf{R}) \equiv \langle f_1(\varepsilon, \mathbf{p}_{\mathrm{F}}, \mathbf{R})\rangle_{\mathrm{FS}}, \qquad f_{\mathrm{T}}(\varepsilon, \mathbf{R}) \equiv \langle f_3(\varepsilon, \mathbf{p}_{\mathrm{F}}, \mathbf{R})\rangle_{\mathrm{FS}}. \tag{2.48}$$

Here, the labels L and T refer to to the original nomenclature of longitudinal and transverse mode for diffusive superconductors. They are also referred to as the energy and charge mode, respectively. As a result of the momentum average, the (anti)symmetry in Eq. (2.45) reduces to f_{L} (f_{T}) being an odd (even) function of energy.

For transport that is not fully diffusive, partial Fermi-surface averages for only right-moving (left-moving) quasiparticles can be of interest as well. In order to obtain quantities that have the same energy symmetry as the full averages in Eq. (2.48), we define the combinations

$$f_{1\rightarrow} = \frac{\langle h\rangle_{+} - \langle \tilde{h}\rangle_{-}}{2}, \qquad f_{1\leftarrow} = \frac{\langle h\rangle_{-} - \langle \tilde{h}\rangle_{+}}{2}, \tag{2.49}$$

$$f_{3\rightarrow} = \frac{\langle h\rangle_{+} + \langle \tilde{h}\rangle_{-}}{2}, \qquad f_{3\leftarrow} = \frac{\langle h\rangle_{-} + \langle \tilde{h}\rangle_{+}}{2}. \tag{2.50}$$

They are energy-like and charge-like modes for quasiparticles that are right-moving or left-moving since they have a positive or negative group velocity, respectively.

It is possible to generalize the definitions given above to the case of non-trivial spin-structure. As an example, we consider the case of non-degenerate spin polarization along the spin z-axis. Then $\hat{f}$ changes to

$$\hat{f} = (f_{1,0}\sigma_0 + f_{1,z}\sigma_3)\hat{1} + (f_{3,0}\sigma_0 + f_{3,z}\sigma_3)\hat{\tau}_3) \tag{2.51}$$

$$= \begin{pmatrix} h_0 + h_z\sigma_z & 0 \\ 0 & -\tilde{h}_0 - \tilde{h}_z\sigma_z \end{pmatrix}. \tag{2.52}$$

The spin-splitting thus introduces two additional modes that have, in the diffusive case, been referred to as spin-imbalance mode ($f_{1,z}$) and spin-energy mode ($f_{3,z}$)[51]. Completely analogous to the spin-degenerate case we can define (partial) Fermi-surface averages for the two additional modes by adding the respective spin label to Eqs. (2.48) – (2.50).

Lastly, we mention that it is possible to transfer between the distributions x and h by using the relations

$$x = h + \gamma^{\mathrm{R}}\tilde{h}\tilde{\gamma}^{\mathrm{A}}, \tag{2.53}$$

and the inverse

$$h = \sum_{n=0}^{\infty} \left(\gamma^{\mathrm{R}}\tilde{\gamma}^{\mathrm{R}}\right)^n \left(x - \gamma^{\mathrm{R}}\tilde{x}\tilde{\gamma}^{\mathrm{A}}\right) \left(\gamma^{\mathrm{A}}\tilde{\gamma}^{\mathrm{A}}\right)^n. \tag{2.54}$$

Analogous expressions exist for $\tilde{x}$ and $\tilde{h}$[45]. Note especially that in the normal state where $\gamma^{\mathrm{X}} = \tilde{\gamma}^{\mathrm{X}} = 0$, we have $x = h$ and $\tilde{x} = \tilde{h}$.

The main reason to solve the equation of motion for x is that the solution theory is developed further than for h. We mention here the boundary conditions, see Sec. 2.3.3, and a solution method that is numerically advantageous, discussed in Sec. 3.2.1. The transformation to h provides an tool to analyse the non-equilibrium state in terms of concepts that are well-established in the theory of diffusive systems.

2.3.2 Splitting of the distribution function

In addition to different parametrizations of the Keldysh Green's function $\hat{g}^{\mathrm{K}}$, the underlying distribution functions x and h can be split into a (local) equilibrium part and a so-called anomalous part that captures the non-equilibrium contributions, as introduced in Ref. [45]. The most natural starting point is to generalize Eq. (2.47) to allow for locally varying electrochemical potential and temperature,

$$h(\mathbf{R})^{\mathrm{le}} = h^{\mathrm{le}}(\varepsilon, \phi(\mathbf{R}), T(\mathbf{R})) \equiv \tanh \frac{\varepsilon - e\phi(\mathbf{R})}{2k_{\mathrm{B}}T(\mathbf{R})}. \tag{2.55}$$

We refer $h^{\mathrm{le}}(\mathbf{R})$ as the local equilibrium distribution. For a given full non-equilibrium distribution $h(\mathbf{R})$, we can then define the anomalous distribution as

$$h^{\mathrm{a}}(\mathbf{R}) \equiv h(\mathbf{R}) - h^{\mathrm{le}}(\mathbf{R}). \tag{2.56}$$

It thus captures all non-equilibrium effects that can not be described through a spatially varying chemical potential or temperature. In the following we will not explicitly write out the dependence on the spatial coordinate. Based on the above definitions, we can analogously split x into a local-equilibrium component

$$x^{\mathrm{le}} \equiv h^{\mathrm{le}} + \gamma^{\mathrm{R}}\tilde{h}^{\mathrm{le}}\tilde{\gamma}^{\mathrm{A}} = \tanh \frac{\varepsilon - e\phi}{2k_{\mathrm{B}}T} - \gamma^{\mathrm{R}} \tanh \frac{\varepsilon + e\phi}{2k_{\mathrm{B}}T}\tilde{\gamma}^{\mathrm{A}}, \tag{2.57}$$

and an anomalous component

$$x^{\mathrm{a}} \equiv x - x^{\mathrm{le}}. \tag{2.58}$$

Since $\hat{g}^{\mathrm{K}}$ is in linear in h (or x), these definitions can be used to similarly split

$$\hat{g}^{\mathrm{K}} = \hat{g}^{\mathrm{le}} + \hat{g}^{\mathrm{a}}, \tag{2.59}$$

by using only the local-equilibrium or anomalous part of the parametrizing distribution in Eq. (2.35) or Eq. (2.41) . For an observable A that is linear in $\hat{g}^{\mathrm{K}}$, see also Sec. 2.5, this then naturally gives

$$A = A^{\mathrm{le}} + A^{\mathrm{a}}. \tag{2.60}$$

As we will see in Sec. 2.5 this splitting allows to distinguish, for example, the charge current carried by quasiparticles and by the condensate. We note also that the modes introduced in Sec. 2.3.1 can be split into local-equilibrium and anomalous parts. Taking the energy mode f_1 in the spin-degenerate case as an example, we have

$$\begin{aligned} f_1(\varepsilon, \mathbf{p}_\mathrm{F}, \mathbf{R}) &= \frac{h(\varepsilon, \mathbf{p}_\mathrm{F}, \mathbf{R}) - \tilde{h}(\varepsilon, \mathbf{p}_\mathrm{F}, \mathbf{R})}{2} \\ &= \frac{h^\mathrm{le}(\varepsilon, \mathbf{R}) - \tilde{h}^\mathrm{le}(\varepsilon, \mathbf{R})}{2} + \frac{h^\mathrm{a}(\varepsilon, \mathbf{p}_\mathrm{F}, \mathbf{R}) - \tilde{h}^\mathrm{a}(\varepsilon, \mathbf{p}_\mathrm{F}, \mathbf{R})}{2} \\ &= f_1^\mathrm{le}(\varepsilon, \mathbf{R}) + f_1^\mathrm{a}(\varepsilon, \mathbf{p}_\mathrm{F}, \mathbf{R}). \end{aligned} \tag{2.61}$$

Note that the local-equilibrium part f_1^le does, by definition, not depend on the momentum orientation $\mathbf{p}_\mathrm{F}$. This splitting is equally possible for the charge mode f_3.

Additionally, the splitting makes the numerical solution of the equation of motion for x, Eq. (2.36), more stable. Since x^le is entirely determined by the local quantities ϕ and T, it does not have to be propagated along trajectories. Instead, we only need to solve the equation of motion for the anomalous function x^a. The equation of motion for x^a is, in the stationary state, given by Eq. (3.10) with the replacements

$$x \to x^\mathrm{a}, \tag{2.62}$$

$$\Delta^\mathrm{K} \to \Delta^\mathrm{K} + \Delta^\mathrm{R}\tilde{h}^\mathrm{le} + h^\mathrm{le}\Delta^\mathrm{A}, \tag{2.63}$$

$$E^\mathrm{K} \to E^\mathrm{K} - \left(E^\mathrm{R}h^\mathrm{le} - h^\mathrm{le}E^\mathrm{A}\right) - i\hbar\mathbf{v}_\mathrm{F}\cdot\nabla h^\mathrm{le}. \tag{2.64}$$

The local electrochemical potential $\phi(\mathbf{R})$ enters these transformed self-energies through h^le, $\tilde{h}^\mathrm{le}$, and

$$\mathbf{v}_\mathrm{F}\cdot\nabla h^\mathrm{le} = -\mathbf{v}_\mathrm{F}\cdot\left(\nabla\mu + \frac{\varepsilon-\mu}{T}\nabla T\right)\frac{dh^\mathrm{le}}{d\varepsilon}, \tag{2.65}$$

where $\mu = e\phi$. As a consequence, ϕ has to updated after each solution step by means of the definition in Sec. 2.5 until self-consistency, similar to the self-energies in Sec. 2.4. More details and generalizations of the concepts introduced here can be found in Ref. [45].

2.3.3 Boundary Conditions

The solution formulas in Sec. 3.2.1 allow the propagation of the coherence functions and distribution functions in a system with constant pairing strength. Special care has to be taken, however, at an interface between a superconducting and a normal-metal region, or two different superconductors. Such atomically sharp

interfaces are beyond quasiclassical theory and boundary conditions need to be derived externally, for example using scattering theory. All results presented in this thesis assume that scattering at the interface is specular, that is, the momentum parallel to the surface is conserved in the scattering process. The corresponding boundary conditions have been derived, for both sets of function, in the spin-degenerate case[52] and for general spin structure[53]. Generalizations to a fully general boundary condition, e.g., for multiband systems or diffusive interfaces, exist[45] as well as alternative formulations using a t-matrix approach[54]. We follow the form used in [53]. The interface itself is described by the associated normal-state scattering matrix, for electrons it reads

$$\mathcal{S}_\mathrm{e} = \begin{pmatrix} \mathcal{S}_\mathrm{R} & \mathcal{S}_\mathrm{D} \\ \mathcal{S}_\mathrm{D} & -\mathcal{S}_\mathrm{R} \end{pmatrix}, \tag{2.66}$$

and the matrix for holes $\mathcal{S}_\mathrm{h} = \tilde{\mathcal{S}}_\mathrm{e}^\dagger$. For a system with two independent spin components, the elements can be parametrized as

$$\mathcal{S}_R = \begin{pmatrix} \sqrt{R_\uparrow} e^{i\vartheta/2} & 0 \\ 0 & \sqrt{R_\downarrow} e^{-i\vartheta/2} \end{pmatrix}, \qquad \mathcal{S}_D = \begin{pmatrix} \sqrt{D_\uparrow} e^{i\vartheta/2} & 0 \\ 0 & \sqrt{D_\downarrow} e^{-i\vartheta/2} \end{pmatrix}. \tag{2.67}$$

Here, we use ϑ to denote so-called spin-mixing angle of the interface and the probabilities for reflection, R_σ, and transmission, D_σ, have to In order for the resulting scattering matrix to be unitary, $\mathcal{S}_e^\dagger \mathcal{S}_e = \mathbb{1}$, the probabilities satisfy $R_\sigma + D_\sigma = 1$. In the spin-degenerate case, we just have $\vartheta = 0$, $R_\uparrow = R_\downarrow$, and $D_\uparrow = D_\downarrow$.

We label the functions on the two sides of a given interface by indices 1 and 2. Incoming functions are indicated by small letters, e.g, γ_1^R and x_2. Outgoing functions are then represented as capital letters with the respective index, for example Γ_1^R and X_1. A sketch of the different incoming and outgoing functions can be seen in Fig. 2.2. As an example, we specify the outgoing retarded coherence function Γ_1^R and the distribution function X_1 on side 1, which are propagated away from the interface in the direction of $\mathbf{v}_\mathrm{F}^\mathrm{1o}$. Their boundary conditions read

$$\Gamma_1^\mathrm{R} = r_{1l}^\mathrm{R} \gamma_1^\mathrm{R} S_\mathrm{R}^\dagger + t_{1l}^\mathrm{R} \gamma_2^\mathrm{R} S_\mathrm{D}^\dagger, \tag{2.68}$$

$$X_1 = r_{1l}^\mathrm{R} x_1 \tilde{r}_{1r}^\mathrm{A} + t_{1l}^\mathrm{R} x_2 \tilde{t}_{1r}^\mathrm{A} - a_{1l}^\mathrm{R} \tilde{x}_2 \tilde{a}_{1r}^\mathrm{A}. \tag{2.69}$$

The equations use the definitions

$$r_{1l}^R = \frac{\mathcal{S}_R - \gamma_2^R \mathcal{S}_R^\dagger \tilde{\gamma}_2^R}{1 - \gamma_1^R \mathcal{S}_D^\dagger \tilde{\gamma}_2^R \mathcal{S}_D - \gamma_2^R \mathcal{S}_R^\dagger \tilde{\gamma}_2^R \mathcal{S}_R}, \tag{2.70}$$

$$t_{1l}^R = \frac{\mathcal{S}_D - \gamma_1^R \mathcal{S}_D^\dagger \tilde{\gamma}_2^R}{1 - \gamma_1^R \mathcal{S}_D^\dagger \tilde{\gamma}_2^R \mathcal{S}_D - \gamma_2^R \mathcal{S}_R^\dagger \tilde{\gamma}_2^R \mathcal{S}_R}, \tag{2.71}$$

$$a_{1l}^R = -\left(r_{1l}^R \gamma_1^R \mathcal{S}_R^\dagger \mathcal{S}_R + t_{1l}^R \gamma_2^R \mathcal{S}_D^\dagger \mathcal{S}_R + \mathcal{S}_R \gamma_1^R\right) \left(\mathcal{S}_D - \tilde{\gamma}_2^R \mathcal{S}_D \gamma_1^R\right)^{-1}. \tag{2.72}$$

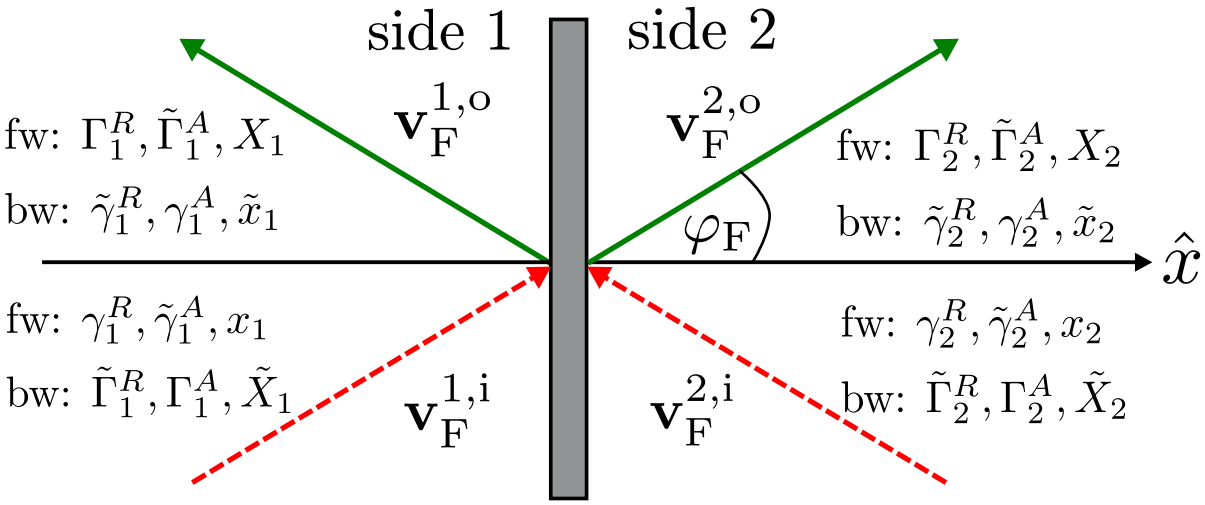

Figure 2.2: *Sketch of the different functions of the trajectories that are coupled for specular reflection at an interface between two regions. The labels "fw" and "bw" indicate if the given functions move in the direction of the respective* $\mathbf{v}_\mathrm{F}$ *or opposite to it.*

In the stationary case that we consider here, the advanced quantities can be obtained by the symmetries $\tilde{r}_{1r}^\mathrm{A} = (r_{1l}^\mathrm{R})^\dagger$, $\tilde{t}_{1r}^\mathrm{A} = (t_{1l}^\mathrm{R})^\dagger$, and $\tilde{a}_{1r}^\mathrm{A} = (a_{1l}^\mathrm{R})^\dagger$. All quantities in the above example, as well as γ, are still matrices in spin space. Implicitly, it is assumed in Eqs. (2.70) – (2.72) that we do not have a fully reflective ($D_\sigma = 0$) or fully transmissive ($D_\sigma = 1$) interface for either of the two spin components. The simpler boundary conditions for these two special cases can be derived following the original references. Boundary conditions for the functions on the other side of the interface can be obtained by exchanging the indices 1 and 2 in the above quantities, up to an unimportant global sign in r_{2l}^R, t_{2l}^R, and a_{2l}^R.

The different momentum orientations shown in Fig. 2.2 can be expressed as angles to the $\hat{x}$ axis in momentum space. In a quasi one-dimensional system, an incoming trajectory $\mathbf{v}_\mathrm{F}^{1,\mathrm{i}}$, with the angle φ_F, scattered into the reflected outgoing trajectory $\mathbf{v}_\mathrm{F}^{1,\mathrm{o}}$ with momentum angle

$$\varphi_\mathrm{F}' = \pi - \varphi_\mathrm{F}. \tag{2.73}$$

Specular scattering at the interface thus mixes different trajectories. The boundary condition for Γ_1^R. Eq. (2.68), is thus a functional dependence of the form

$$\Gamma_1^\mathrm{R}(\varphi_\mathrm{F}') = f\left(\gamma_1^\mathrm{R}(\varphi_\mathrm{F}), \tilde{\gamma}_1^\mathrm{R}(\varphi_\mathrm{F}'), \gamma_2^\mathrm{R}(\varphi_\mathrm{F}'), \tilde{\gamma}_2^\mathrm{R}(\varphi_\mathrm{F})\right). \tag{2.74}$$

With slight changes to Eq. (2.73), the same boundary conditions are valid in two-dimensional systems, we will return to this in Sec. 3.3.5. We can model a tunnel cone via a transparency that depends on the momentum orientation, we use

$$D(\varphi_\mathrm{F}) = D_0(e^{-\beta \sin^2 \varphi_\mathrm{F}} - e^{-\beta})/(1 - e^{-\beta}). \tag{2.75}$$

in the appended papers.

2.4 Self-energies

In Sec. 2.2 we introduced the elements of the self-energy matrix $\check{h}$. In order to obtain physical results all self-energies must be determined self-consistently when solving the Eilenberger equation, Eq. (2.22). In this work we use

$$\check{h} = \check{h}_{\mathrm{MF}} + \check{h}_{\mathrm{s}}, \tag{2.76}$$

where the two terms describe the mean-field superconducting order parameter and scalar impurity scattering, respectively.

The first term, $\check{h}_{\mathrm{MF}}$, has the Keldysh-space structure

$$\check{h}_{\mathrm{MF}} = \begin{pmatrix} \hat{\Delta}^{\mathrm{R}}_{\mathrm{MF}} & 0 \\ 0 & \hat{\Delta}^{\mathrm{A}}_{\mathrm{MF}}, \end{pmatrix} \tag{2.77}$$

so that the Keldysh component $\hat{h}^{\mathrm{K}}_{\mathrm{MF}}$ is zero. For the mean-field component, the retarded and advanced self-energies are identical[45] and their Nambu-space elements read

$$\hat{\Delta}^{\mathrm{R,A}}_{\mathrm{MF}} = (\Delta'\hat{\tau}_1 - \Delta''\hat{\tau}_2)i\sigma_2 = \begin{pmatrix} 0 & \Delta \\ \Delta^* & 0 \end{pmatrix} i\sigma_2, \tag{2.78}$$

where Δ' (Δ'') denotes the real (imaginary) part of the order parameter and $i\sigma_2$ signals a spin-singlet order parameter. In the general case we can have different pairing channels, corresponding to s-wave, p-wave, d-wave, ... superconductivity. The complex, scalar function Δ itself can then be written as

$$\Delta(\varphi_{\mathrm{F}}) = \sum_{\Gamma} \Delta_\Gamma \eta_\Gamma(\varphi_{\mathrm{F}}), \tag{2.79}$$

where the index $\Gamma = s, p, d, \ldots$ marks the respective pairing, and $\eta(\varphi_{\mathrm{F}})$ is the basis function for a given channel. The basis functions can be chosen real, and for the s-wave and d-wave superconductors that we will consider the basis functions read

$$\eta_s(\varphi_{\mathrm{F}}) = 1, \qquad \eta_d(\varphi_{\mathrm{F}}) = \sqrt{2}\cos\left(2\phi_{\mathrm{F}} - 2\alpha\right), \tag{2.80}$$

where α is the misalignment angle between the main crystal axis and a grain boundary. For the pairing channel Γ the self-consistency equation for the order parameter then reads

$$\Delta_\Gamma(\mathbf{R}) = \mathcal{N}_{\mathrm{F}}\lambda_\Gamma \int_{-\varepsilon_c}^{\varepsilon_c} \frac{d\varepsilon}{8\pi i} \left\langle \mathrm{tr}_{\mathrm{spin}} \left[i\sigma_2 \eta_\Gamma(\mathbf{p}_{\mathrm{F}}) f^{\mathrm{K}}(\mathbf{p}_{\mathrm{F}}, \mathbf{R}, \varepsilon) \right] \right\rangle_{\mathrm{FS}}, \tag{2.81}$$

where λ_Γ is the pairing interaction strength in channel Γ and η_Γ is the respective basis function. Note that the trace in Nambu space has already been taken in

Eq. (2.81), only a trace over the spin degrees of freedom remains. The singlet mean-field order parameter is thus (by assumption) spin-degenerate. Lastly, we note that we eliminate high-energy cutoff ε_c in favour of the critical temperature T_c by subtracting the linearised gap equation, see also[42].

The second term in Eq. (2.76), $\check{h}_s$, describes scattering on scalar, non-magnetic impurities. Assuming a dilute concentration of impurities n_i we can write

$$\check{h}_s = n_i \check{t} \equiv n_i \begin{pmatrix} \hat{t}^R & \hat{t}^K \\ 0 & \hat{t}^A \end{pmatrix}. \tag{2.82}$$

Generally, this leads to an integral equation for the three elements of the t-matrix [55]. For a momentum-independent (s-wave) scattering strength u_0 and in the non-crossing approximation the t-matrix equation simplifies to

$$\hat{t}^{R,A} = u_0 \hat{1} + u_0 \mathcal{N}_F \left\langle \hat{g}^{R,A} \right\rangle_{FS} \hat{t}^{R,A} \tag{2.83}$$

$$\hat{t}^K = \mathcal{N}_F \hat{t}^R \left\langle \hat{g}^K \right\rangle_{FS} \hat{t}^A. \tag{2.84}$$

The solution is then found to be

$$\hat{t}^{R,A} = \frac{u_0 \hat{1} + u_0^2 \mathcal{N}_F \left\langle \hat{g}^{R,A} \right\rangle_{FS}}{\hat{1} - \left[u_0 \mathcal{N}_F \left\langle \hat{g}^{R,A} \right\rangle_{FS} \right]^2}, \tag{2.85}$$

$$\hat{t}^K = \mathcal{N}_F \hat{t}^R \left\langle \hat{g}^K \right\rangle_{FS} \hat{t}^A. \tag{2.86}$$

Note that the denominator in Eq. (2.85) is the inverse of a unit matrix. We can rewrite these expressions by defining the scattering energy Γ_u and the scattering phase shift δ_0 as

$$\Gamma_u \equiv \frac{n_i}{\pi \mathcal{N}_F}, \qquad \delta_0 \equiv \arctan(\pi u_0 \mathcal{N}_F). \tag{2.87}$$

The combination

$$\Gamma \equiv \Gamma_u \sin^2 \delta_0, \tag{2.88}$$

is called the pair-breaking energy and can be related to the normal-state mean free path

$$\ell = \frac{\hbar v_F}{2\Gamma}. \tag{2.89}$$

In terms of the parameters in Eq. (2.87) the retarded and advanced self-energies for scalar impurity scattering read

$$\hat{h}_s^{R,A} = n_i \hat{t}^{R,A} = \pi \Gamma_u \frac{(\pi \cos \delta_0 \ \ \sin \delta_0)\hat{1} + \sin^2 \delta_0 \left\langle \hat{g}^{R,A} \right\rangle_{FS}}{\pi^2 \cos^2 \delta_0 - \sin^2 \delta_0 \left\langle \hat{g}^{R,A} \right\rangle_{FS}^2}. \tag{2.90}$$

Combining Eq. (2.82) and (2.86), we can write $\hat{h}^{\mathrm{K}}$ as

$$\hat{h}_{\mathrm{s}}^{\mathrm{K}} = \frac{1}{\pi\Gamma_{\mathrm{u}}}\hat{h}^{\mathrm{R}}\left\langle\hat{g}^{\mathrm{K}}\right\rangle_{\mathrm{FS}}\hat{h}^{\mathrm{A}}, \tag{2.91}$$

which can be written out by inserting Eq. (2.90).

In Papers I, III, and IV we restrict ourselves to two limiting cases of this general expression. Firstly, the weak-scattering Born limit, obtained by letting $\delta_0 \to 0$ and $\Gamma_u \to \infty$ such that Γ in Eq. (2.88) is constant. In this case we find

$$\hat{h}_{\mathrm{s,Born}}^{\mathrm{R,A}} = \frac{\Gamma}{\pi}\left\langle\hat{g}^{\mathrm{R,A}}\right\rangle_{\mathrm{FS}}, \qquad \hat{h}_{\mathrm{s,Born}}^{\mathrm{K}} = \frac{\Gamma}{\pi}\left\langle\hat{g}^{\mathrm{K}}\right\rangle_{\mathrm{FS}}. \tag{2.92}$$

Secondly, we have the case of the strong-scattering unitary limit, meaning that $\delta \to \pi/2$ or $u_0 \to \infty$. The self-energies then become

$$\hat{h}_{\mathrm{s,uni}}^{\mathrm{R,A}} = -\pi\Gamma\frac{\left\langle\hat{g}^{\mathrm{R,A}}\right\rangle_{\mathrm{FS}}}{\left\langle\hat{g}^{\mathrm{R,A}}\right\rangle_{\mathrm{FS}}^2}, \qquad \hat{h}_{\mathrm{s,uni}}^{\mathrm{K}} = \pi\Gamma\frac{\left\langle\hat{g}^{\mathrm{R}}\right\rangle_{\mathrm{FS}}\left\langle\hat{g}^{\mathrm{K}}\right\rangle_{\mathrm{FS}}\left\langle\hat{g}^{\mathrm{A}}\right\rangle_{\mathrm{FS}}}{\left\langle\hat{g}^{\mathrm{R}}\right\rangle_{\mathrm{FS}}^2\left\langle\hat{g}^{\mathrm{A}}\right\rangle_{\mathrm{FS}}^2}. \tag{2.93}$$

Eqs. (2.90) – (2.93) hold for arbitrary order-parameter symmetry.

2.5 Observables

Once the quasiclassical Green's function $\check{g}(\mathbf{R}, \varepsilon, \varphi_{\mathrm{F}})$ is obtained we can calculate physical observables. Technically, expressions for physical observables are derived by performing the quasiclassical approximation on the underlying expression in terms of the full Green's function[42].

Most observables that are of interest in non-equilibrium situations are defined in terms of the Keldysh Green's function $\hat{g}^{\mathrm{K}}$. The main benefit of introducing the non-equilibrium modes in Sec. 2.3.1 is then that we can express observables entirely in terms of a momentum- and spin-resolved density of states and the non-equilibrium modes, as we will outline below. In the following we assume that there is at most a single spin polarization axis that we choose as the spin z axis. The full spin structure of $\hat{g}^{\mathrm{R,A}}$, as given in Eq. (2.28), then simplifies to

$$\hat{g}^{\mathrm{R,A}} = \begin{pmatrix} g^{\mathrm{R}} & f^{\mathrm{R}} \\ \tilde{f}^{\mathrm{R}} & \tilde{g}^{\mathrm{R}} \end{pmatrix} = \begin{pmatrix} g_0\sigma_0 + g_z\sigma_3 & (f_0\sigma_0 + f_z\sigma_3)i\sigma_2 \\ i\sigma_2(\tilde{f}_0\sigma_0 - \tilde{f}_z\sigma_3) & \tilde{g}_0\sigma_0 + \tilde{g}_z\sigma_3 \end{pmatrix}^{\mathrm{R,A}}. \tag{2.94}$$

Taking the top-left element as an example, we label the elements in spin space as

$$g^{\mathrm{R,A}} = \begin{pmatrix} g_+ & 0 \\ 0 & g_- \end{pmatrix}^{\mathrm{R,A}} \equiv \begin{pmatrix} g_0 + g_z & 0 \\ 0 & g_0 - g_z \end{pmatrix}^{\mathrm{R,A}} \tag{2.95}$$

and analogously for $\tilde{g}^{\mathrm{R}}$.

The momentum-resolved density of states for the a spin component $\sigma = \uparrow, \downarrow$ is then

$$\mathcal{N}_{\uparrow(\downarrow)}(\mathbf{p}_\mathrm{F}, \mathbf{R}, \varepsilon) \equiv -\frac{1}{\pi}\mathrm{Im}\; g^R_{+(-)}(\mathbf{p}_\mathrm{F}, \mathbf{R}, \varepsilon). \tag{2.96}$$

Averaging over the Fermi surface and spin then gives "full" density of states

$$\mathcal{N}(\mathbf{R}, \varepsilon) = \mathcal{N}_\mathrm{F} \sum_{\sigma=\uparrow,\downarrow} \langle \mathcal{N}_\sigma(\mathbf{p}_\mathrm{F}, \mathbf{R}, \varepsilon)\rangle_\mathrm{FS} = 2\mathcal{N}_\mathrm{F} \frac{\left\langle -\mathrm{Im}\; g_0^\mathrm{R}(\mathbf{p}_\mathrm{F}, \mathbf{R}, \varepsilon)\right\rangle_\mathrm{FS}}{\pi}. \tag{2.97}$$

We can now combine Eq. (2.52) and Eq. (**??**) to express observables entirely in terms of $\mathcal{N}_\sigma(\mathbf{p}_\mathrm{F}, \mathbf{R}, \varepsilon)$, Eq. (2.96), and the non-equilibrium modes in Eq. (2.52). In the following, we do not write out the arguments on those two sets of functions. Lastly, we note that in the spin-degenerate case, $\mathcal{N}_\uparrow = \mathcal{N}_\downarrow$ and the expressions below reduce to the those provided in Papers I-IV. The charge current density, in terms of $\hat{g}^\mathrm{K}$ given by

$$\mathbf{j}(\mathbf{R}) = e\mathcal{N}_\mathrm{F} \int_{-\infty}^{\infty} \frac{\mathrm{d}\varepsilon}{8\pi i} \left\langle \mathrm{Tr}\left[\mathbf{v}_\mathrm{F}\hat{\tau}_3\hat{g}^\mathrm{K}(\mathbf{p}_\mathrm{F}, \mathbf{R}, \varepsilon)\right]\right\rangle_\mathrm{FS}, \tag{2.98}$$

becomes

$$\mathbf{j}(\mathbf{R}) = -e\mathcal{N}_\mathrm{F} \int_{-\infty}^{\infty} \mathrm{d}\varepsilon \left\langle \mathbf{v}_\mathrm{F}\left(f_{1,0}\frac{\mathcal{N}_\uparrow + \mathcal{N}_\downarrow}{2} + f_{3,z}\frac{\mathcal{N}_\uparrow - \mathcal{N}_\downarrow}{2}\right)\right\rangle_\mathrm{FS}. \tag{2.99}$$

An expression for the electro-chemical potential can be derived by requiring local charge neutrality to first order in Δ/E_F,[56] giving

$$e\phi(\mathbf{R}) = \frac{1}{2}\int_{-\infty}^{\infty} \frac{\mathrm{d}\varepsilon}{8\pi i} \left\langle \mathrm{Tr}\; \hat{g}^\mathrm{K}(\mathbf{p}_\mathrm{F}, \mathbf{R}, \varepsilon)\right\rangle_\mathrm{FS}. \tag{2.100}$$

In terms of the non-equilibrium modes, it reads

$$e\phi(\mathbf{R}) = -\frac{1}{2}\int_{-\infty}^{\infty} \mathrm{d}\varepsilon \left\langle f_{3,0}\frac{\mathcal{N}_\uparrow + \mathcal{N}_\downarrow}{2} + f_{1,z}\frac{\mathcal{N}_\uparrow - \mathcal{N}_\downarrow}{2}\right\rangle_\mathrm{FS}. \tag{2.101}$$

In Paper I and III, we use in addition to this Fermi-surface averaged potential, a left-mover and right-mover potential, defined in analogy to the normal state for the spin-degenerate case as

$$\phi_\pm := \phi - \frac{1}{2e}\int_{-\infty}^{\infty} \frac{d\varepsilon}{2} \left(\langle \mathcal{X}^\mathrm{a}\rangle_\pm + \langle \tilde{\mathcal{X}}^\mathrm{a}\rangle_\mp\right), \tag{2.102}$$

While compiling this thesis, we noticed that a more natural definition is

$$e\phi_{\rightleftarrows} := -\frac{1}{2}\int_{-\infty}^{\infty} d\varepsilon\ \langle h(\varepsilon,\mathbf{p}_\mathrm{F})\mathcal{N}(\varepsilon,\mathbf{p}_\mathrm{F})\rangle_{\pm} + \langle \tilde{h}(\varepsilon,\mathbf{p}_\mathrm{F})\mathcal{N}(\varepsilon,\mathbf{p}_\mathrm{F})\rangle_{\mp}, \tag{2.103}$$

which satisfies

$$\phi(\mathbf{R}) = \frac{\phi_{\rightarrow}+\phi_{\leftarrow}}{2}. \tag{2.104}$$

also in the superconducting state. Similarly, we can rewrite the energy current

$$\mathbf{j}^{\mathrm{th}}(\mathbf{R}) = \mathcal{N}_\mathrm{F}\int_{-\infty}^{\infty}\frac{\mathrm{d}\varepsilon}{8\pi i}\ \varepsilon\left\langle \mathbf{v}_\mathrm{F}\hat{g}^{\mathrm{K}}(\mathbf{p}_\mathrm{F},\mathbf{R},\varepsilon)\right\rangle_{\mathrm{FS}}, \tag{2.105}$$

$$= -\mathcal{N}_\mathrm{F}\int_{-\infty}^{\infty}\mathrm{d}\varepsilon\ \varepsilon\ \left\langle \mathbf{v}_\mathrm{F}\left(f_{3,0}\frac{\mathcal{N}_\uparrow+\mathcal{N}_\downarrow}{2}+f_{1,z}\frac{\mathcal{N}_\uparrow-\mathcal{N}_\downarrow}{2}\right)\right\rangle_{\mathrm{FS}}, \tag{2.106}$$

and the magnetization along the spin-polarization axis z,

$$M_z(\mathbf{p}_\mathrm{F},\mathbf{R},\varepsilon) - M_{\mathrm{z,ext}} = -\mu_\mathrm{B}\mathcal{N}_\mathrm{F}\int_{-\infty}^{\infty}\frac{\mathrm{d}\varepsilon}{8\pi i}\ \left\langle \sigma_z\hat{g}^{\mathrm{K}}(\mathbf{p}_\mathrm{F},\mathbf{R},\varepsilon)\right\rangle_{\mathrm{FS}} \tag{2.107}$$

$$= \mu_\mathrm{B}\mathcal{N}_\mathrm{F}\int_{-\infty}^{\infty}\mathrm{d}\varepsilon\ \left\langle f_{1,0}\frac{\mathcal{N}_\uparrow-\mathcal{N}_\downarrow}{2}+f_{3,z}\frac{\mathcal{N}_\uparrow+\mathcal{N}_\downarrow}{2}\right\rangle_{\mathrm{FS}}. \tag{2.108}$$

Here $M_{\mathrm{z,ext}} = 2\mu_\mathrm{B}^2\mathcal{N}_\mathrm{F}B_z(\mathbf{R})$. The last identity shows that a spin polarization can be created in two different ways. Either by a spin-split density of states, for example by an applied magnetic field, this magnetization also exists in equilibrium. Injection from a ferromagnet or through an spin-active interface with $D_\uparrow \neq D_\downarrow$ creates a non-zero $f_{3,z}$, resulting in a non-equilibrium magnetization.

3 Solution strategies

This chapter outlines what a self-consistent solution means within the framework of quasiclassical theory and reviews the solution methods that were used for the work presented in this thesis.

3.1 Self-consistency of solutions

An central part of the work presented in this thesis was to not only solve the Eilenberger equation, Eq. (2.22), but to find self-consistent solutions. This means that the self-energy matrix $\check{h}$ has to be determined such that it is consistent with the solution $\check{g}$ to the equation of motion.

The requirement of self-consistency is necessary to ensure that the obtained solutions fulfil fundamental physical requirements such as conservation laws, as we show for charge conservation in Appendix A. Nevertheless, self-consistency is often neglected in the literature, especially in non-equilibrium situations. This can be justifiable in cases, e.g, if the applied bias or external drive is small so that self-consistency can be expected to give only small corrections.

Starting from an initial guess for all self-energies, the general recipe consists of three steps:

1. For a given guess of $\check{h}$ solve the Eilenberger equation for $\check{g}$.
2. Use $\check{g}$ to obtain a new guess $\check{h}_{\text{new}}$.
3. Unless both $\check{g}$ and $\check{h}$ did not change – at least up to a desired accuracy – go back to step 1 and use $\check{h}_{\text{new}}$ as the given guess for all self-energies.

Depending on the solution method, it it is essentially a one-step process to solve for $\check{g}$ for a given set of self-energies. In contrast, finding a self-consistent guess for the self-energies $\check{h}$ is typically an iterative procedure that can take many iterations of the above three steps. The problem can be seen as a fix-point problem and methods such as Anderson acceleration[57] can be used to speed to the process.

3.2 1D: Stepping method

In Papers I-III we investigate systems that are either one-dimensional, such as a nanowire, or quasi one-dimensional by translational invariance normal to the transport direction. For a numerical solution, the spatial coordinate along the transport direction then has to be discretised on a finite grid of points. Both the self-energies and the solution are then only defined on the grid points. To solve the equations of motion for the parametrizing functions, we use a method of propagation functions discussed in Sec. 3.2.1. Using the obtained analytic expression we can propagate the functions along trajectories "step-by-step" from one point on the grid to the next, we refer to this as a *stepping method*. The underlying assumption is that the self energies are constant between neighbouring grid points as sketched in Fig. 3.1, and thus piecewise continuous. We note here that some care has to be taken in choosing the correct profile in order to ensure the proper behaviour of the self-consistency equations in this case[58]. One we have found the set of parametrizing functions on all grid points, we can construct $\check{g}$ and proceed with the self-consistency scheme outlined in Sec. 3.1.

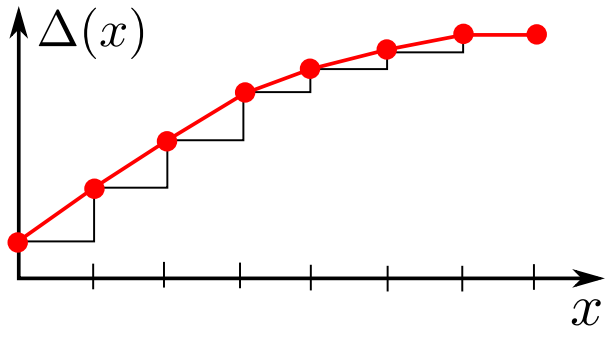

Figure 3.1: *Profile of piece-wise constant self-energies, here the order parameter $\Delta(x)$.*
Grid points are indicated in red. The self-energies and solutions are assumed constant between neighbouring points. When plotting the final results, we might interpolate between neighbouring points to obtain the smooth, red profile.

3.2.1 Propagating functions

In Ref. [45] formal solutions of Eqs. (2.32) and Eq. (2.36) in terms of three propagation functions were derived. Here we use those formal expressions to derive a solution to the equations of motion in a region of constant self-energies.

We start by defining $E^{\mathrm{X}} = \varepsilon - \Sigma^{\mathrm{X}}$, $\tilde{E}^{\mathrm{X}} = -\varepsilon - \tilde{\Sigma}^{\mathrm{X}}$, $E^{\mathrm{K}} = -\Sigma^{\mathrm{K}}$ and $\tilde{E}^{\mathrm{K}} = -\tilde{\Sigma}^{\mathrm{K}}$, and rewrite Eq. (2.32) as

$$i\partial\gamma^{\mathrm{X}} - \gamma^{\mathrm{X}}\tilde{\Delta}^{\mathrm{X}}\gamma^{\mathrm{X}} + E^{\mathrm{X}}\gamma^{\mathrm{X}} - \gamma^{\mathrm{X}}\tilde{E}^{\mathrm{X}} + \Delta^{\mathrm{X}} = 0, \quad \text{with } \gamma^{\mathrm{X}}(0) = \gamma_i^{\mathrm{X}}, \tag{3.1}$$

where, here and in the following, $\mathrm{X} = \mathrm{R}, \mathrm{A}$ marks retarded or advanced version of the equation, $\partial \equiv \hbar \mathbf{v}_{\mathrm{F}} \cdot \nabla$, and ρ specifies the position along a given trajectory. Given a solution $\gamma^{\mathrm{X}}(\rho)$ to the Eilenberger equation we can obtain three functions

the $U^{\mathrm{X}}(\rho), V^{\mathrm{X}}(\rho),$ and $W^{\mathrm{X}}(\rho)$ through

$$i\partial U^{\mathrm{X}} + \left(E^{\mathrm{X}} - \gamma^{\mathrm{X}}\tilde{\Delta}^{\mathrm{X}}\right) U^{\mathrm{X}} = 0, \quad U^{\mathrm{X}}(0) = \mathbb{1}, \tag{3.2}$$

$$i\partial V^{\mathrm{X}} - V^{\mathrm{X}}\left(\tilde{E}^{\mathrm{X}} + \tilde{\Delta}^{\mathrm{X}}\gamma^{\mathrm{X}}\right) = 0, \quad V^{X}(0) = \mathbb{1}, \tag{3.3}$$

$$i\partial W^{\mathrm{X}} + V^{\mathrm{X}}\tilde{\Delta}^{\mathrm{X}}U^{\mathrm{X}} = 0, \quad W^{X}(0) = 0. \tag{3.4}$$

Let us assume that for our given solution $\gamma^{\mathrm{X}}(\rho) \equiv \gamma_0^{\mathrm{X}}(\rho)$ we have obtained the three functions $U_0^{\mathrm{X}}, V_0^{\mathrm{X}}$, and W_0^{X}. The benefit of these propagators is that for a change of the initial condition $\gamma^{\mathrm{X}}(0)$ of differential equation,

$$\gamma^{\mathrm{X}}(0) = \gamma_i^{\mathrm{X}} \to \gamma^{\mathrm{X}}(0) = \gamma_i^{\mathrm{X}} + \delta^{\mathrm{X}} \tag{3.5}$$

we do not have to solve any differential equations. Instead, we obtain the new set of functions for the new initial condition via

$$U^{X}(\rho) = U_0^{X}(\rho)\left[\mathbb{1} + \delta^{X}W_0^{X}(\rho)\right]^{-1}, \tag{3.6}$$

$$V^{X}(\rho) = \left[\mathbb{1} + W_0^{X}(\rho)\delta^{X}\right]^{-1} V_0^{X}(\rho), \tag{3.7}$$

$$W^{X}(\rho) = \left[\mathbb{1} + W_0^{X}(\rho)\delta^{X}\right]^{-1} W_0^{X}(\rho) = W_0^{X}(\rho)\left[\mathbb{1} + \delta^{X}W_0^{X}(\rho)\right]^{-1}, \tag{3.8}$$

and our new solution $\gamma^{\mathrm{X}}(\rho)$ via

$$\gamma^{X}(\rho) = \gamma_0^{X}(\rho) + U_0^{X}(\rho)\delta^{X}V^{X}(\rho) = \gamma_0^{X}(\rho) + U^{X}(\rho)\delta^{X}V_0^{X}(\rho). \tag{3.9}$$

That the general solution can be constructed out of a particular solution is a well-known property of Ricatti equations[59]. The three operator functions U, V, and W can, however, also be used to construct a solution to the equation of motion for the distribution function x. We start by rewriting Eq. (2.36) as

$$i\partial x + (E - \gamma\tilde{\Delta})^{\mathrm{R}}x - x(E + \Delta\tilde{\gamma})^{\mathrm{A}} = \gamma^{\mathrm{R}}\tilde{E}^{\mathrm{K}}\tilde{\gamma}^{\mathrm{A}} + \Delta^{\mathrm{K}}\tilde{\gamma}^{\mathrm{A}} + \gamma^{\mathrm{R}}\tilde{\Delta}^{\mathrm{K}} + E^{\mathrm{K}}, \tag{3.10}$$

where the right-hand side defines

$$I^{\mathrm{K}} = \gamma^{\mathrm{R}}\tilde{E}^{\mathrm{K}}\tilde{\gamma}^{\mathrm{A}} + \Delta^{\mathrm{K}}\tilde{\gamma}^{\mathrm{A}} + \gamma^{\mathrm{R}}\tilde{\Delta}^{\mathrm{K}} + E^{\mathrm{K}}. \tag{3.11}$$

Formally, the solution can be written as

$$x(\rho) = S_U^{\mathrm{R}}(\rho, 0)x(0)\tilde{S}_V^{\mathrm{A}}(0, \rho) - i\int_0^{\rho} S_U^{\mathrm{R}}(\rho, \rho')I^{\mathrm{K}}(\rho')\tilde{S}_V^{\mathrm{A}}(\rho', \rho)\mathrm{d}\rho', \tag{3.12}$$

where

$$S_U^{X}(\rho, \rho') \equiv U^{X}(\rho)\left(U^{X}(\rho')\right)^{-1}, \quad S_V^{X}(\rho', \rho) \equiv \left(V^{X}(\rho')\right)^{-1} V^{X}(\rho). \tag{3.13}$$

We apply this method to propagation in a region of constant selfenergies, assuming that γ^{X}, x, and all self-energies have only non-zero components along a single spin-quantization axis that we can choose to be the spin z axis. In this case, we can write

$$\gamma^X(\rho) = \mathrm{diag}(\gamma^{\mathrm{X}}_\uparrow, \gamma^{\mathrm{X}}_\downarrow) i\sigma_2, \qquad x(\rho) = \mathrm{diag}(x_\uparrow, x_\downarrow) \tag{3.14}$$

$$\Delta^X(\rho) = \mathrm{diag}(\Delta^{\mathrm{X}}_\uparrow, \Delta^{\mathrm{X}}_\downarrow) i\sigma_2, \qquad \Sigma^X(\rho) = \mathrm{diag}(\Sigma^{\mathrm{X}}_\uparrow, \Sigma^{\mathrm{X}}_\downarrow). \tag{3.15}$$

Up to a factor of $i\sigma_2$, all objects can thus be written as diagonal matrices in spin space. In the following $\sigma = \uparrow, \downarrow$ denotes one of the two components and $\underline{\sigma}$ the opposite-spin component, i.e., $\underline{\uparrow} = \downarrow$. For γ^{X} with a spin structure as in Eq. (3.14) the bulk solution $\gamma^{\mathrm{X}}_{\mathrm{bulk}}$ for each component reads

$$\gamma^{\mathrm{R}}_{\mathrm{bulk},\sigma} = -\frac{\Delta_{0,\sigma}}{\varepsilon - (\Sigma_\sigma - \tilde{\Sigma}_{\underline{\sigma}})/2 + i\sqrt{\Delta_{0,\sigma}\tilde{\Delta}_{0,\underline{\sigma}} - (\varepsilon - (\Sigma_\sigma - \tilde{\Sigma}_{\underline{\sigma}})/2\ )^2}}.$$

Denoting the bulk solution $\gamma^{\mathrm{X}}_0 \equiv \mathrm{diag}(\gamma^{\mathrm{X}}_{0,\uparrow}, \gamma^{\mathrm{X}}_{0,\downarrow}) i\sigma_2$ we then find

$$U^{\mathrm{X}}_0 = \exp\left[i\left(E^{\mathrm{X}} - \gamma^{\mathrm{X}}_0 \tilde{\Delta}^{\mathrm{X}}\right)\rho\right], \tag{3.16}$$

$$V^{\mathrm{X}}_0 = \exp\left[-i\left(\tilde{E}^{\mathrm{X}} + \tilde{\Delta}^{\mathrm{X}}\gamma^{\mathrm{X}}_0\right)\rho\right] \tag{3.17}$$

$$W^{\mathrm{X}}_0 = \tilde{\Delta}^X \left(w^{\mathrm{X}}_0\right)^{-1} \left(\exp\left[i w^{\mathrm{X}}_0 \rho\right] - 1\right). \tag{3.18}$$

Note that all thee functions are spin matrices, U_0 and V_0 are spin diagonal while $W_0 = i\sigma_2 \mathrm{diag}(W_\uparrow, W_\downarrow)$. The matrix $w^X_0 \equiv \mathrm{diag}(w^X_{0,\uparrow}, w^X_{0,\downarrow})$ has the elements

$$w^{\mathrm{X}}_{0,\sigma} \equiv \left(E^X_\sigma - \tilde{E}^X_{\underline{\sigma}} + 2\gamma^X_{0,\sigma}\tilde{\Delta}^X_{\underline{\sigma}}\right). \tag{3.19}$$

Using $\delta^X = \gamma^X(0) - \gamma^X_{\mathrm{bulk}}$ and the shorthand

$$D^{\mathrm{X}}_\sigma \equiv \delta^{\mathrm{X}}_\sigma \tilde{\Delta}^{\mathrm{X}}_{\underline{\sigma}} (w^{\mathrm{X}}_{0,\sigma})^{-1}, \tag{3.20}$$

the combination of Eqs. (3.6)–(3.9) can be written per spin component as

$$\gamma^{\mathrm{X}}_\sigma = \gamma^{\mathrm{X}}_{\mathrm{bulk},\sigma} + \frac{\delta^{\mathrm{X}}_\sigma}{(1 + D^{\mathrm{X}}_\sigma)\exp(-i w^{\mathrm{X}}_{0,\sigma}\rho) - D^{\mathrm{X}}_\sigma}. \tag{3.21}$$

For a x with spin structure as in Eq. (3.14), evaluating the integral in Eq. (3.12) then gives for the component σ the result

$$\begin{aligned} x_\sigma(\rho) = U^{\mathrm{R}}_\sigma(\rho) \Bigg[& x_\sigma(0) - \frac{1 - e^{-i\beta_{1,\sigma}\rho}}{\beta_{1,\sigma}} \left(1 + D^{\mathrm{R}}_\sigma\right) I^{\mathrm{K}}_{0,\sigma} \left(1 + \tilde{D}^A_{\underline{\sigma}}\right) \\ & - \frac{1 - e^{-i\beta_{2,\sigma}\rho}}{\beta_{2,\sigma}} \left(D^{\mathrm{R}}_\sigma I^{\mathrm{K}}_{0,\sigma} \tilde{D}^{\mathrm{A}}_{\underline{\sigma}} + D^{\mathrm{R}}_\sigma \left(\gamma^{\mathrm{R}}_{0,\sigma} \tilde{E}^{\mathrm{K}}_{\underline{\sigma}} + \Delta^{\mathrm{K}}_\sigma\right) \tilde{\delta}^{\mathrm{A}}_{\underline{\sigma}} + \delta^{\mathrm{R}}_\sigma \left(\tilde{E}^{\mathrm{K}}_{\underline{\sigma}} \tilde{\gamma}^{\mathrm{A}}_{0,\underline{\sigma}} + \tilde{\Delta}^{\mathrm{K}}_{\underline{\sigma}}\right) \tilde{D}^{\mathrm{A}}_{\underline{\sigma}} - \delta^{\mathrm{R}}_\sigma \tilde{E}^{\mathrm{K}}_{\underline{\sigma}} \tilde{\delta}^{\mathrm{A}}_{\underline{\sigma}} \right) \\ & + \frac{1 - e^{-i\beta_{3,\sigma}\rho}}{\beta_{3,\sigma}} \left(1 + D^{\mathrm{R}}_\sigma\right) \left(\gamma^{\mathrm{R}}_{0,\sigma} \tilde{E}^{\mathrm{K}}_{\underline{\sigma}} \tilde{\delta}^{\mathrm{A}}_{\underline{\sigma}} + \Delta^{\mathrm{K}}_\sigma \tilde{\delta}^{\mathrm{A}}_{\underline{\sigma}} + I^{\mathrm{K}}_{0,\sigma} \tilde{D}^{\mathrm{A}}_{\underline{\sigma}} \right) \\ & + \frac{1 - e^{-i\beta_{4,\sigma}\rho}}{\beta_{4,\sigma}} \left(\delta^{\mathrm{R}}_\sigma \tilde{E}^{\mathrm{K}}_{\underline{\sigma}} \tilde{\gamma}^{\mathrm{A}}_{0,\underline{\sigma}} + \delta^{\mathrm{R}}_\sigma \tilde{\Delta}^{\mathrm{K}}_{\underline{\sigma}} + D^{\mathrm{R}}_\sigma I^{\mathrm{K}}_{0,\sigma} \right) \left(1 + \tilde{D}^{\mathrm{A}}_{\underline{\sigma}}\right) \Bigg] \tilde{V}^{\mathrm{A}}_\sigma(\rho), \end{aligned} \tag{3.22}$$

where D^{X}_{σ} is defined in Eq. (3.20) and the $\beta_{i,\sigma}$ are given by

$$\beta_{1,\sigma} \equiv E^{\mathrm{R}}_{\sigma} - E^{\mathrm{A}}_{\sigma} + \gamma^{\mathrm{R}}_{\sigma}\tilde{\Delta}^{\mathrm{R}}_{\underline{\sigma}} + \tilde{\gamma}^{\mathrm{A}}_{\underline{\sigma}}\Delta^{\mathrm{A}}_{\sigma} = 2i\ \mathrm{Im}\left(E^{\mathrm{R}} + \gamma^{\mathrm{R}}_{\sigma}\tilde{\Delta}^{\mathrm{R}}_{\underline{\sigma}}\right), \tag{3.23}$$

$$\beta_{2,\sigma} \equiv \tilde{E}^{\mathrm{R}}_{\underline{\sigma}} - \tilde{E}^{\mathrm{A}}_{\underline{\sigma}} - \gamma^{\mathrm{R}}_{\sigma}\tilde{\Delta}^{\mathrm{R}}_{\underline{\sigma}} - \tilde{\gamma}^{\mathrm{A}}_{\underline{\sigma}}\Delta^{\mathrm{A}}_{\sigma} = 2i\ \mathrm{Im}\left(\tilde{E}^{\mathrm{R}}_{\underline{\sigma}} - \gamma^{\mathrm{R}}_{\sigma}\tilde{\Delta}^{\mathrm{R}}_{\underline{\sigma}}\right), \tag{3.24}$$

$$\beta_{3,\sigma} \equiv E^{\mathrm{R}}_{\sigma} - \tilde{E}^{\mathrm{A}}_{\underline{\sigma}} + \gamma^{\mathrm{R}}_{\sigma}\tilde{\Delta}^{\mathrm{R}}_{\underline{\sigma}} - \tilde{\gamma}^{\mathrm{A}}_{\underline{\sigma}}\Delta^{\mathrm{A}}_{\sigma} = E^{\mathrm{R}}_{\sigma} - \tilde{E}^{\mathrm{A}}_{\underline{\sigma}} + 2\ \mathrm{Re}\left(\gamma^{\mathrm{R}}_{\sigma}\tilde{\Delta}^{\mathrm{R}}_{\underline{\sigma}}\right), \tag{3.25}$$

$$\beta_{4,\sigma} \equiv \tilde{E}^{\mathrm{R}}_{\underline{\sigma}} - E^{\mathrm{A}}_{\sigma} - \gamma^{\mathrm{R}}_{\sigma}\tilde{\Delta}^{\mathrm{R}}_{\underline{\sigma}} + \tilde{\gamma}^{\mathrm{A}}_{\underline{\sigma}}\Delta^{\mathrm{A}}_{\sigma} = -\beta^{*}_{3,\sigma}. \tag{3.26}$$

Additionally, we use Eq. (3.11) to define

$$I^{\mathrm{K}}_{0,\sigma} \equiv -\gamma^{\mathrm{R}}_{0,\sigma}\tilde{E}^{\mathrm{K}}_{\underline{\sigma}}\tilde{\gamma}^{\mathrm{A}}_{0,\underline{\sigma}} - \Delta^{\mathrm{K}}_{\sigma}\tilde{\gamma}^{\mathrm{A}}_{0,\underline{\sigma}} - \gamma^{\mathrm{R}}_{0,\sigma}\tilde{\Delta}^{\mathrm{K}}_{\underline{\sigma}} + E^{\mathrm{K}}_{\sigma} \tag{3.27}$$

Lastly, we note that when solving for the anomalous function x^{a} as the replacements given in Eqs. (2.58)–(2.64) have to be made in the formula provided above.

3.3 2D: Finite Element Method

A Finite Element Method, or FEM, is a general strategy for the numerical solution of partial differential equations. Such methods are particular useful in spatial dimensions larger than one. As the name suggest the core idea is to split the domain where a solution is wanted into finite-sized elements. The original differential equation is translated into an integral equation for each element. These integral equations can be translated into algebraic equations using so-called *Galerkin methods* which provide an approximate solution of the differential equation. The strength of the method is then that the original differential equation has been translated into a linear-algebra problem that is often easy and fast to solve. This chapter consists of two parts. Firstly, we give a brief introduction to the key concepts of finite element methods, and we refer to one of the many textbooks on FEMs[60] for a more detailed introduction. Secondly, we outline a FEM for Eilenberger quasiclassical theory.

3.3.1 Key concepts in short examples

We start with a simple example to illustrate the key concepts of FEMs. We consider a diffusion-type equation in one dimension,

$$f''(x) = -2 \qquad \text{with boundary conditions } f(0) = 0, f'(0) = 2, \tag{3.28}$$

for $x \in [0, 2]$. In this case the equation can be readily solved analytically, and we find

$$f(x) = -x^2 + 2x = -(x-1)^2 + 1. \tag{3.29}$$

We can multiply this with a, for now unspecified, test function $\phi(x)$ and integrate over the domain to obtain

$$\int_0^2 f''(x)\phi(x)\mathrm{d}x = -2\int_0^2 \phi(x)\mathrm{d}x. \tag{3.30}$$

Integration by parts then gives

$$f'(2)\phi(2) - f'(0)\phi(0) - \int_0^2 f'(x)\phi'(x)\mathrm{d}x = -2\int_0^2 \phi(x)\mathrm{d}x. \tag{3.31}$$

This is the so-called *weak form* of the differential equation. A solution f_w is accordingly called a *weak solution* since it does not have to satisfy Eq. (3.28) in every point x but only the integral equation Eq (3.31). An exact solution f to the original differential equation is clearly always a weak solution as well. Theoretically a weak solution can always be found in the space of infinite-order polynomials by constructing a polynomial that agrees with a given solution $f(x)$ point-wise, for example by polynomial interpolation.

In practice we might not have a solution to the original differential equation at hand, so we need a solution strategy for the weak form. Unfortunately no general solution strategy for integral equations such as the weak form exists. However, strategies to obtain approximate solutions f_h exist in the form of *Galerkin methods*. We will discuss here the simpler case of a continuous Galerkin (CG) method. First, we chose $N+1$ node points such that $x_0 = 0, x_1, x_2, \ldots, x_N, x_{N+1} = 2$. This gives a natural splitting of our domain into $N+1$ segments of length $h_{j+1} = x_{j+1} - x_j$, the finite elements in our one-dimensional example. The Galerkin method then assumes that the approximate solution can be written as sum of piecewise-continuous polynomials up to a finite order k,

$$f_w(x) \approx \sum_{i=1}^{N} c_i\ \phi_i(x). \tag{3.32}$$

It is advantageous to choose functions that satisfy

$$\phi_i(x_j) = \begin{cases} 1 & \text{if } i = j \\ 0 & \text{if } i \neq j \end{cases}. \tag{3.33}$$

One common choice of basis functions with this property are Lagrange polynomials. For the simplest case of $k = 1$, they read

$$\phi_i(x) = \begin{cases} (x - x_{j-1})/h_j & \text{if } x_{j-1} < x < x_j \\ (x_{j+1} - x)/(h_{j+1}) & \text{if } x_j < x < x_{j+1} \\ 0 & \text{otherwise} \end{cases}. \tag{3.34}$$

An example for $N = 4$ nodes with $\Delta h = \text{const.}$ is shown in Fig. 3.2. Each function

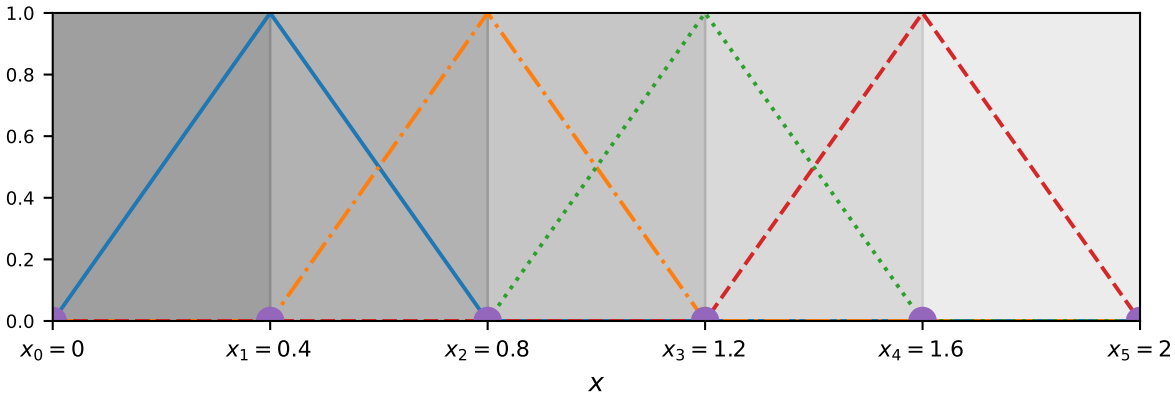

Figure 3.2: *The four basis functions ϕ_i for $N = 4$ in the domain $x \in [0, 2]$. Here we have five elements $\Omega_i = (x_{i-1}, x_i)$, coloured in different shades of grey.*

$\phi_i(x)$ is only non-zero in the two segments connected to x_i, and all of them vanish on the boundary ($x = 0$ and $x = 2$), so the two boundary terms in Eq. (3.31) vanish. Inserting Eq. (3.32) into Eq. (3.31), and choosing $\phi(x) = \phi_i(x)$ gives an equation

$$\sum_{j=1}^{N} \int_0^2 c_j \phi_j'(x)\phi_i'(x)\mathrm{d}x = \int_0^2 2\phi_i(x)\mathrm{d}x \ . \tag{3.35}$$

The first term is only non-zero if $\phi_i(x)$ and $\phi_j(x)$ are both non-zero in the same segment, hence each choice of $\phi_i(x)$ gives only contributions for some of the coefficients c_j. Varying the different $\phi_i(x)$ gives then a set of equations that can be written in matrix form

$$A\mathbf{c} = \mathbf{b},$$

where the elements of A and $\mathbf{b}$ are determined by

$$A_{ij} = \int_0^2 \phi_i'(x)\phi_j'(x)\mathrm{d}x, \qquad b_i = \int_0^2 2\phi_i(x)\ \mathrm{d}x. \tag{3.36}$$

In our example with $N = 4$ and $h_i = h = \text{const.}$ we get the equation system

$$\begin{pmatrix} 2 & -1 & 0 & 0 \\ -1 & 2 & -1 & 0 \\ 0 & -1 & 2 & -1 \\ 0 & 0 & -1 & 2 \end{pmatrix} \begin{pmatrix} c_1 \\ c_2 \\ c_3 \\ c_4 \end{pmatrix} = 2h^2 \begin{pmatrix} 1 \\ 1 \\ 1 \\ 1 \end{pmatrix}.$$

The equation system has a unique solution since A is invertible. We note further A is *banded*, meaning $A_{ij} = 0$ if $|i-j| > p$ for a certain p, and hence *sparse*. Finite-element matrices are often sparse which is advantageous for a numerical solution

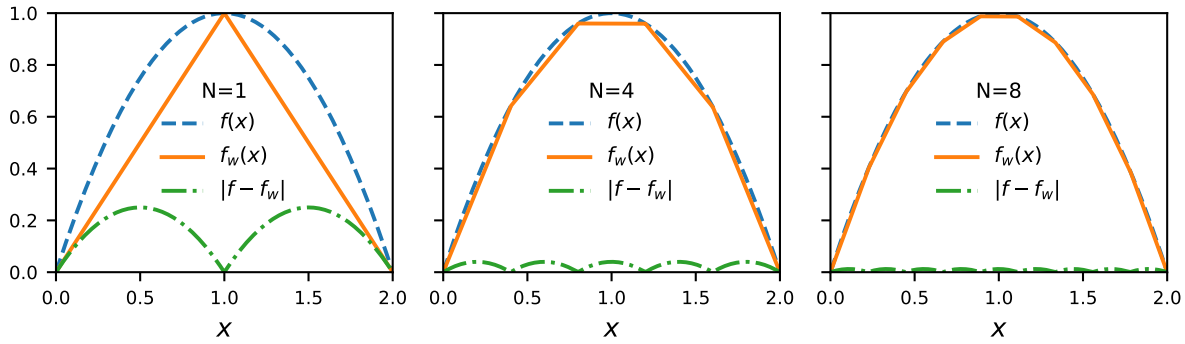

Figure 3.3: *Comparison of the analytic solution $f(x)$ (dashed blue) to the approximate solution $f_w(x)$ (solid orange) and the difference between the two functions $|f - f_w|(x)$ (dotted green) for different values of N.*

of the equation systems. Explicitly, one finds $c_1 = c_4 = 16/25, c_2 = c_3 = 24/25$, the resulting solution is shown in the central panel of Fig. 3.3. Comparison to the other panels in the same figure shows that the difference between the approximate solution $f_w(x)$ and the true solution $f(x)$ gets smaller with increasing number of nodes N. Note that the weak solution agrees with the analytic solution exactly at the nodes x_i. Intuitively, we expect that as $N \to \infty$, the weak solution will (for "well-behaved" problems) converge to the analytic solution of the differential equation. It is possible to use higher-order polynomials as the basis functions. This typically leads to better convergence of f_w to the solution f of the original differential equation but comes at a higher numerical cost through additional nodes and larger equation systems. Looking at this one-dimensional case it might seem like we have not gained much compared to using a finite difference method that can also be translated into a matrix equation. The strength of a FEM is, however, that the translation of the underlying differential equation into a weak form can be done independently of the dimension. The translation into a matrix equation via a Galerkin method then follows a standard recipe that is independent of the specific equation.

3.3.2 Discontinuous Galerkin method for Eilenberger quasiclassical theory

As discussed in Sect. 2.3, the equations of motion of the parametrizing functions for the quasiclassical Green's function $\check{g}$ are *transport equations*. It is well known that for such equations a FEM with continuous basis functions, as the one used in the above example, can lead to unphysical solutions that require special treatment [60–62]. As a result, a *discontinuous* Galerkin (DG) method was developed, originally in the context of the neutron transport equation[63, 64]. The main difference is that the nodes, or degrees of freedom, of the approximating function are not shared between neighbouring cells but rather defined cell-wise, as indicated

in Fig. 3.4.

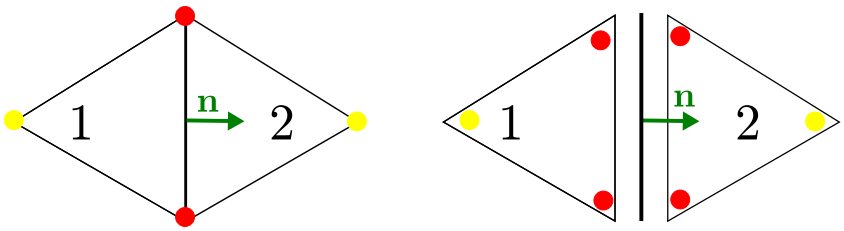

Figure 3.4: *Left: In a CG method the function is continuous across cell edges through the shared red nodes. Right: In a DG method, the function nodes are not shared and the function can be discontinuous across the cell edge. The displacement of the two cells is purely illustrative.*

The functions can be discontinuous between cells since jumps at element edges are allowed, which gives the method its name. This means that the weak solution is not globally continuous, in contrast to a CG method. Technically the solutions obtained in the stepping method, discussed in Sec. 3.2, are also only piecewise and not globally continuous. Additionally, transport equations get mapped into weak forms that penalize large discontinuities across element edges[62].

Figure 3.5:
Triangulation of a domain Ω (light grey) into triangles T_j, with the inflow and outflow boundaries $\partial\Omega_-$ (red) and $\partial\Omega_+$ (green) for one direction of $\mathbf{v}_\mathrm{F}$, and the collection of internal edges τ (orange).

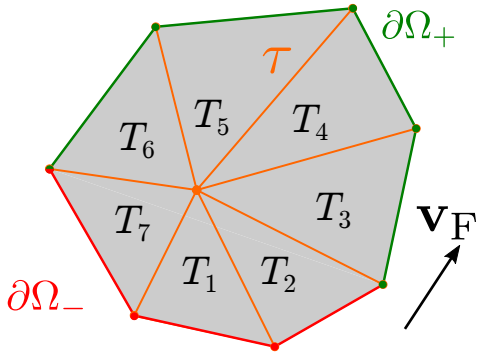

In two dimensions, the equivalent of splitting the domain into different segments in Sect. 3.3.1 is a triangulation $\mathcal{T}$ of the domain Ω into triangles. For transport equations, the domain boundary $\partial\Omega$ is further split into the so-called inflow boundary ($\partial\Omega_-$) and outflow boundary ($\partial\Omega_+$),

$$\partial\Omega_- \equiv \{\mathbf{R} \in \partial\Omega \mid \mathbf{v}_\mathrm{F} \cdot \mathbf{n}(\mathbf{R}) < 0\}\,, \quad \partial\Omega_+ \equiv \{\mathbf{R} \in \partial\Omega \mid \mathbf{v}_\mathrm{F} \cdot \mathbf{n}(\mathbf{R}) \geq 0\}\,, \tag{3.37}$$

which depends on the transport direction $\mathbf{v}_\mathrm{F}$. Each edge of a triangle is then either part of the inflow boundary, outflow boundary, or it is an internal edge. The collection of all internal edges is labelled as τ. The concepts are visualized in Fig. 3.5.

3.3.3 Coherence function

For ease of notation we will restrict ourselves to the spin-degenerate case here, and comment on the generalization to several spin components in Sec. 3.3.6. In this case Eq. (2.32) can be rewritten as a scalar equation for scalar retarded function γ^R

$$i\hbar \mathbf{v}_\mathrm{F} \cdot \nabla \gamma^\mathrm{R} + 2\varepsilon\gamma^\mathrm{R} + \gamma^\mathrm{R}\tilde{\Delta}^\mathrm{R}\gamma^\mathrm{R} - \Sigma^\mathrm{R}\gamma^\mathrm{R} + \gamma^\mathrm{R}\tilde{\Sigma}^\mathrm{R} = -\Delta^\mathrm{R}. \tag{3.38}$$

Note that the only difference to the general case is the change of sign in the quadratic term.

To obtain the weak form, we multiply Eq. (3.38) with a test function ϕ and integrate over our domain to find

$$i\hbar \int_\Omega \phi \ \mathbf{v}_\mathrm{F} \cdot \nabla\gamma \ \mathrm{d}\Omega + \int_\Omega \phi \left(2\varepsilon\gamma + \gamma\tilde{\Delta}\gamma - \Sigma\gamma + \gamma\tilde{\Sigma}\right) \mathrm{d}\Omega = -\int_\Omega \phi\Delta \ \mathrm{d}\Omega. \tag{3.39}$$

Only the first term on the left-hand side needs further rearrangements while the other terms can be treated analogously to our example in Sect. 3.3.1. To proceed, the integration over Ω is split up into a sum of integrals over each triangle T_j in the triangulation $\mathcal{T}$. For each triangle, we then perform a partial integration over the first term on the left-hand side containing the directional derivative $\mathbf{v}_\mathrm{F} \cdot \nabla$. This results in

$$\begin{aligned}
&\sum_{T_j\in\mathcal{T}} i\hbar \int_{\partial\Omega_j} \phi \ (\gamma\mathbf{v}_\mathrm{F}) \cdot \mathbf{n}_j \ \mathrm{d}s_j - i\hbar \int_{T_j} \gamma\mathbf{v}_\mathrm{F} \cdot (\nabla\phi)\mathrm{d}\Omega_j \\
&+ \int_{T_j} \phi \left(2\varepsilon\gamma + \gamma\tilde{\Delta}\gamma - \Sigma\gamma + \gamma\tilde{\Sigma}\right) \mathrm{d}\Omega_j = -\sum_{T_j\in\mathcal{T}} \int_{T_j} \phi\Delta \ \mathrm{d}\Omega_j.
\end{aligned} \tag{3.40}$$

Here, the first term on the left-hand side is an integral over the boundary $\partial\Omega_j$ of a triangle T_j, consisting of three edges. The remaining terms are integrations of the entire area Ω_j. How exactly the boundary term gets treated depends if we solve for the retarded function γ^R, the advanced function γ^A, or the associated tilde functions $\tilde{\gamma}^{\mathrm{R,A}}$. In following, we assume that we want to find the retarded function γ^R.

Each internal edge $\tau_j \in \tau$ is shared by two cells and thus integrated over twice in the sum over all the boundary integrals. Following[65] summing this double integration over each edge allows to rewrite the first term on the left-hand side in Eq. (3.40) as

$$\begin{aligned}
&\sum_{T_j\in\mathcal{T}} \int_{\partial\Omega_j} \phi \ (\gamma\mathbf{v}_\mathrm{F}) \cdot \mathbf{n}_j \ \mathrm{d}s_j = \sum_{\tau_j} \int_{\tau_j} \{\gamma\mathbf{v}_\mathrm{F}\} \cdot [\phi] \ \mathrm{d}\tau_j \\
&+ \sum_{\partial\Omega_j\in\partial\Omega_+} \int_{s_j} (\mathbf{n}_j \cdot \mathbf{v}_\mathrm{F}) \ \gamma\phi \ \mathrm{d}s_j + \sum_{\partial\Omega_j\in\partial\Omega_-} \int_{s_j} (\mathbf{n}_j \cdot \mathbf{v}_\mathrm{F}) \ \gamma\phi \ \mathrm{d}s_j,
\end{aligned} \tag{3.41}$$

where the first summation on the right-hand side is over individual edges rather than closed boundaries of each triangle, the remaining two terms are either on the inflow or outflow boundary. For edges on the inflow boundary ($\partial\Omega_-$), we need to specify a boundary value $\gamma_{\mathrm{B}}^{\mathrm{R}}$. The function value is unknown on the outflow boundary ($\partial\Omega_+$) and determined in the solution step. Internal edges (τ_j) are integrated over twice in the sum over all triangles. Thus the difference of function values, in this case of ϕ, in the two cells sharing the edge enter the weak form. In Eq. (3.45), the jump operator $[\dots]$ is defined as

$$[\mathbf{a}] \equiv \mathbf{a}_1 \cdot \mathbf{n}_1 + \mathbf{a}_2 \cdot \mathbf{n}_2, \quad [\phi] \equiv \phi_1 \mathbf{n}_1 + \phi_2 \mathbf{n}_2, \tag{3.42}$$

where $\mathbf{n}_1$ and $\mathbf{n}_2$ are the outward-pointing normals to the edge between the two cells, and the index on $\mathbf{a}$ or ϕ refers to the function values in one of the two cells. As the name suggests, the jump operator is a measure for the difference of the respective function in two neighbouring cells. Following Ref. [66], we use the so-called upwind value $\{\dots\}_u$, given by

$$\left\{\gamma^R \mathbf{v}_{\mathrm{F}}\right\}_u \equiv \begin{cases} \gamma_1^R \mathbf{v}_{\mathrm{F}} & \text{if } \mathbf{v}_{\mathrm{F}} \cdot \mathbf{n}_1 > 0 \\ \gamma_2^R \mathbf{v}_{\mathrm{F}} & \text{if } \mathbf{v}_{\mathrm{F}} \cdot \mathbf{n}_1 < 0 \\ \left\{\gamma^R\right\} \mathbf{v}_{\mathrm{F}} & \text{if } \mathbf{v}_{\mathrm{F}} \cdot \mathbf{n}_1 = 0 \end{cases}, \tag{3.43}$$

where $\{\dots\}$ is the average operator,

$$\{\mathbf{a}\} \equiv \frac{1}{2}\left(\mathbf{a}_1 + \mathbf{a}_2\right), \quad \{\phi\} \equiv \frac{1}{2}\left(\phi_1 + \phi_2\right). \tag{3.44}$$

The upwind value propagates function values over cell edges from one cell into the other in along with the transport direction. In total, the derivative $\mathbf{v}_{\mathrm{F}} \cdot \nabla\gamma$ has thus been transformed into edge integrals that enforce flow of the "vector field" $\gamma\mathbf{v}_{\mathrm{F}}$ in the direction of the respective momentum from the inflow boundary to the outflow boundary. This enforced flow direction is the equivalent of the propagation along trajectories along $\mathbf{v}_{\mathrm{F}}$ in the stepping method. The tilde function $\tilde{\gamma}^R$, and the advanced function γ^{A}, propagate in the opposite direction of $\mathbf{v}_{\mathrm{F}}$. In the weak form, this translates into a swapping of the inflow and outflow boundaries, as well as a replacement of the upwind value in Eq. (3.43) with a corresponding downwind value, for these two functions. The final weak form becomes

$$\begin{aligned} & i\hbar \sum_{\tau_j} \int_{\tau_j} \left\{\gamma^{\mathrm{R}} \mathbf{v}_{\mathrm{F}}\right\}_u [\phi] \; \mathrm{d}\tau_j + i\hbar \sum_{\partial\Omega_j \in \partial\Omega_+} \int_{\partial\Omega_j} (\gamma^{\mathrm{R}} \mathbf{n}_j \cdot \mathbf{v}_{\mathrm{F}}) \phi \; \mathrm{d}s_j \\ & - i\hbar \sum_j \int_{T_j} (\gamma^{\mathrm{R}} \mathbf{v}_{\mathrm{F}}) \cdot \nabla\phi \; \mathrm{d}\Omega_j + \sum_j \int_{T_j} \left(2\varepsilon\gamma^{\mathrm{R}} + \gamma^{\mathrm{R}}\tilde{\Delta}\gamma^{\mathrm{R}} - \Sigma\gamma^{\mathrm{R}} + \gamma^{\mathrm{R}}\tilde{\Sigma}\right) \phi \; \mathrm{d}\Omega_j \\ & \quad \stackrel{!}{=} -\sum_j \int_{T_j} \Delta\phi \; \mathrm{d}\Omega - i\hbar \sum_{\partial\Omega_j \in \partial\Omega_-} \int_{\partial\Omega_j} (\mathbf{n}_j \cdot \mathbf{v}_{\mathrm{F}}) \phi \; \gamma_B^{\mathrm{R}} \; \mathrm{d}s_j. \end{aligned} \tag{3.45}$$

The weak form in Eq. (3.45) then gets translated into a matrix equation in a similar way as done in the example in Sec. 3.3.1. One complication that arises for the coherence function is the non-linear term $\gamma\tilde{\Delta}\gamma$ which results in a non-linear matrix equation. The system can thus not be solved by matrix inversion. Instead, we iteratively find an (approximate) zero to the so-called residual, defined via

$$R(\gamma, \phi) \equiv L(\gamma, \phi) - a(\phi). \tag{3.46}$$

In order to speed up this iterative solution we can use Newton iterations, this requires knowledge of the multi-dimensional Jacobian of the the weak form. As a weak form, it can be obtained via the Gateaux derivative

$$J(\delta\gamma, \gamma, \phi) \equiv \lim_{h\to 0} \frac{R(\gamma + h\ \delta\gamma, \phi) - R(\gamma, \phi)}{h}. \tag{3.47}$$

Explicitly, we find for the retarded function

$$\begin{aligned} &i\hbar \sum_{\tau_j} \int_{\tau_j} \left\{\delta\gamma^{\mathrm{R}}\mathbf{v}_{\mathrm{F}}\right\}_u [\phi]\ \mathrm{d}\tau_j - i\hbar \sum_j \int_{T_j} (\delta\gamma^{\mathrm{R}}\mathbf{v}_{\mathrm{F}}) \cdot \nabla\phi\ \mathrm{d}\Omega_j + i\hbar \sum_{\partial\Omega_j \in \partial\Omega_+} \int_{\partial\Omega_j} (\delta\gamma^{\mathrm{R}}\mathbf{n}_j \cdot \mathbf{v}_{\mathrm{F}})\phi\ \mathrm{d}s_j \\ &+ \sum_j \int_{T_j} \left(2\varepsilon\delta\gamma^{\mathrm{R}} + 2\delta\gamma^{\mathrm{R}}\tilde{\Delta}\gamma^{\mathrm{R}} - \Sigma^{\mathrm{R}}\delta\gamma^{\mathrm{R}} + \delta\gamma^{\mathrm{R}}\tilde{\Sigma}\right)\phi\ \mathrm{d}\Omega_j \end{aligned} \tag{3.48}$$

Notice that the resulting weak form is linear in the variation $\delta\gamma^{\mathrm{R}}$. The expression can be translated into a matrix along similar lines as the weak form. Starting from guess of γ^{R}, this can be used iterate γ^{R} by using Newton-Raphson iterations as outlined in Paper IV.

3.3.4 Distribution function

In the spin-degenerate case the differential equation for the distribution function x, Eq. (2.36), can be simplified to

$$\begin{aligned} i\hbar\mathbf{v}_{\mathrm{F}} \cdot \nabla x - \left(\Sigma - \gamma\tilde{\Delta}\right)^{\mathrm{R}} x + x\left(\Sigma + \Delta\tilde{\gamma}\right)^{\mathrm{A}} \\ = \gamma^{\mathrm{R}}\tilde{\Sigma}^{\mathrm{K}}\tilde{\gamma}^{\mathrm{A}} - \Delta^{\mathrm{K}}\tilde{\gamma}^{\mathrm{A}} - \gamma^{\mathrm{R}}\tilde{\Delta}^{\mathrm{K}} - \Sigma^{\mathrm{K}} \equiv I_s^{\mathrm{K}} \end{aligned} \tag{3.49}$$

Note that the right-hand side is independent of x and defines the I^{K} as given in Eq. (3.11). The reformulation as a weak form proceeds largely along the same lines as that of the coherence function γ^{R}. Again, we multiply by a test function ϕ, integrate over the domain, and split the integration into a sum of integrals over each triangle T_j. After a partial integration, the derivative term $\mathbf{v}_{\mathrm{F}} \cdot \nabla x$ gets transformed in edge integrals on the inflow boundary, the outflow boundary, or

an interior edge. The resulting weak form can then be written as

$$
\begin{aligned}
&i\hbar \sum_{\tau_j} \int_{\tau_j} \{x\mathbf{v}_\mathrm{F}\}_u [\phi] \; \mathrm{d}\tau_j + i\hbar \sum_{\partial\Omega_j \in \partial\Omega_+} \int_{\partial\Omega_j} (x\, \mathbf{n}_j \cdot \mathbf{v}_\mathrm{F})\phi \; \mathrm{d}s_j \\
&- i\hbar \sum_{j} \int_{T_j} (x\mathbf{v}_\mathrm{F}) \cdot \nabla\phi \; \mathrm{d}\Omega_j - \sum_{T_j \in \mathcal{T}} \int_{T_j} \left[\left(\Sigma - \gamma\tilde{\Delta}\right)^\mathrm{R} x - x \left(\Delta\tilde{\gamma} + \Sigma\right)^\mathrm{A} \right] \phi \; \mathrm{d}\Omega_j \\
&= \sum_{T_j \in \mathcal{T}} \int_{T_j} I_s^\mathrm{K} \phi \; \mathrm{d}\Omega_j - i\hbar \sum_{\partial\Omega_j \in \partial\Omega_-} \int_{\partial\Omega_j} (\mathbf{n}_j \cdot \mathbf{v}_\mathrm{F})\phi \; x_B \; \mathrm{d}s_j,
\end{aligned}
\tag{3.50}
$$

where I_s^K is defined in Eq. (3.49). The jump and average operators, as well as the upwind value, are defined analogously to those for the coherence function, see Eqs. (3.42)–(3.44). Just as for the coherence function, boundary values for x have to be provided on the inflow boundary $\partial\Omega_-$, while the upwind value propagates function values in the direction of the momentum orientation $\mathbf{v}_\mathrm{F}$ through cells toward to the outflow boundary. For the "tilde" distribution function $\tilde{x}$ the role of inflow and outflow boundaries are swapped and a downwind value has to be used in the first term on the left-hand side. This is again analogous to the case of $\tilde{\gamma}^\mathrm{R}$. The weak form in Eq. (3.50) is linear in x. As a result, the weak solution x_w can be found by matrix inversion and does not require an iterative solution procedure, in contrast to the coherence function γ. In that sense it is numerically easier to solve for the distribution function.

3.3.5 Boundary conditions and coupling to reservoirs

As outline in Sect. 3.3.2, boundary values $\gamma_\mathrm{B}^\mathrm{X}$ or x_B have to be specified on the (momentum-dependent) inflow boundary $\partial\Omega_-$. In two dimensions, the domain boundary $\partial\Omega$ is approximated as a collection of straight-line segments, each with a fixed normal $\mathbf{n}$. Each boundary is then treated using the boundary conditions outlined in Sec. 2.3.3. If the normal has an angle α_n to the $\hat{x}$ axis, then specular relates an incoming trajectory with momentum angle φ_F to the outgoing trajectory

$$
\varphi_\mathrm{F}' = \pi - \varphi_\mathrm{F} + 2\alpha_n. \tag{3.51}
$$

Each boundary segment is one edge of a cell, depending on the order of approximating polynomials there are N_edge nodes on the given edge. It is then enough to apply the boundary conditions at the nodes. To simulate an open boundary, we associate a virtual "reservoir" node to each edge node. In the case of a superconducting reservoir, the order parameter in this reservoir point is then update using an incoming bulk function and the outgoing function from the boundary condition. A normal-metal reservoir with a fixed chemical potential or temperature that is different from the simulated system need no such updating procedure. For further details, we refer to Paper IV.

3.3.6 Generalization to the spin-dependent problems

The above concepts can be straightforwardly generalized to the case of more than one spin component or other internal degrees of freedom such as multiple bands. As an example, we take the case of a general two-by-two spin structure of the coherence function $\gamma = (\gamma_0 + \vec{\gamma} \cdot \vec{\sigma})\, i\sigma_2$, where $\vec{\gamma} = (\gamma_x, \gamma_y, \gamma_z)^{\mathrm{T}}$ and $\sigma = (\sigma_x, \sigma_y, \sigma_z)^{\mathrm{T}}$. This can be rewritten in terms of four coupled scalar equations as

$$i\hbar \mathbf{v}_{\mathrm{F}} \cdot \nabla \begin{pmatrix} \gamma_0 \\ \gamma_x \\ \gamma_y \\ \gamma_z \end{pmatrix} = \begin{pmatrix} f_0 \\ f_x \\ f_y \\ f_z \end{pmatrix}, \tag{3.52}$$

where the different f_i will generally introduce a coupling between the equations. The derivation of a weak form for each component is now analogous to the one for a scalar function if the scalar test function $\phi(\mathbf{R})$ gets replace with a corresponding four-component vector of four independent test function $\vec{\phi}(\mathbf{R}) = (\phi_0, \phi_x, \phi_y, \phi_z)$, and the four functions are solved simultaneously.

4 Superconductors in equilibrium

This chapter gives an overview of the main *equilibrium* properties of superconductors. Especially important for our purposes is the different influence of impurities on s-wave and d-wave superconductors in equilibrium since this gives a degree of intuition on the expected non-equilibrium behaviour, as well as the surface properties of d-wave superconductors.

4.1 Influence of impurities

4.1.1 Impurity scattering in a s-wave superconductor

The s-wave order parameter is isotropic

$$\Delta(\varphi_\mathrm{F}) = \Delta_0, \tag{4.1}$$

meaning the magnitude and sign of the order parameter are independent of the position on the Fermi surface. For a homogeneous bulk system, in equilibrium and in the absence of superflow, all possible momentum orientations are then equivalent which implies

$$\hat{g}^{\mathrm{R,A,K}} = \left\langle \hat{g}^{\mathrm{R,A,K}} \right\rangle_{\mathrm{FS}}. \tag{4.2}$$

We thus find

$$\left\langle \hat{g}^{\mathrm{R,A}} \right\rangle_{\mathrm{FS}}^2 = (\hat{g}^{\mathrm{R,A}})^2 = -\pi^2, \tag{4.3}$$

$$\left\langle \hat{g}^{\mathrm{R}} \right\rangle_{\mathrm{FS}} \left\langle \hat{g}^{\mathrm{K}} \right\rangle_{\mathrm{FS}} \left\langle \hat{g}^{\mathrm{A}} \right\rangle_{\mathrm{FS}} = \hat{g}^{\mathrm{R}}\hat{g}^{\mathrm{K}}\hat{g}^{\mathrm{A}} = -\hat{g}^{\mathrm{K}}\hat{g}^{\mathrm{A}}\hat{g}^{\mathrm{A}} = \pi^2\hat{g}^{\mathrm{K}} \tag{4.4}$$

where we used the normalization condition of $\check{g}$, Eq. (2.25). As a consequence, Eq. (2.90) and Eq. (2.91) simplify to

$$\hat{h}_\mathrm{s}^{\mathrm{R,A}} = \Gamma_\mathrm{u}\left(\cos\delta\sin\delta\hat{1} + \frac{\sin^2\delta_0}{\pi}\hat{g}^{\mathrm{R,A}}\right), \tag{4.5}$$

The first term is an energy-independent constant that can be absorbed into the chemical potential, the second term is proportional to $\hat{g}^{\mathrm{R,A}}$ itself. For the Keldysh component we then obtain

$$\hat{h}_\mathrm{s}^{\mathrm{K}} = \frac{\Gamma_u}{\pi}\sin^2\delta_0\ \hat{g}^{\mathrm{K}} = \frac{\Gamma}{\pi}\hat{g}^{\mathrm{K}}. \tag{4.6}$$

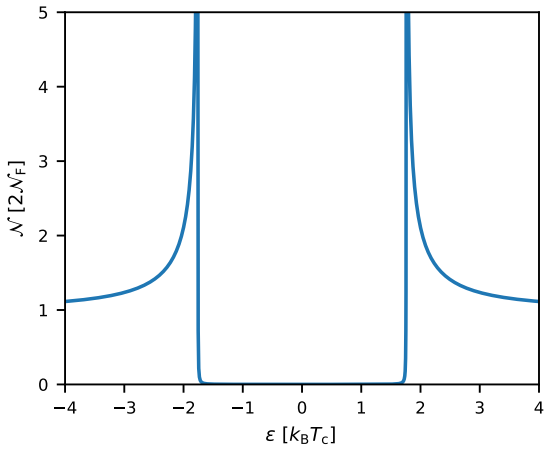

(a) *Density of states $\mathcal{N}(\varepsilon)$ for a homogeneous s-wave superconductor in the absence of current flow for $\eta = 1e-3$.*

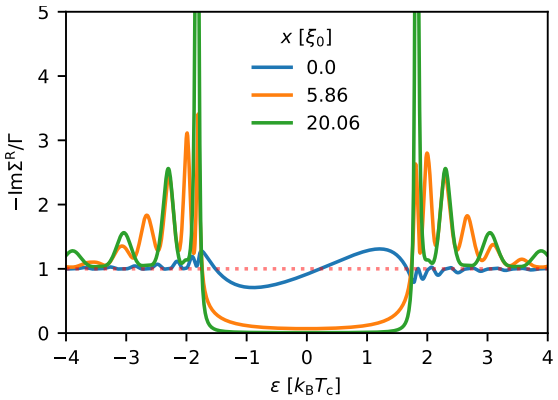

(b) *Induced electron-hole asymmetry in* Im Σ^{R} *for intermediate phase shifts close to a surface. Here are $D = 1$, $\delta_0 = (\pi/10)$, $\ell = 10\xi_0$. The normal-state value is shown as a red, dotted line.*

Figure 4.1: *Bulk density of states and effects of impurities close to interfaces in an s-wave SC, in both cases $T = 0.1T_{\mathrm{c}}$.*

For scalar impurities, the self-energy matrix $\check{h}_{\mathrm{s}}$ is thus either proportional to the Nambu-space unit matrix or the respective element of $\check{g}$. Then, $\check{h}_{\mathrm{s}}$ and $\check{g}$ commute and the respective term drops out of the steady-state Eilenberger equation, Eq. (2.22). In equilibrium the bulk Green's function $\check{g}$ is thus unaltered by scalar impurities, as is any quantity derived from it. This is the case for the mean-field order parameter Δ_0, the critical temperature T_{c}, and even the density of states $\mathcal{N}(\varepsilon)$. The latter is shown in Fig. 4.1a. That s-wave pairing is, for a spatially homogeneous system, not affected by elastic scattering on non-magnetic impurities is the content of Anderson's theorem[68]. The latter, however, assumes time-reversal invariance and will thus not hold in the presence of current flow. The transport behaviour of an s-wave superconductor, especially in non-equilibrium, is thus affected by scalar impurities. Eq. (4.2) and the arguments outlined above for the bulk do not hold for spatially inhomogeneous systems either. As an example, scattering with an intermediate phase shift $\delta_0 \in (0, \pi/2)$ induces an electron-hole asymmetry in Σ^{R} in the vicinity of the surface between a normal-metal and a superconductor, seen in Fig. 4.1b. The oscillations visible for energies larger than Δ are so-called Tomasch oscillations[69, 70], that appear around spatial inhomogeneities in the order parameter. We will return to the asymmetry in the impurity self-energy in Sec. 5.3.2.

4.1.2 Impurity scattering in a d-wave superconductor

For a d-wave SC the order parameter can be written as

$$\Delta(\varphi_\mathrm{F}) = \Delta_0 \sqrt{2} \cos 2\left(\varphi_\mathrm{F} - \alpha\right), \tag{4.7}$$

where α is the misalignment angle between the crystal a axis and a grain boundary. There are two main differences to the uniform s-wave case. Firstly, the order parameter magnitude changes over the Fermi surface and includes four nodes where the order parameter is zero. Secondly, if we are not at a node, changing the momentum angle by 90° means that Δ changes sign, corresponding to a phase shift of π. This leads to new physics in d-wave SCs, both in the bulk and at surfaces.

The bulk, momentum-resolved density of states $\mathcal{N}_\mathrm{F}(\varepsilon, \varphi_\mathrm{F})$ is shown for $\varphi_\mathrm{F} \in (0, \pi/4)$ in Fig. 4.2a, and the Fermi-surface average $\mathcal{N}_\mathrm{F}$ in Fig. 4.2b.

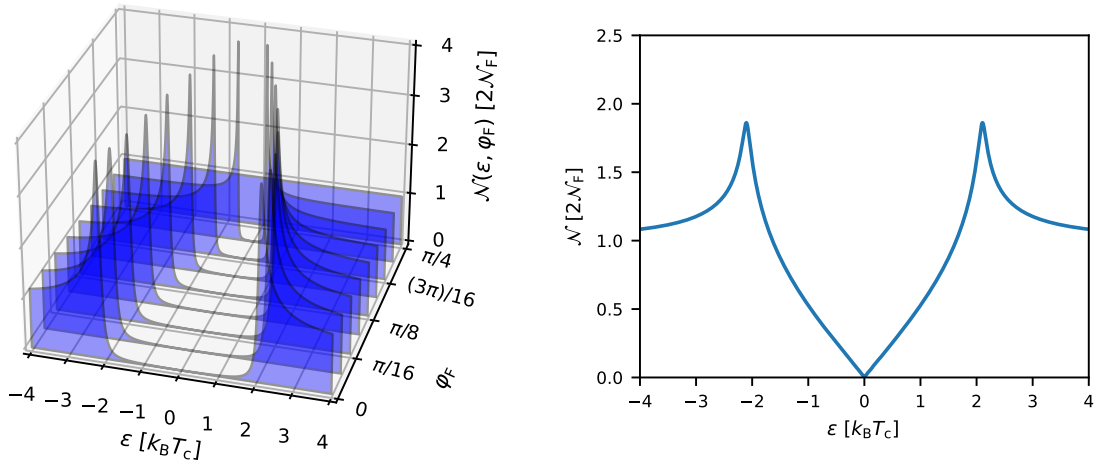

(a) *Momentum-resolved* $\mathcal{N}_\mathrm{F}(\varepsilon, \varphi_\mathrm{F})$.

(b) *Fermi-surface averaged* $\mathcal{N}_\mathrm{F}(\varepsilon)$.

Figure 4.2: *Density of states for the bulk of a clean d-wave superconductor.*

For a given orientation of φ_F, $\mathcal{N}_\mathrm{F}(\varepsilon, \varphi_\mathrm{F})$ is similar to an s-wave spectrum with a varying width of the energy gap Δ. The FS average then is profoundly different from the s-wave case. Around zero energy it is a roughly linear function of energy, indicating the presence of low-lying excitations, in contrast to the fully gapped s-wave spectrum.

The arguments presented in Sec. 4.1.1 do not hold for the d-wave case. Since the order parameter varies with momentum orientation and impurity scattering mixes different momenta, a d-wave superconductor is not insensitive to scalar impurities. Scattering on scalar impurities is said to be pair-breaking[71], and the the pair-breaking parameter Γ suppresses the bulk order parameter Δ_0, shown in Fig. 4.3, as well as the critical temperature T_c[67]. There is a critical $\Gamma_\mathrm{c} \approx 0.28\pi k_\mathrm{B} T_{\mathrm{c}0}$ where the order parameter vanishes. By Eqs. (2.20) and (2.89), this corresponds

to a minimum mean free path $\ell_c \approx 3.57\xi_0$ below which a d-wave order parameter is fully suppressed. Importantly, ℓ_c is always larger than the superconducting coherence length ξ_0.

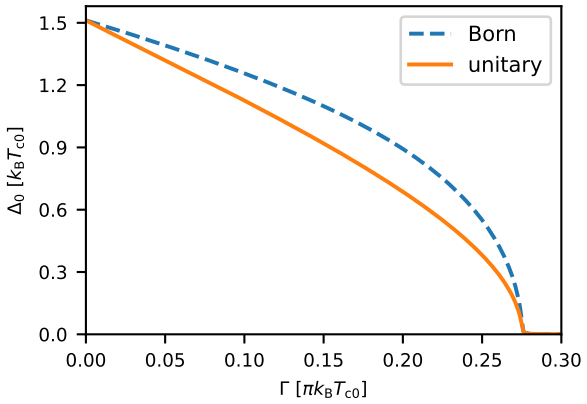

Figure 4.3: *Dependence of the bulk d-wave order parameter on impurity concentration for the Born and unitary limits, here for* $T = 0.1T_{c0}$.

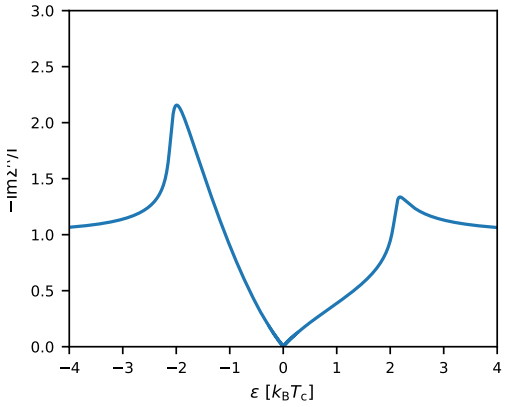

(a) *The imaginary part* Σ^R *for a scattering phase shift* $\delta_0 = \pi/10$. *It is not electron-hole symmetric since* $\mathrm{Im}\ \Sigma^R(\varepsilon) \neq \mathrm{Im}\ \Sigma^R(-\varepsilon)$.

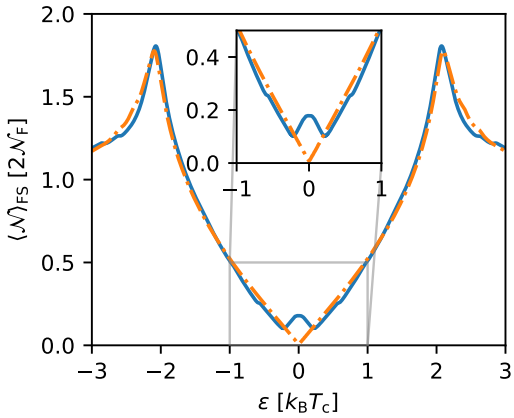

(b) *Creation of an impurity band in the DOS for unitary-limit scattering (blue solid line) compared to the Born limit (dashed orange line), both for* $\ell = 100\xi_0$ *at* $T = 0.1T_c$.

Figure 4.4: *Effects of impurity scattering on the bulk properties of a d-wave SC.*

For a phase shift δ_0 in between the Born and unitary limits, meaning $\delta_0 \in (0, \pi/2)$, the diagonal elements Σ^R and $\tilde{\Sigma}^R$ of $\hat{h}^R$ in Eq. (2.90), are not electron-hole symmetric. An example of this asymmetry for one value of δ_0 can be seen in Fig. 4.4a. This electron-hole asymmetry has been argued to lead to a large thermoelectric effect even in the bulk of a d-wave superconductor[72]. Additionally, such scattering for intermediate phase shifts leads to the creation of an impurity band in the density of states that appears at finite energy and moves toward $\varepsilon = 0$ in the unitary limit [73], shown in Fig. 4.4b.

4.2 Surface physics in a d-wave superconductor

In addition to the differences in the bulk properties, new physics can appear in d-wave superconductors at surfaces with a normal $\hat{n}$ that is misaligned with the crystal axis, seen in Fig. 4.5.

For a finite misalignment angle α the d-wave order parameter "rotates" in momentum-space. If α is an odd multiple of $\pi/4$ the nodes are parallel to the k_x and k_y axes. The bulk properties of a d-wave SC, discussed above, are not affected by this.

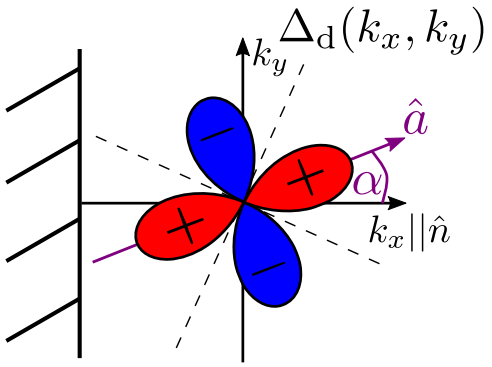

Figure 4.5: *The angle α measures the misalignment of the crystal $\hat{a}$ axis and the normal of a crystal surface.*

Specular scattering at surfaces, however, connects different momenta on the Fermi surface and hence different values of Δ.

At an interface that is parallel to the k_y-direction in Fig. 4.5, the momentum shifts as $\varphi_{\mathrm{F}} \to \pi - \varphi_{\mathrm{F}}$, see Sec. 2.3.3. For incoming trajectories that satisfy

$$\frac{\pi}{4} - \alpha < \varphi_{\mathrm{F}} < \frac{\pi}{4} + \alpha, \tag{4.8}$$

this means that the order parameter changes sign, or acquires a phase shift of π, between the incoming and outgoing trajectory[74]. At $\alpha = \pi/4$, this is then the case for all incoming trajectories. The sign change $\Delta \to -\Delta$ upon reflection results in a bound state at zero energy, the so-called midgap state[75]. The name reflects the fact that it is located at the Fermi energy, and thus in the middle of the energy gap for each momentum orientation.

To see this within quasiclassical theory, let us assume an interface with finite transparency D and neglect the suppression of the (real) order parameter in a clean system with spin degeneracy. For any angle $\varphi_{\mathrm{F}} \neq 0$, the incoming bulk coherence functions $\gamma(\varphi_{\mathrm{F}})$ and $\tilde{\gamma}(\pi - \varphi_{\mathrm{F}})$ on the outgoing trajectory read

$$\gamma_{\mathrm{in}}^{R}(\varphi_{\mathrm{F}}) \equiv \frac{\Delta}{\varepsilon + i\Omega}, \qquad \tilde{\gamma}^{R}(\pi - \varphi_{\mathrm{F}}) \equiv \frac{\Delta}{\varepsilon + i\Omega}, \tag{4.9}$$

where $\Omega = \sqrt{\Delta^2(\varphi_{\mathrm{F}}) - (\varepsilon + i\eta)^2}$, and we assumed that the incoming trajectory has a negative sign of Δ. In the following, we will not write out the angle φ_{F} explicitly. Note that ε implicitly contains a small imaginary part for the retarded function. Through the boundary conditions, we find the outgoing function at the

interface, and can then use Eq. (3.9) to obtain the spatial dependence

$$\Gamma^R(x) = -\gamma_{\text{in}}^R \frac{\varepsilon(R+1) + i\Omega D - e^{-x'}(R+1)(\varepsilon + i\Omega)}{\varepsilon(R+1) + i\Omega D - e^{-x'}(R+1)(\varepsilon - i\Omega)}, \tag{4.10}$$

where $x' = 2\Omega x/(\hbar v_{\text{F}} \cos\varphi_{\text{F}})$. We then find the retarded Green's function

$$g^{\text{R}} = \frac{-i\pi}{2} \frac{1 - \Gamma^{\text{R}}\tilde{\gamma}^{\text{R}}}{1 + \Gamma^{\text{R}}\tilde{\gamma}^{\text{R}}} \tag{4.11}$$

$$= \frac{-i\pi}{2} \left[\frac{\varepsilon}{\Omega} \left(1 - e^{-x'} \frac{(R+1)\varepsilon}{\varepsilon(R+1) + iD\Omega} \right) - e^{-x'} \frac{(R+1)\Omega}{\varepsilon(R+1) + i\Omega D} \right]. \tag{4.12}$$

From this, we can obtain the momentum-resolved density of states per spin via Eq. (2.96). For subgap energies we find the midgap state,

$$\mathcal{N}_\sigma(|\varepsilon| < |\Delta(\varphi_{\text{F}})|, \varphi_F, x) = \frac{\pi\Delta(R+1)}{2\sqrt{R}} \frac{1}{\pi} \frac{\Gamma}{\varepsilon^2 + \Gamma^2} e^{-2x'}, \tag{4.13}$$

where $x' = x/(\cos\varphi_{\text{F}}\xi_{\text{Andreev}})$. This is a Lorentzian around zero energy with a width given by

$$\Gamma = \frac{D\Delta}{2\sqrt{R}}. \tag{4.14}$$

Interface transparency thus broadens the bound states. The midgap state decays away from the surface on the length scale of Andreev reflection, $\xi_{\text{Andreev}} = \hbar v_{\text{F}}/\sqrt{\Delta^2 - \varepsilon^2}$. In the limit $D \to 0$ ($R \to 1$), the Lorentzian narrows to a δ-distribution, integration then gives the spectral weight $\pi\Delta$ of the bound state.

The bound state will be additionally broadened by impurities. Noting that the off-diagonal impurity renormalization vanishes for a d-wave order parameter since $\left\langle f^{\text{R}} \right\rangle_{\text{FS}} \propto \langle \Delta(\varphi_{\text{F}}) \rangle_{\text{FS}} = 0$, one finds by insertion into Eqs. (2.92)–(2.93) that

$$\Sigma_{\text{Born}}(\varepsilon) = \frac{\Gamma_s}{\pi} \left\langle g^{\text{R}}(\varepsilon) \right\rangle_{\text{FS}}, \Sigma_{\text{unitary}} = \pi\Gamma_s \frac{1}{\langle g^{\text{R}}(\varepsilon) \rangle_{\text{FS}}}. \tag{4.15}$$

Here Γ_{s} is the scattering energy due to scalar impurities. By Eq. (2.97), the imaginary part of Σ is thus proportional to the density of states. Since the bound state is peaked around $\varepsilon = 0$, we thus expect a large broadening of the bound state in the Born limit and less broadening in the unitary limit. A detailed analysis shows that the impurity broadening is Im $\Sigma_{\text{Born}} \propto \Gamma_{\text{s}}$ and Im $\Sigma_{\text{uni}} \propto \sqrt{\Gamma_s}$[76], while the broadening in the bulk is larger in the unitary limit .

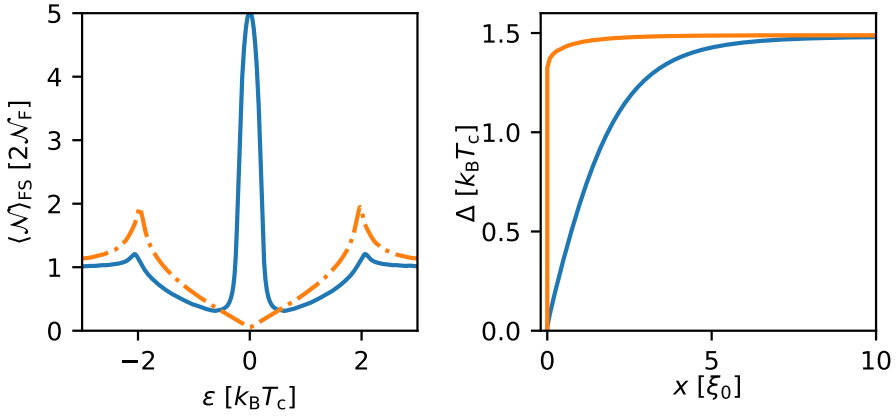

Figure 4.6:
Left: Comparison of the density of states $\mathcal{N}_F(\varepsilon)$ at an interface with a tunnel cone according to Eq. (2.75) with $D_0 = 0.2$ and $\beta = 1$. Right: Suppression of the order parameter close to the surface. In both cases, $\alpha = 0$ (orange) and $\alpha = \pi/4$(blue). Results for the Born limit with $\ell = 100\xi_0$ at $T = 0.1T_c$.

One example for the resulting difference in the density of states between $\alpha = 0$ and $\alpha = \pi/4$ is shown in the left panel of Fig. 4.6. The presence of such ABS leads to strong suppression of the order parameter near the surface, shown in the right panel of the same figure. These midgap states are a fingerprint of d-wave superconductors. They do not occur at boundaries of s-wave superconductors to normal metals or the vacuum. The MGS have been extensively studied in literature, for example the influence of surface roughness[77]. They also comes at a high cost in free energy that gets reduced in the presence of additional, subdominant order parameter components[78]. As we will see Ch. 5 the difference in the surface spectrum for different misalignment angles also changes the transport behaviour.

4.3 mixed $d + is$ order parameter

As the name suggests, a $d + is$ SC has an order parameter of the combination

$$\Delta(\varphi_F) = \Delta_d \sqrt{2} \cos 2(\varphi_F - \alpha) + i\Delta_s, \tag{4.16}$$

where Δ_d and Δ_s give the magnitude of the respective component. In equilibrium, the two components are thus shifted in phase by $\pi/2$. It is implicitly assumed that the d-wave component is dominant $\Delta_d \gg \Delta_s$, and the two gaps have two different critical temperatures that satisfy $T_{c,s} \ll T_{c,d}$. For temperatures $T \lesssim T_{c,s} \ll T_{c,d}$, the s-wave component is very small in the bulk and does not affect the bulk properties which are dominated by the larger d-wave component. Scattering on pair-breaking interfaces, meaning for $\alpha \neq 0$, lead to an increase of Δ_s close to such

an interface[22]. A self-consistent profile of the spatial dependence $\Delta_\mathrm{d}(x)$ and $\Delta_\mathrm{s}(x)$ in equilibrium is shown in Fig. 4.7a. This suggests that the sub-dominant component mostly affects the surface physics. Indeed, an observable consequence is that the midgap states get split away from zero energy to, for a clean system, $\varepsilon = \pm\Delta_\mathrm{s}$, as seen in Fig. 4.7b. The influence on the transport behaviour will be studied in Chap. 5.

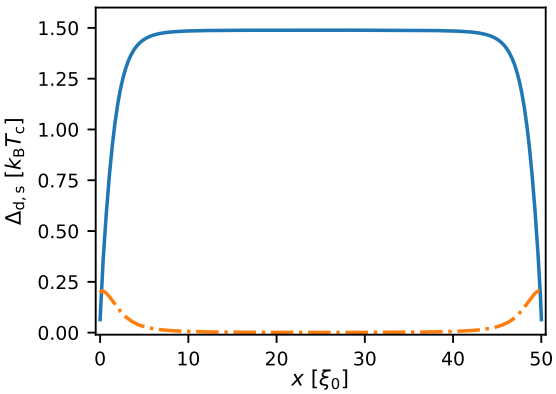

(a) *Spatial dependencies of* Δ_d *and* Δ_s.

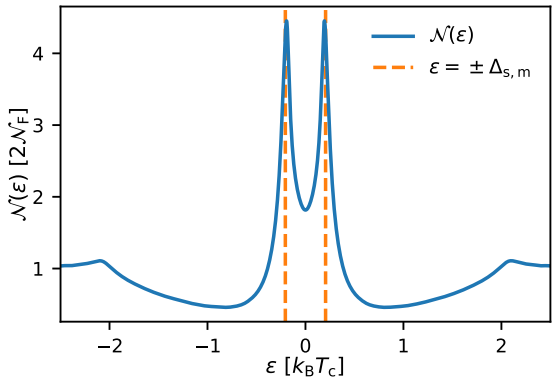

(b) *Shift of the surface ABS to an energy on the order of* $\pm\Delta_\mathrm{s}$.

Figure 4.7: *Enhancement of a sub-dominant order parameter* Δ_s *close to a partially reflective pair-breaking surface where the dominant d-wave pairing is suppressed. The interfaces is characterized by* $D_0 = 0.5$ *and* $\beta = 1$, *see Eq.* (2.75), *and a misalignment angle of* $\alpha = \pi/4$. *The temperature* $T = 0.1T_\mathrm{c,d} \approx 0.5T_\mathrm{c,s}$ *and we have* $\Gamma = 0.01\pi k_\mathrm{B}T_\mathrm{c}$ *in the Born limit.*

5 Transport in superconductors

This section will provide background and additional information for the results of the appended papers. The general type of system we considered is sketched in Fig. 5.1.

It consists of a central superconducting region, denoted S of width w and length L, coupled to the left and right to normal-metal reservoirs, denoted N. By assumption, the reservoirs are large compared to the central superconducting system so that the left (L) and right(R) reservoir remain at their respective equilibrium distributions, characterized by their separate electrochemical potentials $\mu_{\mathrm{L/R}}$ and temperatures $T_{\mathrm{L/R}}$. At the contact between the central region and the reservoirs there can be insulating barriers, denoted I, which we model as interfaces of finite transparency. Using the abbreviations of the different components we call such systems a NISIN structure. We discuss deviations from this general structure if required.

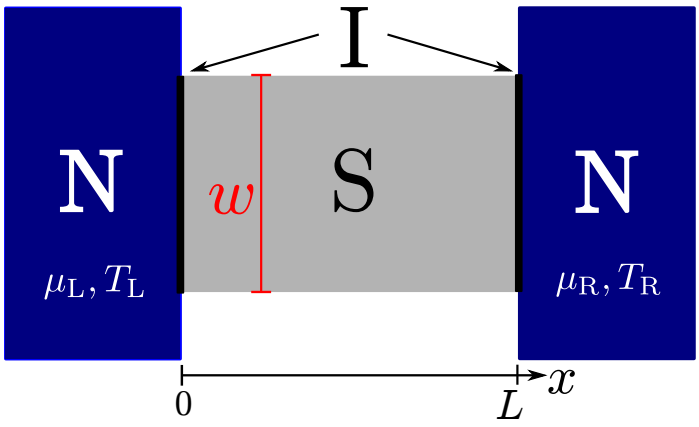

Figure 5.1:
General structure of the setups we consider. A superconductor (S), of length L and width w, is contacted via insulating barriers (I) to a normal-metal reservoir (N) to the left and right. Transport occurs between the reservoirs in the x direction.

5.1 Nonequilibrium in the normal state

As a simple example for the introduced concepts, such as the modes of the nonequilibrium distribution, we briefly review their behaviour in the normal state. To this end, we consider the central region in Fig. 5.1 to be replaced by a spin-degenerate normal metal, so we only have the energy-like mode $f_{1,0} = f_1$ and charge-like mode $f_{3,0} = f_3$ to consider.

Each normal-metal reservoir is described by a Fermi distribution at an electrochemical potential $\mu_{\mathrm{L(R)}} = e\phi_{\mathrm{L(R)}}$ and temperature $T_{\mathrm{L(R)}}$ so that h reads as defined in Eq. (2.47). Taking the left reservoir as an example, the energy-like and charge-like modes incoming from the reservoir are then simply

$$f_1^{\text{left res.}}(\varepsilon, v_{\mathrm{F}}^x > 0) = \frac{1}{2}\left(\tanh\frac{\varepsilon - e\phi_{\mathrm{L}}}{2k_{\mathrm{B}}T_{\mathrm{L}}} + \tanh\frac{\varepsilon + e\phi_{\mathrm{L}}}{2k_{\mathrm{B}}T_{\mathrm{L}}}\right), \tag{5.1}$$

$$f_3^{\text{left res.}}(\varepsilon, v_{\mathrm{F}}^x > 0) = \frac{1}{2}\left(\tanh\frac{\varepsilon - e\phi_{\mathrm{L}}}{2k_{\mathrm{B}}T_{\mathrm{L}}} - \tanh\frac{\varepsilon + e\phi_{\mathrm{L}}}{2k_{\mathrm{B}}T_{\mathrm{L}}}\right). \tag{5.2}$$

Note that the charge mode is only non-zero for finite values of ϕ_{L} and cannot be created by a temperature alone. Fig. 5.2 shows the two modes for a finite and zero voltage at different temperatures. A finite ϕ_L creates step-like structures of width $2e\phi_{\mathrm{L}}$ in both modes, while higher temperatures broaden the steps.

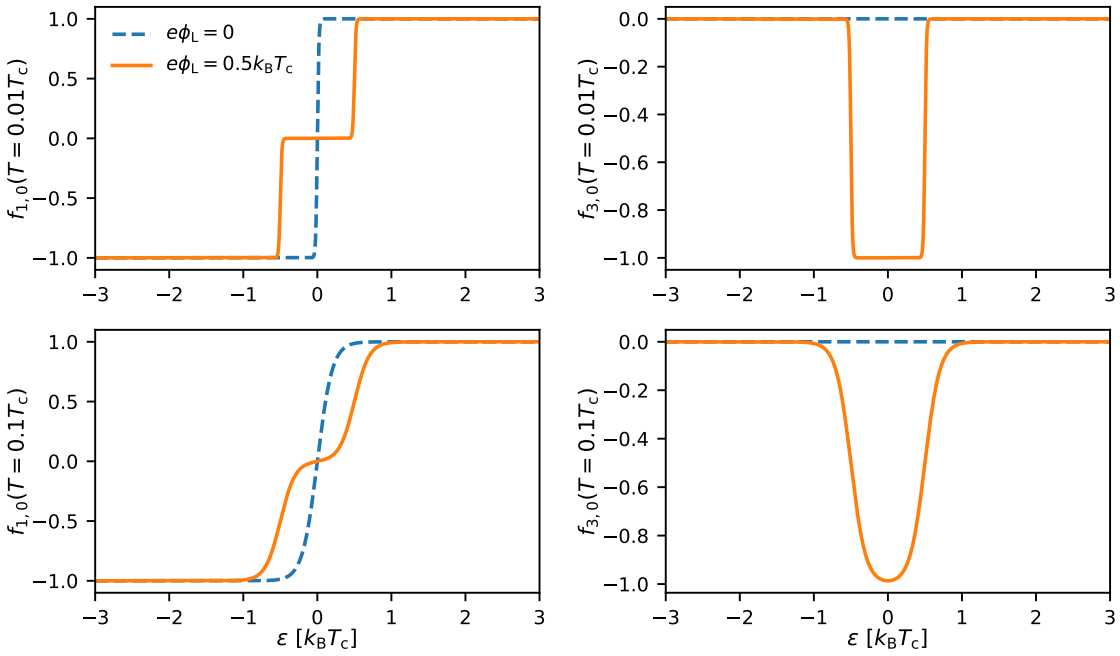

Figure 5.2: *Energy-like (left column) and charge-like (right column) modes in a reservoir with $e\phi_{\mathrm{L}} = 0.5k_{\mathrm{B}}T_{\mathrm{c}}$ (solid orange), and their shape for $e\phi_{\mathrm{L}} = 0$ at the same temperature (dashed blue). In the top row $T = 0.01T_{\mathrm{c}}$, in the bottom row $T = 0.1T_{\mathrm{c}}$.*

For simplicity we assume $\phi_{\mathrm{L}} > \phi_{\mathrm{R}} = 0$ and a constant temperature T everywhere. The starting guess for the incoming function from the right reservoir and in the central region is then an equilibrium distribution. The distribution entering the central region at the left insulating barrier, see Fig. 5.1, will then depend on the interface transparency D,

$$f_{1(3)}(\varepsilon, \mathbf{v}_{\mathrm{F}}^x, x > 0) = D\ f_{1(3)}^{\text{left res.}}(\varepsilon, \mathbf{v}_{\mathrm{F}}^x) + (1 - D)\ f_{1(3)}(\varepsilon, \mathbf{v}_{\mathrm{F}}^x < 0, x > 0), \tag{5.3}$$

so that the function entering the normal region from the left is a weighted mixture of the blue and orange curves in Fig. 5.2.

The spatial variation of the distribution is found by solving the equation of motion for x as outlined in Sec. 3.2. Once the impurity self-energies are self-consistently determined the charge current is conserved everywhere. For left-movers, right-movers, and the FS average show the Fig. 5.3 shows the energy mode and Fig. 5.4 the charge mode, both for left-movers, right-movers, and FS-averaged, as defined in Sec. 2.3.1. Comparison to Fig. 5.2 shows that the left-mover (right-mover) modes agree with the reservoir modes at the right (left) system edge at $x = L = 20\xi_0$ ($x = 0$), this is only the case for fully transparent interfaces with $D = 1$.

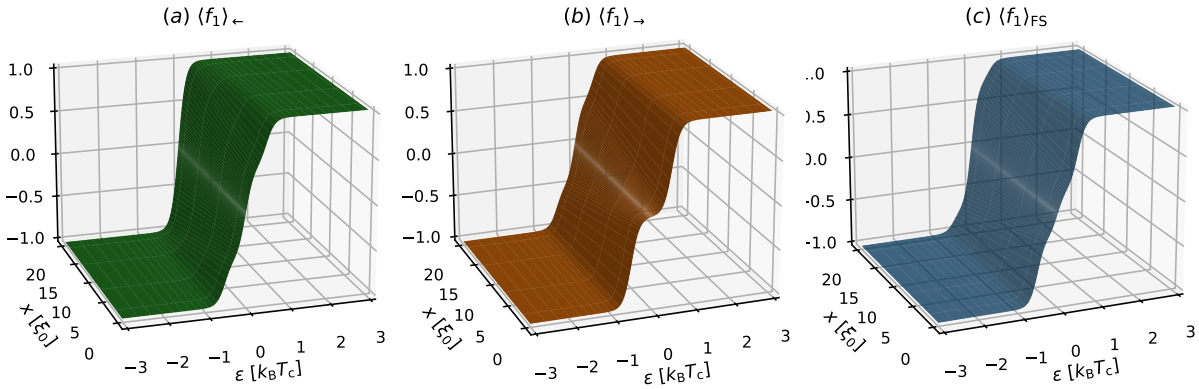

Figure 5.3: *The energy-like mode for (a) left-movers, (b) right-movers, and (c) FS-averaged. Here we have $D = 1$, $\ell = L/2$ and $T = 0.1k_{\mathrm{B}}T_{\mathrm{c}}$.*

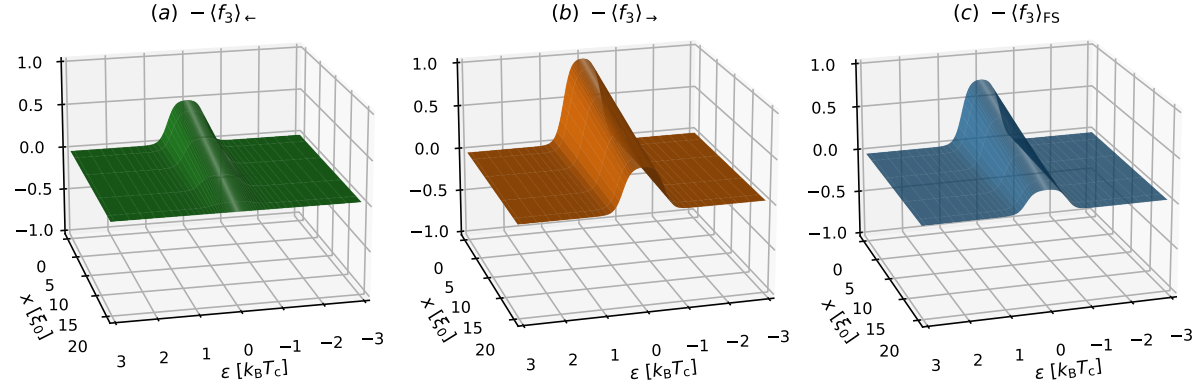

Figure 5.4: *The charge mode for (a) left-movers, (b) right-movers, and (c) FS-averaged. Note that we show $-\langle f_3\rangle_{\rightarrow/\leftarrow/\mathrm{FS}}$ is shown and the x and ε axes are flipped compared to Fig. 5.3.*

Even for $D = 1$, the FS-average of both modes has jumps compared to the reservoir distributions since it is the local average of left- and right-mover distributions. Additionally, we see that $\langle f_i\rangle_{\rightarrow} \neq \langle f_i\rangle_{\leftarrow} \neq \langle f_i\rangle_{\mathrm{FS}}$ for both modes, indicating that

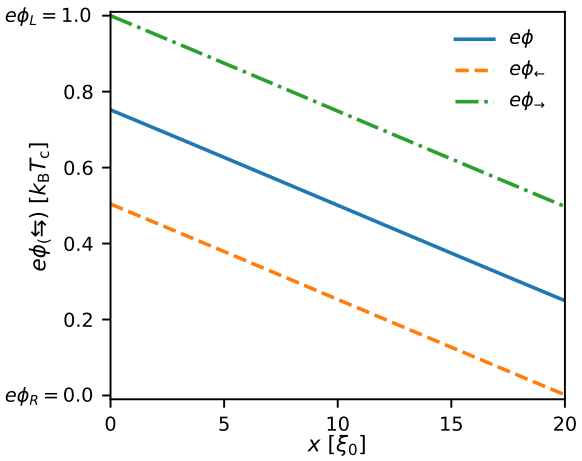

Figure 5.5: *Left-mover and right-mover potentials in the normal state for the results shown in Figs. 5.3–5.4.*

the transport is not fully diffusive.

Studying the non-equilibrium modes gives insight into the physics on an energy- and momentum-resolved level. As a complimentary approach, we can use the left-mover and right-mover potentials, see Eq. (2.103), that are shown in Fig. 5.5. The right-mover (left-mover) potential $\phi_{\rightarrow}$ ($\phi_{\leftarrow}$) connects to the potential of the left (right) reservoir at the left (right) system edge. The average potential ϕ, however, has jumps even for the fully transparent interface considered here. We can interpret those jumps as a contact resistance between the reservoir and the system[33].

In both viewpoints of the problem, we see mixing between left-movers and right-movers in the central region. The "strength" of this mixing is determined by the ratio of the mean free path to the system length, ℓ/L. The smaller the ratio the more diffusive transport becomes . Noting that in the normal state, $x = h$, the equation of motion for h obtained from Eq. (2.36) is simply

$$i\hbar \mathbf{v}_{\mathrm{F}} \cdot \nabla h - \Sigma^{\mathrm{R}} h + h\Sigma^{\mathrm{A}} = -\Sigma^{\mathrm{K}}. \tag{5.4}$$

In the Born limit the self-energies for the normal state are $\Sigma^{\mathrm{R}} = -i\Gamma$, $\Sigma^{\mathrm{A}} = i\Gamma$, and $\Sigma^{\mathrm{K}} = -2i\Gamma \langle h \rangle_{\mathrm{FS}}$. A solution step of length x in a region of constant self-energies is then found to be

$$h(\varepsilon, x, v_{\mathrm{F}}^x > 0) = e^{-x/\ell \cos\varphi_{\mathrm{F}}} h(\varepsilon, 0, v_{\mathrm{F}}^x > 0) + (1 - e^{-x/\ell \cos\varphi_{\mathrm{F}}}) \langle h \rangle_{\mathrm{FS}} (\varepsilon, x). \tag{5.5}$$

For propagation in the x direction the momentum-dependent effective path length becomes $x/\cos\varphi_{\mathrm{F}}$. Hence, the information about the initial occupation is lost on a scale of ℓ, and instead the occupation is driven towards the Fermi-surface average of the occupation for the given energy, $\langle h \rangle_{\mathrm{FS}} (\varepsilon)$. This is what we would expect since we include only elastic scattering processes but not inelastic ones. The occupation for a given energy can then only be redistributed over the available momentum orientations on the Fermi surface but not scattered to different energies.

5.2 Voltage bias in the superconducting state

If a potential difference $\mu_L \neq \mu_R$ is applied between the reservoirs at equal temperature $T_L = T_R$ then the structure is under a pure voltage bias. The superconductor is assumed to be grounded so that we have $\mu_S = 0$ in the central region. In the attached papers we compare our results to a non-self-consistent scattering approach, so we briefly review it here within quasiclassical theory.

5.2.1 Interface conductance

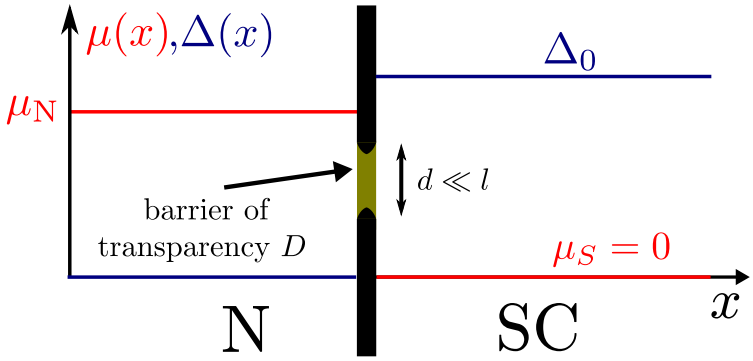

Figure 5.6: *A pinhole contact between a normal metal reservoir at potential μ and a grounded superconductor. The voltage drop occurs exactly at the interface and $\Delta(x) = \Delta_0$ in the SC, $\Delta(x) = 0$ in the normal metal.*

Let us assume a symmetric system, meaning that the left and right insulating barrier have equal transparencies D. Then the potential difference should be applied symmetrically around μ_S, for example $\mu_L = -\mu_R$. The problem can then be reduced to studying an individual normal-metal reservoir (N) at connected via an insulating barrier (I) to a grounded superconductor (S), or NIS system, with a potential difference $V = |\mu|$ applied. The question of interest is then in the current-voltage relation $I(V)$, or alternatively the differential conductance $G(V) = dI/dV$ of such an interface.

In a simple, non self-consistent model the order parameter can be assumed constant up to the interface while the voltage drop from μ_N to 0 exactly at the interface. Implicitly, this means that we have either interface with very low transparency or a Sharvin-type pinhole contact[79]. We will assume the latter case here and sketch this simplified model in Fig. 5.6.

For simplicity, we consider the current on the normal side of the interface and assume the spin degenerate case. As in Sec. 2.3.3, we adopt the convention that capital letters denote functions outgoing from the interface and small letters denote incoming ones nd do not write out v_F^x explicitly. From the definition of the charge current, Eq. (2.98), we find the current in the x direction to be

$$j_x = -e\mathcal{N}_F \int_{-\infty}^{\infty} \frac{d\varepsilon}{2} \frac{\left\langle \mathbf{v}_F(x_N - \tilde{X}_N + \tilde{\Gamma}_N^R x_N \Gamma_N^A)\right\rangle_+ + \left\langle \mathbf{v}_F(X_N - \Gamma_N^R \tilde{x}_N \tilde{\Gamma}^A - \tilde{x}_N)\right\rangle_-}{2}. \quad (5.6)$$

The incoming functions on the normal-metal side (N) and superconducting side (S) for $\mathbf{v}_\mathrm{F}$ pointing toward the interface are

$$\gamma_\mathrm{N}(v_\mathrm{F}^x > 0) = 0, \qquad x_\mathrm{N}(\varepsilon, v_\mathrm{F}^x > 0) = \tanh\frac{\varepsilon - eV}{2T}, \tag{5.7}$$

$$\gamma_\mathrm{S}^\mathrm{R}(\varepsilon, v_\mathrm{F}^x < 0) = \gamma_\mathrm{bulk}^\mathrm{R}(\Delta_0, \varphi_\mathrm{F}), \qquad x_\mathrm{S}(\varepsilon, v_\mathrm{F}^x < 0) = \tanh\frac{\varepsilon}{2T}\left(1 - |\gamma_\mathrm{S}^\mathrm{R}|^2\right). \tag{5.8}$$

The outgoing functions on each side are then obtained by using the boundary conditions outlined in Sec. 2.3.3. The coherence function on the normal side is simply

$$\Gamma_\mathrm{N}^\mathrm{R} = D\mathcal{G}_\mathrm{S}^\mathrm{R}\gamma_\mathrm{s}^\mathrm{R}, \tag{5.9}$$

where $\mathcal{G}_\mathrm{S}^\mathrm{R} = \left(1 + R\gamma_\mathrm{S}^\mathrm{R}\tilde{\gamma}_\mathrm{S}^\mathrm{R}\right)$, with the interface reflectivity $R = 1 - D$, is the value at the interface on the superconducting side. The outgoing distributions can be written in terms of physical probabilities[80] as

$$X_\mathrm{N} = R_\mathrm{ee}x_\mathrm{N} + \overline{T}_\mathrm{ee}x_\mathrm{S} - \overline{T}_{eh}\tilde{x}_\mathrm{S}, \tag{5.10}$$

$$\tilde{X}_\mathrm{N} = R_\mathrm{hh}\tilde{x}_\mathrm{N} + \overline{T}_\mathrm{hh}\tilde{x}_\mathrm{S} - \overline{T}_{he}x_\mathrm{S}. \tag{5.11}$$

The different prefactors in Eqs. (5.10)–(5.11) designate for different transport processes across the interface. Specifically, R_ee denotes reflection of an electron incoming from the normal side and $\overline{T}_\mathrm{ee}$ denotes transmission of an electron incoming from the superconducting side. Lastly, $\overline{T}_\mathrm{eh} = \overline{T}_{\mathrm{e}\leftarrow\mathrm{h}}$ is the so called branch-conversion transmission, meaning a hole incoming from the superconductor gets transmitted as an electron in the normal metal. For each of these processes there is a electron-hole conjugated counterpart where the indices h and e are exchanged.

The probabilities can be expressed in terms of the amplitudes $r_{1l}^\mathrm{R}, t_{1l}^\mathrm{R}$ and a_{1l}^R, see Sec. 2.3.3, and Γ^R. In the normal side they evaluate to

$$R_\mathrm{ee} = |r_{1l}^\mathrm{R}|^2 = |\sqrt{R}(1 + D\gamma_\mathrm{S}^\mathrm{R}\mathcal{G}_\mathrm{S}^\mathrm{R}\tilde{\gamma}_\mathrm{S}^\mathrm{R})|^2, \qquad \overline{T}_\mathrm{ee} = |t_{1l}^\mathrm{R}|^2 = |\sqrt{D}\mathcal{G}_\mathrm{S}^\mathrm{R}|^2, \tag{5.12}$$

$$\overline{T}_\mathrm{eh} = |a_{1l}^\mathrm{R}|^2 = |\sqrt{R}\sqrt{D}\mathcal{G}_\mathrm{S}^\mathrm{R}\gamma_\mathrm{S}^\mathrm{R}|^2, \qquad R_{eh} = |\Gamma_\mathrm{N}^\mathrm{R}|^2 = |D\mathcal{G}_\mathrm{S}^\mathrm{R}\gamma_\mathrm{S}^\mathrm{R}|^2. \tag{5.13}$$

One can also obtain the probabilities from a diagrammatic summation[81]. The electron-hole conjugated terms can be combined by symmetries, and by combining trajectories that are related through specular scattering, see Eq. (2.73), we can also combine the two Fermi surface averages. The final result for the current becomes

$$j_x = -e\mathcal{N}_\mathrm{F}v_\mathrm{F}\int_{-\infty}^{\infty}\mathrm{d}\varepsilon\int_{-\pi/2}^{\pi/2}\frac{\mathrm{d}\varphi_\mathrm{F}}{2\pi}\cos\varphi_\mathrm{F}\left[x_\mathrm{N}\left(1 - R_\mathrm{ee} + R_\mathrm{he}\right) + x_\mathrm{S}\left(\overline{T}_\mathrm{he} - \overline{T}_\mathrm{ee}\right)\right]. \tag{5.14}$$

Note that all probabilities and x_S can still depend on the momentum orientation. The current is then given by $I_x = \mathcal{A} j_x$ where $\mathcal{A}$ is the contact area. For x_N as specified in Eq. (5.7) we find the conductance $G(V) = dI/dV$, normalized to the normal-state value, to be

$$\frac{G(V)}{G_N} = \int_{-\infty}^{\infty} d\varepsilon \int_{-\pi/2}^{\pi/2} \frac{d\varphi_F}{2\pi} \frac{1}{2T} \frac{(1 - R_{ee} + R_{he}) \cos\varphi_F}{\cosh^2[(\varepsilon - eV)/2T]} \tag{5.15}$$

where the normal-state conductance is $G_N = 2e^2 \mathcal{N}_F v_F \mathcal{A} \langle \cos\varphi_F D(\varphi_F) \rangle_+$. Implicitly, we have assumed that the transport probabilities and x_s are not voltage-dependent which is consistent with the model of an unperturbed superconductor. For $T \to 0$, the voltage-dependent part becomes a delta distribution so that the conductance at a voltage V measure the amplitudes at the corresponding energy eV, for a finite temperature T the energy integral averages on the scale of $2T$. Examples for the resulting conductances for an s-wave superconductor are shown in Fig. 5.7. In the low-transparency limit $D \ll 1$ the conductance resembles the bulk density of states, so it can be used as a probe of the spectrum in tunnelling spectroscopy[82, 83].

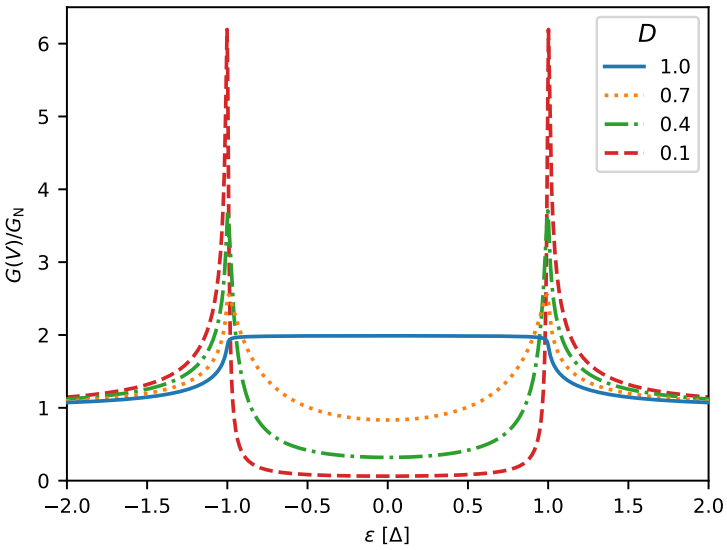

Figure 5.7:
Conductance for the interface between a normal metal and an s-wave superconductor as predicted by Eq. (5.15).
Here a non-selfconsistent result for a clean superconductor at $T = 0.1$.

For a clean s-wave superconductor with momentum-independent interface transparency D, the interface conductance agrees with that obtained by Blonder, Klapwijk, and Tinkham, in the so-called BTK approach[84]. Further evaluation shows that in this case transport probabilities in Eq. (5.12) – (5.13) can be expressed in terms of experimentally accessible parameters such as the energy gap Δ and the interface transparency D, and the model is used to analyse experimental results[85]. It will also serve as a means of comparison for our results. Eq. (5.15) extends the original BTK approach by averaging all transport probabilities over

the Fermi surface average. Additionally, using self-consistently determined values of the transport amplitudes captures corrections due to deviations from the simple model of an unperturbed bulk superconductor.

5.2.2 Beyond the interface

Having obtained an expression for the interface conductance, the natural question is: What happens now with the current that gets injected through the interface? To get some intuition, we can take the equation of motion for x^{a} for a clean s-wave superconductor so that there are is no impurity self-energy. The Keldysh components of $\check{h}_{\mathrm{MF}}$ are also zero, see Sec. 2.4. Let us additionally assume that the coherence function is unperturbed by the low-transparency contact with $D \ll 1$ and the coherence functions for the outgoing trajectory just have their bulk values. In this case Eq. (2.36) can, in the spin degenerate case, be written as

$$i\hbar \mathbf{v}_{\mathrm{F}} \cdot \nabla x^{\mathrm{a}} = -\gamma^{\mathrm{R}} \tilde{\Delta}^{\mathrm{R}}\, x^{\mathrm{a}} - \Delta^{A} \tilde{\gamma}^{A} x^{\mathrm{a}} = -2i\, \mathrm{Im}\left(\gamma^{\mathrm{R}} \tilde{\Delta}^{\mathrm{R}}\right) x^{\mathrm{a}}. \tag{5.16}$$

The solution along the x direction is then of them form

$$x^{\mathrm{a}}(x) = x^{\mathrm{a}}(0) \exp\left(-\frac{2x}{\hbar v_{\mathrm{F}} \cos\varphi_{\mathrm{F}}} \mathrm{Im}(\gamma^{\mathrm{R}} \tilde{\Delta})\right). \tag{5.17}$$

We find

$$\mathrm{Im}(\gamma^{\mathrm{R}} \tilde{\Delta}) = \begin{cases} \sqrt{\Delta^2 - \varepsilon^2} & \text{if } |\varepsilon| < \Delta \\ \mathcal{O}(\eta) & \text{if } |\varepsilon| > \Delta \end{cases}, \tag{5.18}$$

where η is the small imaginary part of energy for retarded functions. Particles injected at an energy eV below the gap will thus decay on a length scale of Andreev reflection $\xi_{\mathrm{Andreev}}(eV) = \hbar v_{\mathrm{F}}/\sqrt{\Delta^2 - (eV)^2}$, while those above propagate unperturbed as quasiparticles since they cannot scatter. If the change of γ at the interface is actually taken into account, the oscillations in γ and $\tilde{\gamma}$ for voltages above the gap also affect the population. In the presence of impurities, the decay becomes additionally dependent on the mean free path, similar to the normal-metal case.

In general, the equation of motion for x^{a} will contain driving terms on the right-hand side. Similar to the normal-state case, the injected population will be driven to a value that is determined by the combination of those driving terms, see Eq. (2.36). For injection voltages below the energy gap, we would still expect the quasiparticle current to decay inside the superconductor if there no quasiparticle states at the given energy. Since the total current has to be conserved, a compensating current carried by the condensate should build up in the superconductor. To capture this transition correctly we need to perform a fully self-consistent calculation that cannot be done analytically.

5.2.3 s-swave order parameter

The aim of paper I was to calculate the charge transport inside an s-wave superconductor self-consistently for different impurity concentrations and interface transparency. In the literature, similar work has been done mostly in the fully diffusive limit[27, 28, 86], or without self-consistency in the clean case[84]. The work that is the most closely related is a series of publications, referenced in its entirety in Paper I, by Sols and Sánchez-Cañizares. Starting from scattering theory with an "asymptotic" self-consistency in the bulk[87], their work culminated in a fully self-consistent quasiclassical theory but only for very small systems ($L \lesssim 3\xi_0$)[88]. Our interest was in somewhat larger systems in the intermediate regime of impurity concentrations between the clean and dirty limits where transport is not fully ballistic or fully diffusive.

Here we will review the results for the setup in Fig. 5.1, a superconductor connected on each end to a reservoir. Additionally, the superconductor has negligible width $w \ll L$ so it essentially a superconducting nanowire. We assume then that there are only two momentum orientations, $v_{\mathrm{F}}^x = \pm 1$, allowed in the wire. While inclusion of additional momenta leads to a certain averaging and reduces the influence of p_s, we have checked that the general results are not strongly affected by this assumption. The setup is shown in Fig. 5.8. Here, we will assume $D_{\mathrm{L}} = D_{\mathrm{R}}$ so that the bias is symmetric, $\mu_{\mathrm{L}} = -\mu_{\mathrm{R}}$. We can then focus on one side of the system to discuss the physics.

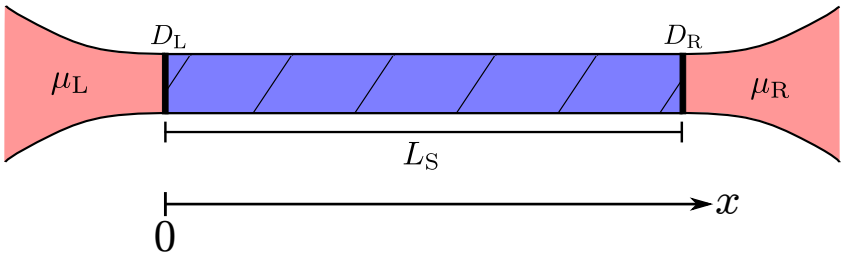

Figure 5.8:
One of the setups in paper I, referred to as ISI system. A superconducting nanowire is coupled to a normal-metal reservoir on the left (L) and right (R) via an insulating barriers of transparency D_{L} (D_{R}).

Once a self-consistent solution is found the injected charge current j is conserved, $j(x) = \text{const.}$. However, the injected quasiparticle current, j^{a}, is converted into current carried by the condensate, j^{le}, see Fig. 5.9. This identification is possible since the charge current, in the form of Eq. (5.19), reads for the spin degenerate case

$$\mathbf{j}(\mathbf{R}) = -e\mathcal{N}_{\mathrm{F}} \int_{-\infty}^{\infty} \mathrm{d}\varepsilon \ \langle \mathbf{v}_{\mathrm{F}} f_1(\varepsilon, \mathbf{p}_{\mathrm{F}}, \mathbf{R}) \mathcal{N}(\varepsilon, \mathbf{p}_{\mathrm{F}}, \mathbf{R}) \rangle_{\mathrm{FS}} \,, \tag{5.19}$$

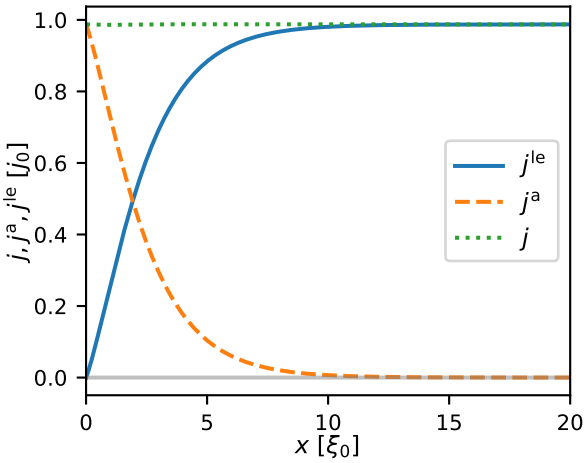

Figure 5.9:
Conversion of quasiparticle current into supercurrent in an s-wave superconductor. Shown are the anomalous current j^{a}, the local-equilibrium current j^{le}, and total current j. Here $D = 1$, $eV = 0.5k_{\mathrm{B}}T_{\mathrm{c}}$, $T = 0.1T_{\mathrm{c}}$, for a superconductor with $\ell = 20\xi_0$.

where we suppress the spin index on $f_1 \equiv f_{1,0}$. Using the splitting of f_1, Eq. (2.61), we arrive at $\mathbf{j}(\mathbf{R}) = \mathbf{j}^{\mathrm{le}}(\mathbf{R}) + \mathbf{j}^{\mathrm{a}}(\mathbf{R})$, where

$$\mathbf{j}^{\mathrm{le}}(\mathbf{R}) = -e\mathcal{N}_{\mathrm{F}} \int_{-\infty}^{\infty} \mathrm{d}\varepsilon \; f_1^{\mathrm{le}}(\varepsilon, \mathbf{R}) \left\langle \mathbf{v}_{\mathrm{F}} \mathcal{N}(\varepsilon, \mathbf{p}_{\mathrm{F}}, \mathbf{R}) \right\rangle_{\mathrm{FS}} = \int_{-\infty}^{\infty} \mathrm{d}\varepsilon \; j^{\mathrm{le}}(\varepsilon, \mathbf{R}), \quad (5.20)$$

$$\mathbf{j}^{\mathrm{a}}(\mathbf{R}) = -e\mathcal{N}_{\mathrm{F}} \int_{-\infty}^{\infty} \mathrm{d}\varepsilon \; \left\langle \mathbf{v}_{\mathrm{F}} f_1^{\mathrm{a}}(\varepsilon, \mathbf{p}_{\mathrm{F}}, \mathbf{R}) \mathcal{N}(\varepsilon, \mathbf{p}_{\mathrm{F}}, \mathbf{R}) \right\rangle_{\mathrm{FS}} = \int_{-\infty}^{\infty} \mathrm{d}\varepsilon \; j^{\mathrm{a}}(\varepsilon, \mathbf{R}). \quad (5.21)$$

On the right-hand side of both equations we have defined the spectral current densities for both quantities. Note that f_1^{le} does, by definition, not depend on the momentum orientation $\mathbf{p}_{\mathrm{F}}$. This shows that $\mathbf{j}^{\mathrm{le}}$ can only be non-zero if the momentum-resolved DOS, $\mathcal{N}(\varepsilon, \mathbf{p}_{\mathrm{F}}, \mathbf{R})$, varies over the Fermi surface.

We will see below how this variation appears in a self-consistent calculation. If ϕ is determined self-consistently, j^{a} is entirely due to differences in the occupation of quasiparticles for different momentum orientations, since f_1^{le} subtracts exactly the momentum-independent part. The variation in $\mathcal{N}(\varepsilon, \mathbf{p}_{\mathrm{F}}, \mathbf{R})$ that carries the condensate current is self-consistently generated from the phase gradient of the superconducting order parameter,

$$\Delta(x) = |\Delta(x)| e^{i\chi(x)}. \quad (5.22)$$

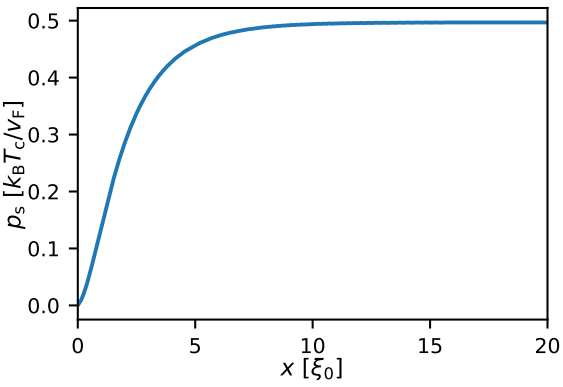

Figure 5.10:
Spatial dependence of the superfluid momentum $p_{\mathrm{s}}(x)$. Parameters are the same in Fig. 5.9.

By a local gauge transform, this is equivalent to a real order parameter Δ and the presence of the so-called superfluid momentum

$$\mathbf{p}_\mathrm{s} \equiv \frac{\hbar}{2}\nabla\chi(x), \tag{5.23}$$

which is shown in Fig. 5.10. In presence of this superfluid momentum, all quasiparticle energies obtain a Doppler shift

$$\varepsilon \to \varepsilon - \mathbf{v}_\mathrm{F}\cdot\mathbf{p}_\mathrm{s}. \tag{5.24}$$

This Doppler shift alters the density of states for different momentum orientations as seen in Fig. 5.11. The density of states gets shifted upward (downward) for positive (negative) momenta, and the Fermi-surface average has a reduced spectral gap compared to the equilibrium shape. Additionally, the original coherence peaks at $\varepsilon = \pm\Delta$ each split into two separate peaks at $\varepsilon = \pm(\Delta \pm v_\mathrm{F}p_\mathrm{S})$.

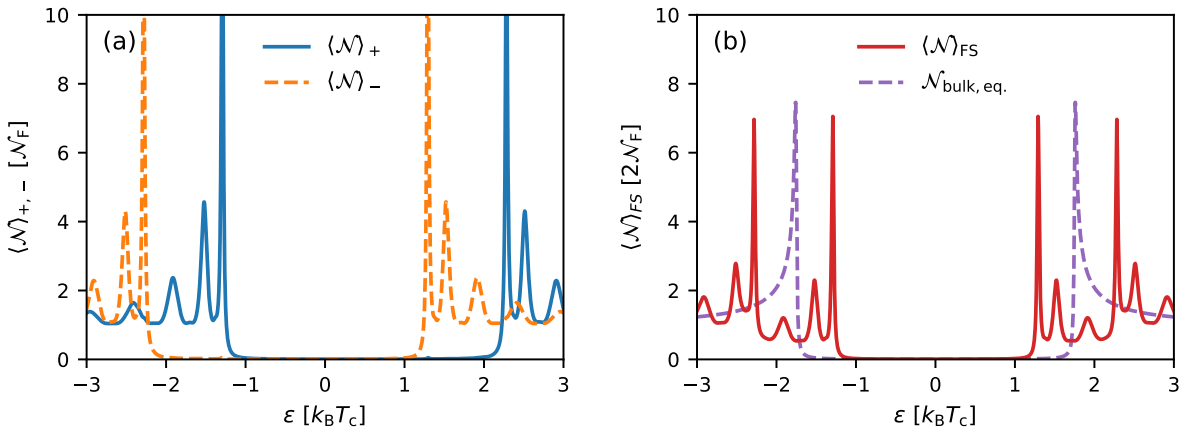

Figure 5.11:
Effect of superflow on the density of states in the center of the superconductor at $x = L/2$. (a) Averaged over positive v_F^x ($\langle\mathcal{N}\rangle_+$) and over negative v_F^x, ($\langle\mathcal{N}\rangle_-$). (b) Averaged over the entire Fermi surface ($\langle\mathcal{N}\rangle_\mathrm{FS}$) in comparison the bulk equilibrium value $\mathcal{N}_\mathrm{bulk}$. Parameters are the same as in Fig. 5.9

The identification of j^a as the quasiparticle current and j^le as current by the condensate is also apparent in the spectral current densities that we have defined in Eq. (5.20)–(5.21). As can be seen in Fig. 5.12 the anomalous part is only nonzero in the bias-window $|\varepsilon| \leq eV$ and decays away from the interface. In contrast, the condensate current is carried in between $\pm(\Delta \pm v_\mathrm{F}p_\mathrm{S})$.

Lastly, we show the right-mover, left-mover, and FS-averaged potential, in Fig. 5.13. They indicate that the right-moving particles are predominantly electron-like while the left-moving ones are predominantly hole-like, reflecting the relaxation of the injected imbalance through Andreev reflection for an injection voltage

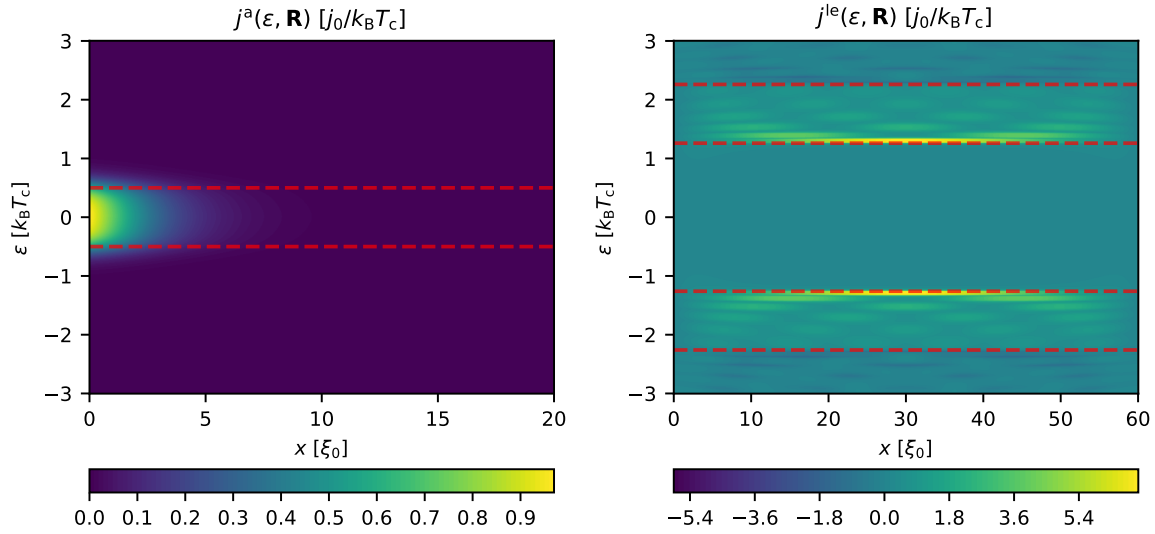

Figure 5.12:
Spectral current densities. The left plot shows $j^{a}(\varepsilon, \mathbf{R})$, and the horizontal red dashed line indicates the bias window. The right plot shows $j^{le}(\varepsilon, \mathbf{R})$, and the dashed lines indicate the $\pm(\Delta \pm v_F p_S)$. Parameters are the same as in Fig. 5.9

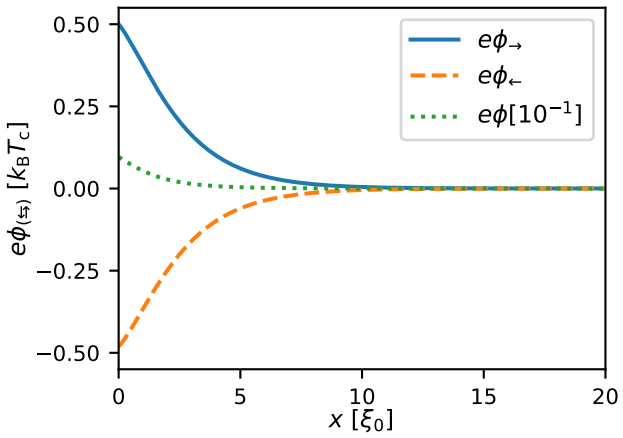

Figure 5.13:
(b) The spatial dependence of the potentials for left-movers $\phi_{\leftarrow}$, right-movers $\phi_{\rightarrow}$, and FS-average ϕ. Note that the latter is enlarged by a factor of 10 for better visibility. Parameters are the same as in Fig. 5.9

$|V| < \Delta/e$. In a perfectly clean system the resulting charge imbalance in the steady would then be zero since each incoming electron gets Andreev reflected, creating a counter-moving hole. The non-zero quasiparticle potential $\phi(x)$ near the interface thus appears as a result of impurity scattering that mixes the left-mover and right-mover branches. For quasiparticle excitations in the superconductor, meaning energies above the gap, $\phi(x)$ is usually referred to as charge imbalance. That there can be difference in the quasiparticle potential compared to the condensate was first measured by Clarke[89], and subsequently a theory of the relaxation was developed for injection voltages above the gap[90, 91]. In the above example, the quasiparticles are only entering the superconductor as

evanescent states, so that the $\phi(x)$ is an evanescent charge imbalance.

For a fully transparent interface, impurity scattering then leads to an increase (decrease) of the current in the case of Andreev reflection (impurity scattering). For finite interface transparency, a back-scattered quasiparticle might not necessarily transfer back into the reservoir so that the opposite effect of a current increase can occur for low-transparency interfaces where Andreev reflection is suppressed. The dependence on the injected current on interface transparency and mean free path is investigated in more detail in paper I.

This decay of injected quasiparticle current with a compensating build-up of a condensate current remains largely unchanged with increasing voltage until we reach voltages that are comparable to Δ/e. At this point, the only stable self-consistent solution we found was that of a vanishing order parameter in the superconductor. This happens at a critical voltage V_c, and part of paper I is an investigation of the underlying mechanism, as well as of the dependence of V_c on interface transparency and impurity concentration. A similar result was reported for a fully diffusive superconducting wire[92] and we found that for increasing impurity concentrations V_c approaches the value in the diffusive limit. Later publications, again for a diffusive wire, report self-consistent solutions with a "bimodal" superconducting state that disappears everywhere but close to the interfaces and relates this to experimentally observed hysteresis in the current-voltage characteristics[93].

5.2.4 d-wave order parameter

Compared to the case of an s-wave superconductor, the theory on transport d-wave superconductors is less well studied. Due to the importance of the surface physics in d-wave superconductors, the main focus of available work is on tunnelling spectroscopy, which can be used to probe such surface effects. Experiments on tunnelling into cuprate superconductors lead to observations of a peak in the conductance at zero bias, or zero-bias conductance peak (ZBCP)[94–96]. Using a generalization of the BTK approach, see Sec. 5.2.1, to d-wave SCs the observed ZBCP were linked to the surface Andreev bound states at pair-breaking interfaces[97, 98]. Non-equilibrium current flow in a d-wave superconductor has not been investigated self-consistently, which drove our interest.

To study a voltage-biased d-wave superconducting film, we use a setup as depicted in Fig. 5.1. In contrast to paper I, the d-wave order parameter inherently requires the inclusion of many trajectories distributed over the Fermi surface. The contacts are tunnel barriers which we describe through a a momentum-dependent transparency according to Eq. (2.75). We model the film as quasi one-dimensional by assuming translational invariance normal to the transport direction $\hat{x}$. Depending on the orientation of the interfaces to the crystal axis, we can tunnel into a so-called [100] surface, meaning we have a misalignment $\alpha = 0$, or into a [110]

surface, meaning $\alpha = \pi/4$. We will discuss both cases separately, and start with the former. We see the results of a self-consistent calculation for one bias voltage in Fig. 5.14 in the Born limit, and in Fig. 5.15 for the unitary limit.

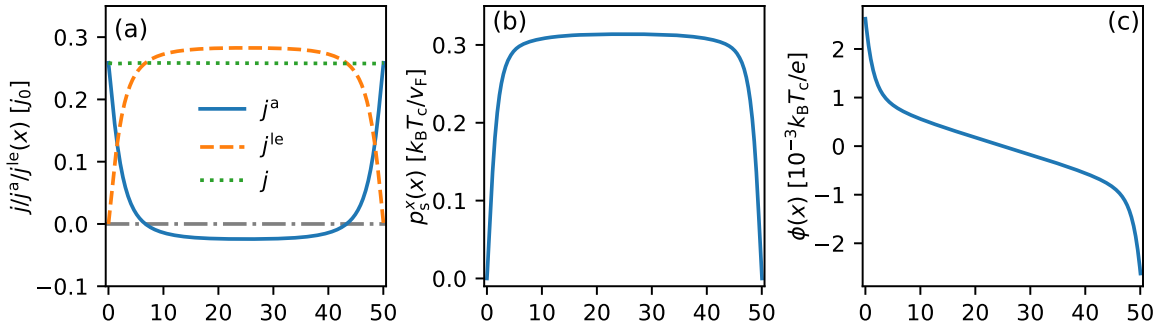

Figure 5.14: *olz(a) The anomalous current j^a, the local-equilibrium current j^{le}, and total current j. (b) The superflow $p_s(x)$. (c) The quasiparticle potential $e\phi(x)$. In this case, we have $D = 1$, $\beta = 1$, $\ell = 100\xi$ in the Born limit, and $\mu_L = -\mu_R = 0.5 k_B T_c$ so that the total bias is $eV = k_B T_c$.*

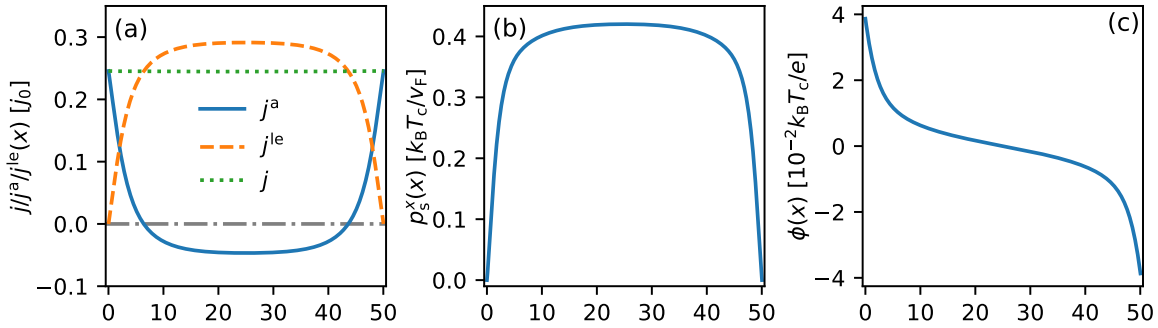

Figure 5.15: *(a) The anomalous current j^a, the local-equilibrium current j^{le}, and total current j. (b) The superflow $p_s(x)$. (c) The quasiparticle potential $e\phi(x)$. In this case, we have $D = 1$, $\beta = 1$, $\ell = 100\xi$ in the unitary limit, and $\mu_L = -\mu_R = 0.5 k_B T_c$ so that the total bias is $eV = k_B T_c$.*

Just as in the s-wave case, the injected quasiparticle current j^a gets converted into condensate current j^{le} inside the superconductor. The condensate is carried by a non-zero superfluid momentum p_S. In contrast to the s-wave case, even for moderate injection voltages there is a counter-flowing quasiparticle current j^a in the center of the superconductor. It is accompanied by a non-zero quasiparticle potential $\phi(x)$ throughout the entire structure, both in the Born and unitary limits and even for a relatively clean system, here $\ell = 100\xi_0 = 2L$. In the unitary limit $\phi(x)$ is an order of magnitude larger, indicating the influence of the impurity band, see Sec. 4.1.2. In the Born limit no such impurity band exist, yet there is non-zero quasiparticle potential $\phi(x)$. In this case the Doppler shift in the bulk creates a finite density of states in an energy range of $|2v_F p_S|$ around zero energy,

seen in Fig. 5.16(b). Additionally, the superflow results in an opposite shift of the DoS for positive and negative v_{F}^x, seen Fig. 5.16(a). In the injection window, this creates an excess of left-moving quasiparticle states for electrons and right-moving ones for holes so that the resulting quasiparticle current is counter-flowing.

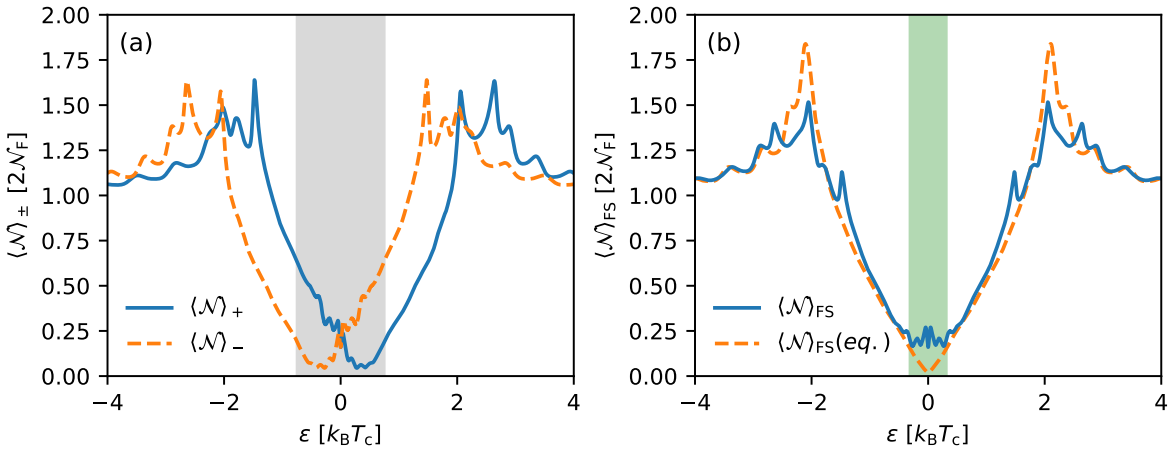

Figure 5.16: *Density of states in the center of the SC in the Born limit. (a) Density of states for $v_{\mathrm{F}}^x > 0$ and $v_{\mathrm{F}}^x < 0$. Shaded in light grey is the energy window of injection voltage $\pm|eV|$. (b) Fermi-surface average compared the bulk equilibrium value, shaded in light the energy window $\pm v_{\mathrm{F}} p_{\mathrm{s}}$.*

Figure 5.17:
Non-selfconsistent interface conductance, here in the Born limit with $\ell = 100\xi_0$ at $T = 0.1T_\mathrm{c}$. The interface has a momentum-dependent transmission given by Eq. (2.75) with $\beta = 0$ and D_0 as given in the legend.

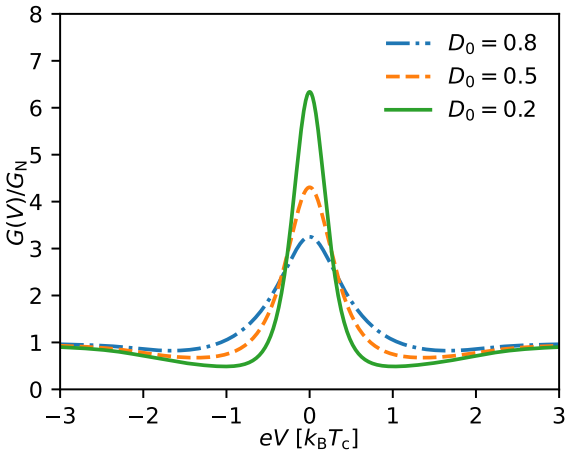

For injection into [110] surfaces, the presence of the surface Andreev bound states leads to a substantial change in the interface conductance. Evaluation the conductance formula, Eq. (5.15), gives a prediction as shown in Fig. 5.17. The behaviour in the center of the system, with a counterflowing quasiparticle current accompanied by a finite quasiparticle potential $\phi(x)$, is largely identical. As we discussed above, the ABS gets shifted to finite energy in the presence of screening currents parallel the surface. In our case, we inject current in the direction of the

surface normal, and find no such shift with increasing current but rather a slight suppression of the bound state with increasing current, seen in Fig. 5.18.

Neglecting the effects of broadening and order parameter suppression, we show in the paper that the effect of superflow along the surface normal only leads to a suppression of the spectral weight

$$\pi|\Delta(\varphi_{\mathrm{F}})| \to \pi\sqrt{\Delta^2(\varphi_{\mathrm{F}}) - (v_{\mathrm{F}}^x p_{\mathrm{S}}^x)^2}. \tag{5.25}$$

implicitly assuming that $|v_{\mathrm{F}}^x p_{\mathrm{S}}^x| < |\Delta(\varphi_{\mathrm{F}})|$, for a small range of momenta around the nodes a non-linear Meissner effect appears[99]. The surface states are thus only weakly affected by the superfluid momentum. As a result, the transport amplitudes that enter the formula for the current at the interface, Eq. (5.14), are not altered as the bias is increased. Our fully self-consistent result for the resulting conductance, discussed in paper III, is in good agreement with the prediction of a scattering approach with self-consistently determined equilibrium values for the amplitudes. This stability in the presence of current flow is not the case for a d-wave order parameter with a sub-dominant s-wave component.

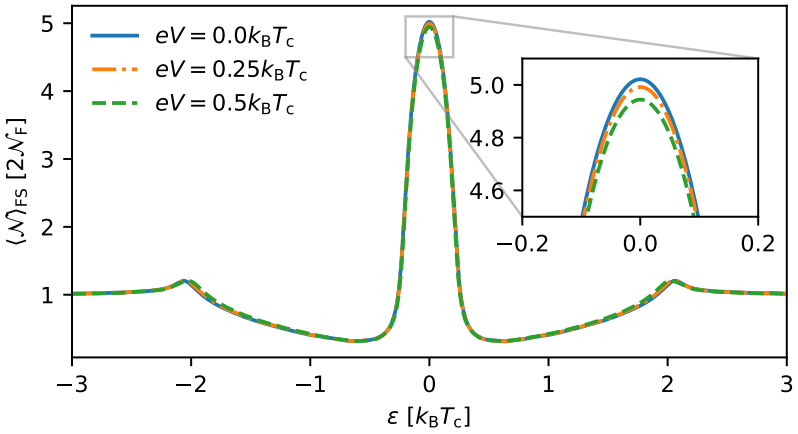

Figure 5.18: *With increasing bias voltage and current, the superflow p_s reduces the height and spectral weight of the ABS, but does not shift it in energy. Parameters are $D_0 = 0.5$, $\beta = 1$ and $\ell = 100\xi_0$ in the Born limit at $T = 0.1T_c$.*

5.2.5 mixed $d + is$ order parameter

Experimentally, the ZBCP discussed in the last section will split if a magnetic field is applied perpendicular to the *ab*-plane,[100] corresponding to shift of the Andreev states in response to screening currents at the surface[77]. A similar splitting of this ZBCP in the *absence* of external magnetic fields is observed in some experiments but not in others[100–102]. The possibility of a such a splitting implies that time-reversal symmetry is broken locally at the surface. This could

be due to the presence of a subdominant order parameter of different symmetry such s or d_{xy} that appears only close to pair-breaking interfaces[22, 77].

As part of paper III, we investigate the influence of current injection on such a sub-dominant s-wave order parameter Δ_s that only appears near the surface since $T_{c,d} \ll T_{c,s}$. As we had discussed in Sec. 4.3, this leads to a splitting of the surface states to $\pm\Delta_s$. Based on a scattering approach, we would expect this splitting to be reflected in the tunnelling conductance when using low-transparency contacts. However, the bound states get broadened through interface transparency and impurities, as we had seen in Sec. 4.2. Additionally, the conductance formula in Eq. (5.15) does not measure the spectrum directly but introduces additional broadening due to temperature. The conductance we obtained in a fully self-consistent calculation, however, disagrees markedly with the prediction of the interface-conductance model, even for low impurity concentrations corresponding to $\ell = 100\xi_0$, as seen in Fig. 5.19.

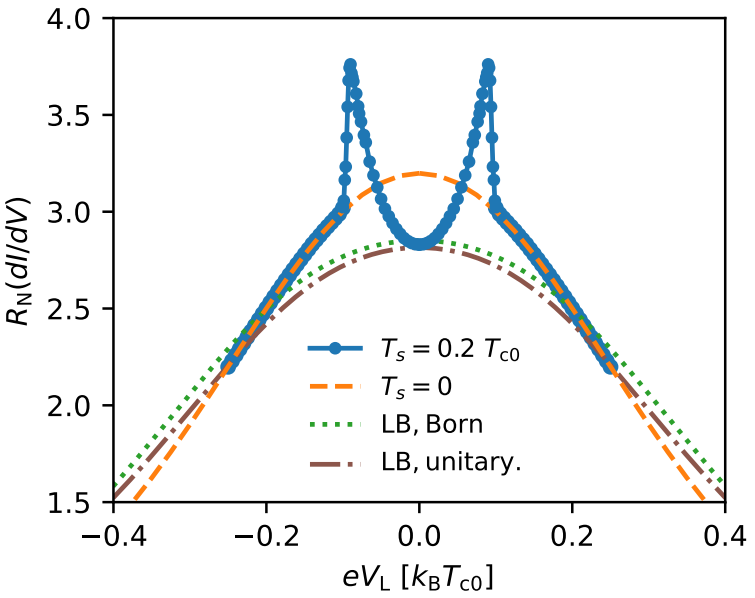

Figure 5.19:
Interface conductance according to Eq. (5.15) compared to the fully self-consistent result with subdominant order (blue) and without (orange). Self-consistent equilibrium transport amplitudes are used for Born and unitary limits for the interface conductance (here abbreviated LB). In all cases, we have $\ell = 100\xi_0$ at $T = 0.1T_c$. The interface is a tunnel cone as in Eq. (2.75) with $D_0 = 0.5$ and $\beta = 1$.

The fully self-consistent result thus predicts an initial steep increase of the conductance, in contrast to a Born- or unitary limit tunnel conductance at the same temperature, where the splitting of the peak is masked due to the temperature broadening of the normal-side distribution. This increase, and the subsequence transition to the conductance of a SC without a sub-dominant component, is the result of the suppression of the sub-dominant component with increasing bias, analysed in paper III. To understand the difference in behaviour, we revisit the

current formula in the non-selfconsistent scattering approach, Eq. (5.14). It read

$$j_x = -e\mathcal{N}_\mathrm{F} \int_{-\infty}^{\infty} \mathrm{d}\varepsilon \int_{-\pi/2}^{\pi/2} \frac{\mathrm{d}\varphi_\mathrm{F}}{2\pi}\, v_\mathrm{F} \cos\varphi_\mathrm{F} \left[x_\mathrm{N} \left(1 - R_\mathrm{ee} + R_\mathrm{he}\right) + x_\mathrm{S} \left(\overline{T}_\mathrm{he} - \overline{T}_\mathrm{ee}\right)\right]. \tag{5.26}$$

In our fully self-consistent approach all terms on the right-hand side depend on voltage:

$$\frac{\mathrm{d}j_x}{\mathrm{d}V} = -e\mathcal{N}_\mathrm{F} \left(A_1 + A_2 + A_3 + A_4\right), \tag{5.27}$$

where the different A_i are given by

$$A_1 = \int_{-\varepsilon_\mathrm{c}}^{\varepsilon_\mathrm{c}} \mathrm{d}\varepsilon \langle v_\mathrm{F}^x \frac{\mathrm{d}x_\mathrm{N}}{\mathrm{d}V} \left(1 - R_\mathrm{ee}(V) + R_\mathrm{he}(V)\right)\rangle_+, \tag{5.28}$$

$$A_2 = \int_{-\varepsilon_\mathrm{c}}^{\varepsilon_\mathrm{c}} \mathrm{d}\varepsilon \langle v_\mathrm{F}^x\, x_\mathrm{N}(V) \frac{\mathrm{d}\left(1 - \mathrm{R_{ee}(V)} + \mathrm{R_{he}(V)}\right)}{\mathrm{d}V} \rangle_+, \tag{5.29}$$

$$A_3 = \int_{-\varepsilon_\mathrm{c}}^{\varepsilon_\mathrm{c}} \mathrm{d}\varepsilon \langle v_\mathrm{F}^x \frac{\mathrm{d}x_\mathrm{S}}{\mathrm{d}V} \left(\bar{T}_\mathrm{he}(V) - \bar{T}_\mathrm{ee}(V)\right)\rangle_+, \tag{5.30}$$

$$A_4 = \int_{-\varepsilon_\mathrm{c}}^{\varepsilon_\mathrm{c}} \mathrm{d}\varepsilon \langle v_\mathrm{F}^x\, x_\mathrm{S}(V) \frac{\mathrm{d}\left(\bar{T}_\mathrm{he}(V) - \bar{T}_\mathrm{ee}(V)\right)}{\mathrm{d}V} \rangle_+, \tag{5.31}$$

with $v_\mathrm{F}^x = v_\mathrm{F} \cos\varphi_\mathrm{F}$. Fig. 5.20 shows that the spectral rearrangements, due to the reduction of Δ_s with increasing voltage, give substantial corrections.

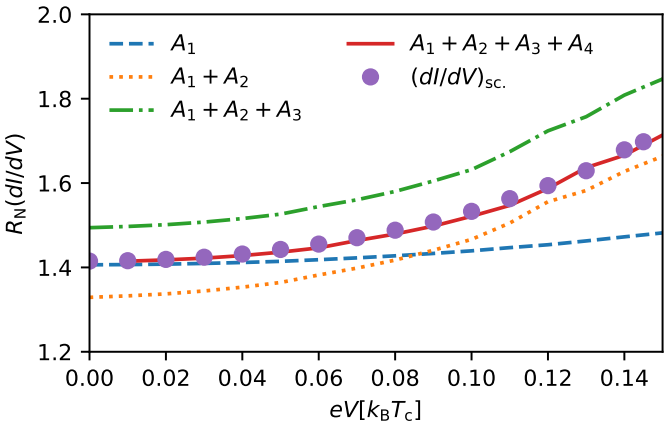

Figure 5.20:
Contributions of the terms A_1–A_4 to the self-consistent conductance.
All results are both in the Born limit for $\ell = 100\xi_0$ at $T = 0.1T_\mathrm{c}$. The interface is a tunnel cone as in Eq. (2.75) with $D_0 = 0.5$ and $\beta = 1$.

5.3 Temperature bias

Let us next consider a different setup with a temperature bias. Application of a fixed temperature difference between the two reservoirs leads to a temperature bias in the central region in Fig. 5.1. We assume the SC to be in a cryostat at temperature T, and the left reservoir to be heated to a slightly higher temperature $T_{\mathrm{L}} = T + \Delta T$. This can in principle lead to a thermoelectric effect and heat flow. Andreev found the heat conductivity of quasiparticles in an s-wave superconductor is exponentially suppressed, $G_{\mathrm{th}} \propto \exp(-\Delta/T)$, as a result of Andreev reflection of injected quasiparticles[103]. The existence of thermoelectric effects in superconductors were somewhat of an elusive question for a long time. Initial results, attributed to Meissner[104, 105] seemed to indicate that there is no thermoelectric effect at all in superconductors. Later Ginzburg argued in terms of a two-fluid model that there is a thermoelectric effect but the induced charge current carried by the "normal fluid", meaning the quasiparticles, is cancelled by a counter-flowing condensate current[106, 107]. The total current thus cancels in the bulk which makes thermoelectric currents difficult to measure. At the contact to a normal metal in an open-circuit setup, however, the quasiparticle current was suggested to fall off close to the contact through the creation of a charge imbalance [108, 109]. This effect was also observed experimentally[110]. Thermoelectric effects in conventional superconductors are thus relatively well-studied[111]. They are also used in superconducting hybrid structures[112]. Our study was motivated by the, in comparison, limited knowledge of thermoelectric effects in unconventional superconductors.

5.3.1 d-wave order parameter

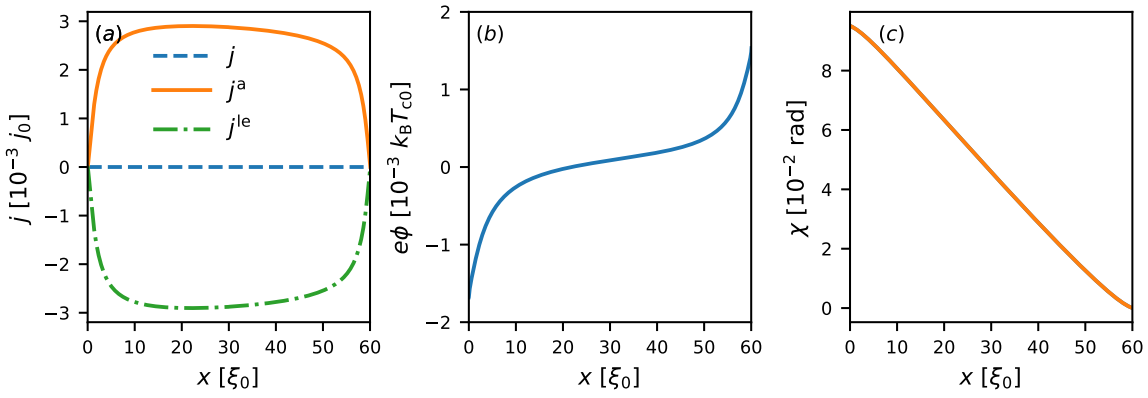

Figure 5.21:
(a) Quasiparticle and condensate current, j^{a} and j^{le}. (b) Spatial profile of $\phi(x)$. (c) The thermophase $\chi(x)$. Here, $D = 1$, $T_{\mathrm{R}} = 0.25T_{\mathrm{c}}$, $T_{\mathrm{L}} = T_{\mathrm{R}} + \Delta T = 0.35T_{\mathrm{c}}$. The mean free path is $\ell = 10\xi_0$ and the scattering phase shift $\delta_0 = 0.9$.

In Paper II we examine the thermoelectric effect in a d-wave superconducting film as a result of an impurity-induced asymmetry between electrons and holes. Recall from Sec. 2.2 that the quasiclassical approximation removes any electron-hole asymmetry due to the band structure. The asymmetry in Σ^{R} for intermediate phase shifts, see Sec. 4.1.2, introduces an asymmetry in the effective mean free path for electrons and holes throughout the film.

A self-consistently determined non-equilibrium steady state shows the expected behaviour for the thermoelectric effect as outlined above. A quasiparticle flow is driven in the direction of the thermal gradient. This flow is dominated by electrons (holes) for positive (negative) values of the phase shift, and determines the charge pileup and resulting gradient of the quasiparticle potential throughout the superconductor. A condensate flow is counter-flowing, driven by a gradient in the thermally induced phase. An example is shown in Fig. 5.21.

A useful concept to understand the results of a thermal bias is, in analogy to the left-mover and right-mover potentials defined in Eq. (2.103), a left-mover and right-mover effective temperature $T_{\mathrm{eff},\leftrightarrows}(\mathbf{R})$. Following[113], we use Eq. (2.50) to define it in analogy to a Sommerfeld expansion as

$$k_{\mathrm{B}}^2 T_{\mathrm{eff},\leftrightarrows}^2(\mathbf{R}) \equiv \frac{6}{\pi^2} \int_0^\infty \mathrm{d}\varepsilon\, \varepsilon \left[\, f_1^{\mathrm{eq}}(\mathbf{R}, \varepsilon, T=0) - \langle f_1(\mathbf{p}_{\mathrm{F}}, \mathbf{R}, \varepsilon)\rangle_{\leftrightarrows}\right], \tag{5.32}$$

and similarly a local Fermi-surface average $\langle T_{\mathrm{eff}}\rangle_{\mathrm{FS}}$. They are, in many aspects, like to the left- and right-mover potentials $\phi_{\leftrightarrows}$ and ϕ in the voltage-bias case. For example, at a fully transparent interfaces the partial average connect to the respective reservoir value, while the average has jumps. An example for the spatial dependencies is shown in Fig. 5.22, and shows the deviation of the energy distribution from a simple linear gradient in the temperature.

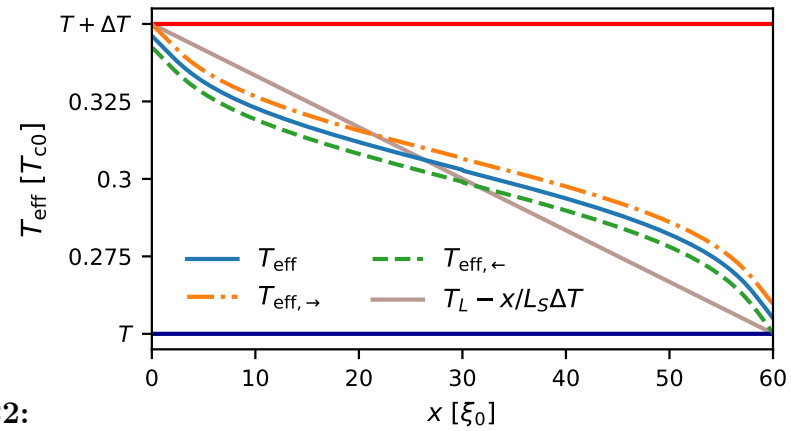

Figure 5.22:
Spatial dependence of the effective temperatures $T_{\mathrm{eff},(\leftrightarrows)}$ in a system with $D = 1$, $T_{\mathrm{R}} = 0.25T_{\mathrm{c}}$, $T_{\mathrm{L}} = T_{\mathrm{R}} + \Delta T = 0.35T_{\mathrm{c}}$. The mean free path is $\ell = 10\xi_0$ and the scattering phase shift $\delta_0 = 0.9$, roughly halfway between the Born and unitary limits.

We proceed in paper II to study the non-linear thermopower of the film,

$$S(T, \Delta T) = -\left.\frac{\mu_{\mathrm{L}} - \mu_{\mathrm{R}}}{\Delta T}\right|_{I=0}, \tag{5.33}$$

as a measure of the voltage build-up as function of applied temperature bias and base temperature. We study the dependence as functions of phase shift, impurity concentration, and interface parameters. An exemplary result for the thermopower is shown in Fig. 5.23.

Figure 5.23:
Example results for the thermopower in a d-wave superconductor as function of base temperature T for different phase shifts. The film has a length $L = 20\xi_0$ with mean free path of $\ell = \xi_0$, we have a good contact with $D = 1.0$, and the bias is $\Delta = 0.1T_{\mathrm{c}0}$. Here, $\overline{\delta}_0 = \delta_0/(\pi/2)$.

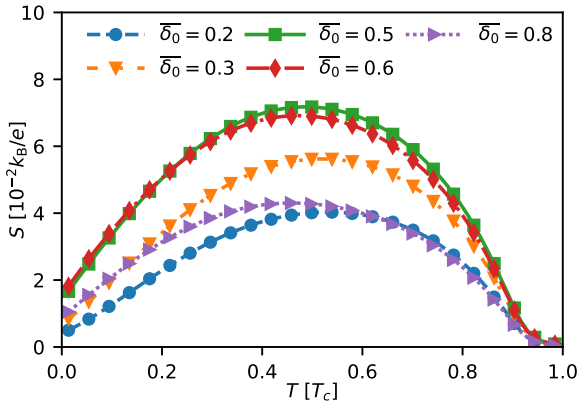

5.3.2 *s*-wave order parameter

The same thermoelectric effect due to impurities also occurs in the case of an *s*-wave SC, although the the effect is smaller since the electron-hole asymmetry exists in equilibrium only close to the interface, see Sec. 4.1.1. The thermopower S is shown for an applied temperature bias of $\Delta T = 0.25T_{\mathrm{c}}$ in Fig. 5.24 for an ideal contact ($D = 1$). It is two orders of magnitude smaller than in the *d*-wave case despite the larger thermal bias. The resulting thermovoltage for lead, a conventional superconductor with $T_{\mathrm{c}} \approx 7.2$ K, is predicted to be on the order of $50 - 100$ nV. This is comparable to experimental results on conventional superconductors on the order of pico- to nanovolt[109, 110].

Figure 5.24:
Thermopower for an s-wave superconductor due to impurity scattering with intermediate phase shift. Here, $\Delta T = 0.25T_{\mathrm{c}}$, $D = 1$, and $\overline{\delta}_0$ specifies the scattering phase shift relative to $\delta_0^{\mathrm{unitary}} = \pi/2$, i.e., $\overline{\delta}_0 = \delta_0/(\pi/2)$. Note that the bulk T_{c} is not affected by the impurities for an s-wave SC.

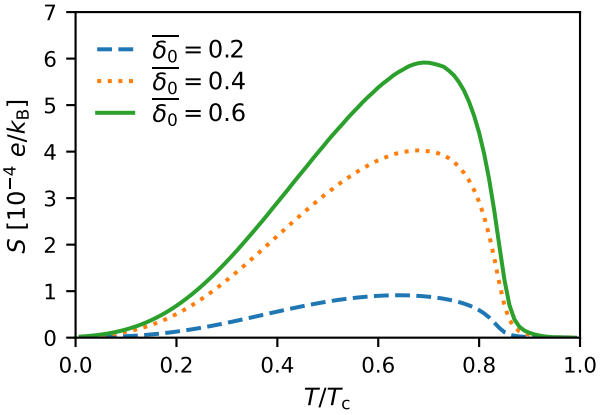

5.4 Transport in two dimensions

Systems in two (or higher) dimensions can show a variety of new effects that are not taken into account in quasi one-dimensional approach considered above. This is due to the additional geometric degrees of freedom. Steady-state current-conservation

$$\nabla \cdot \mathbf{j} = 0, \tag{5.34}$$

just implies $j_x(x) = const.$ in one dimension. In higher dimensions injected current, and the accompanying non-equilibrium distribution, from a small contact can spread out. This should reduce the detrimental impact of the non-equilibrium that we observe in our one-dimensional model system. On the other hand, current can also become focused due to geometric constraints.

Solutions of the quasiclassical theory of superconductivity in higher dimension have been reported in the diffusive limit[114–116], where the Usadel theory can be used[117]. Solution strategies in the non-diffusive case exist[56, 118, 119] but are more rare and often limited to equilibrium transport. An extension to the non-equilibrium case would allow for studies of non-equilibrium phenomena in realistic device geometries, paving the way for closer collaboration with experimental efforts.

In Paper IV we develop a FEM, presented in Sect. 3.3, as a solution technique for transport in dimensions $D \geq 2$ and apply it to two exemplary problems. We will briefly give some background to those problems here.

5.4.1 Effect of impurities on phase crystals

A numerical investigation of a clean, two-dimensional d-wave film found that time-reversal symmetry and translational invariance can be spontaneously broken near pair-breaking interfaces at temperatures below $T^* \approx 0.18T_c$[118].

In this case, the mechanism is not related to sub-dominant pairing but rather the result of an additional phase transition at T^*. The new phase is a so-called phase crystal[120, 121], with spontaneous current flow along the pair-breaking surfaces in peculiar loop patterns. An example of the spontaneous current flow in a small system is shown in Fig. 5.25.

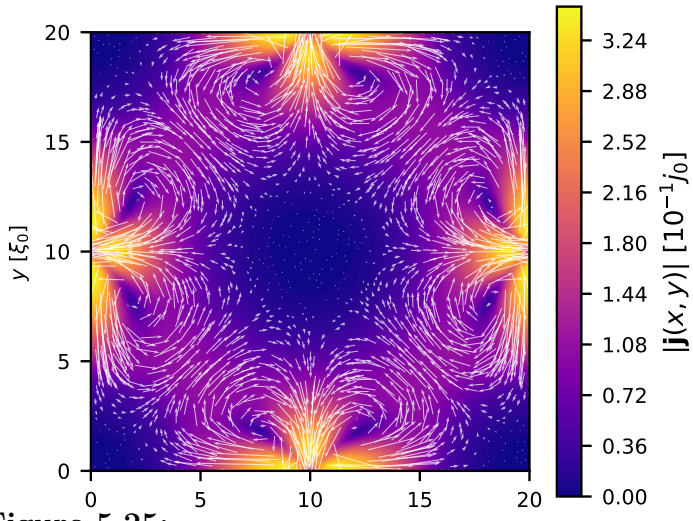

Figure 5.25:
Example for a phase crystal at a temperature of $T = 0.07T_c$ *and* $\Gamma = 5.5 \cdot 10^{-3}\pi k_B T_c$*, corresponding to* $l \approx 180\xi_0$.

Later studies also found the phase in a microscopic tight-binding approach[122]. While randomly-distributed Anderson disorder has been found to suppress the phase crystal, strong correlations stabilize it even in the presence of disorder[123]. The effect of impurities has not been studied within quasiclassical theory, where impurities are included in a homogeneous scattering model rather than with localized disorder. This motivated our investigation in Paper IV.

5.4.2 Current flow in a Dayem bridge

The second part of the project was driven by an interest in a recent experimental effort on superconducting Dayem bridges. At low temperatures, they act as nano scale Josephson junctions in a low-noise SQUID[124, 125]. A rough sketch of the weak link bridge is shown in Fig. 5.26a. To the left and right, it is connected to bulk YBCO film, which we model as superconducting reservoirs. To simulate transport in such a structure, we use a mesh shown in Fig. 5.26b, and solve the underlying transport equation using the FEM method. In Paper IV, we model the groove as a position-dependent mean free path and investigate its influence on the current flow and the order parameter. The geometric constriction into a narrow channel leads to current focussing with an increase in the phase gradient. In the groove, the reduced mean free path suppresses the order parameter even in equilibrium. A further suppression is found in the presence of current flow due to the locally increased momentum p_S.

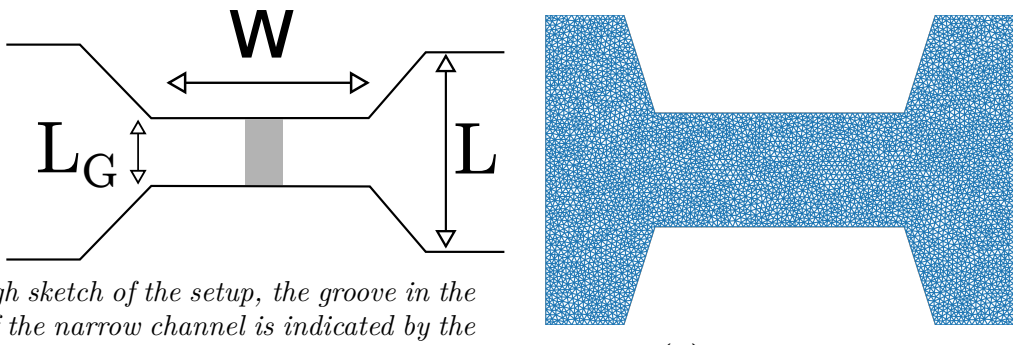

(a) *Rough sketch of the setup, the groove in the center of the narrow channel is indicated by the grey region.*

(b) *Mesh example.*

Figure 5.26: *Grooved Dayem bridge: Sketch and mesh.*

6 Paper overview

The basis of this thesis is the work presented in Papers I-IV which are appended at the end of the thesis. Here we give a brief description and a summary of the main results of these papers.

6.1 Paper I

In this paper we investigate the response of an s-wave superconducting nanowire, connected on one or both ends to a normal-metal reservoir, to an external voltage bias. While the general setup is relatively well-studied, most available literature neglects the requirement of self-consistency of the order parameter which implies non-conservation of charge current. Our main goal was then to perform such a fully self-consistent calculation of the order parameter and self-energies for elastic impurity scattering in non-equilibrium. A substantial part of this publication was the introduction of concepts that can be used to describe the non-equilibrium state in a non-diffusive superconductor, and description of the difference to diffusive transport.

The main finding of the paper is that in the time-independent steady-state, a self-consistent solution can only be found up to a critical voltage $|V_c| \lesssim \Delta_0/e$ after which superconductivity breaks down. We explain the breakdown as a result of two factors. Firstly, the injection of quasiparticles from the reservoirs leads to an occupation of subgap states over a finite lengthscale inside the superconductor. Secondly, a finite phase gradient is required in the superconductor in order to carry the current, this leads to a reduced spectral gap. The two effects combine to suppress the order parameter on the coherence length before superconductivity disappears. We also investigate how V_c depends on the interface transparency and impurity concentration. For high-transparency interfaces and a mean free path ℓ that is short compared to the superconducting coherence length ξ_0 we find that V_c approaches values that have been reported in literature for the diffusive limit.

6.2 Paper II

The second paper is devoted to thermoelectric effects in a d-wave superconducting film connected to normal reservoirs under thermal bias. Earlier results on the bulk linear response had predicted a large thermoelectric effect induced by elastic impurity scattering between the weak-scattering Born and the strong-scattering unitary limit. Our goal was to go beyond the linear response of the bulk and self-consistently calculate the steady-state non-linear response of an experimental setup. At the contacts to the reservoirs, the cancellation between quasiparticle current and condensate current will not be perfect. This leads to a charge pileup in the reservoirs and thus create a thermovoltage V that can be measured. The main result of the paper is an investigation of the thermopower $S = -V/\Delta T$ for different impurity concentrations and scattering strengths. We find that for a good contact and a scattering phase shift halfway between the weak- and strong-scattering limits, this voltage is on the order of a few μV/K and thus experimentally accessible. We further investigate the dependence of the thermopower on the interface transparency and the presence of surface Andreev bound states. The latter suppress the electron-hole asymmetry in the vicinity of the surface which reduces the thermoelectric response.

6.3 Paper III

Publication number three is focused on charge transport in a d-wave film connected to normal-metal reservoirs under voltage bias. Similar to the s-wave case in Paper I, self-consistency is usually neglected in the existing literature, so our aim was to perform such a self-consistent analysis of the transport behaviour. A main point of the investigation in the paper was the influence of surface Andreev bound states on the charge transport. Those have been predicted to give rise a large zero-bias conductance peak (ZBCP). While some experiments are in agreement with this prediction, others observe a splitting of the peak to finite energies. One mechanism suggested in the literature is is a phase-shifted, sub-dominant s-wave order parameter Δ_s that results in a $d + is$ order parameter.

The paper has two main results. For a pure d-wave order parameter, we find that even at voltages far below the gap a counter-flowing quasiparticle current is created, accompanied by a non-vanishing charge imbalance throughout the superconductor. Similar to the s-wave case we find a breakdown of superconductivity for voltages below the gap. Despite the more complicated non-equilibrium state, the conductance of the pure d-wave order parameter is in good agreement with the results in a non-self-consistent scattering model up to the voltages were stable solutions could be obtained. This is markedly different in the case of $d + is$ order parameter. We find that the subdominant pairing gets suppressed quickly as $|eV| \to \Delta_\mathrm{s}$. This suppression results in spectral rearrangements than enhance

the signature of a split ZBCP compared to a non self-consistent approach.

6.4 Paper IV

The last paper that is part of this thesis addresses the question of how to go beyond the one-dimensional models that were studied in papers I-III. To this end, the paper proposes a finite element method for the underlying transport equations of Eilenberger quasiclassical theory. The strength of the method is that the self-energies and the solution to the underlying differential equation can be determined on the same grid. This avoids the frequent interpolation that is necessary in a stepping method in two or three dimensions where the grid of solutions and self-energies cannot be chosen commensurate.

The main results of the paper are the development of the method itself and its applications to two example problems. Firstly, we studied the influence of scalar impurities in phase crystals, meaning the appearance of structured, spontaneous current flow in d-wave superconductors below a temperature $T^* \approx 0.17T_c$. We find that impurities suppress the amount of flow and suppress T^* even if the normal-state mean free path still exceeds size of the flow patterns. Additionally, high impurity concentration can make it energetically favourable for the loop pattern to change the number of loops with increasing temperature. The suppression is quicker in the Born than in the unitary limit which we attribute to reduced surface state broadening in the latter case. Secondly, we investigate the flow of supercurrent in a grooved Dayem bridge based on recent experimental designs. We find that the reduction of the order parameter in the groove leads to a non-linear behaviour in the current-phase relation of the structure. This can lead to a strong suppression of the order parameter in the groove even though the flow is non-dissipative.

7 Conclusion & Outlook

In this thesis we investigated the stationary non-equilibrium in mesoscopic superconductors coupled to normal-metal reservoirs. Specifically, we have studied conventional s-wave and unconventional d-wave superconductors under a voltage or temperature bias between the reservoirs. To this end, we calculated the stationary non-linear response using the quasiclassical theory of superconductivity in the general formulation by Eilenberger, Larkin-Ovchinnikov, and Eliashberg. The vast majority of previous work on non-equilibrium superconductivity has been on conventional superconductors, often in the limit of fully diffusive transport. Part of the work in this thesis was then a generalization of the concepts used in the diffusive regime to the case of "intermediately" dirty systems where transport is neither fully ballistic nor fully diffusive. An additional challenge that had to be overcome was that we aimed at a fully self-consistent solution of the underlying transport equations in non-equilibrium. This is essential for fundamental physical reasons and numerically effective solution strategies for this had to be found.

As a starting point we used those tools and strategies to study an s-wave superconducting nanowire connected to voltage-biased reservoirs. In this case a comparison to earlier work, either in the fully ballistic and fully diffusive regime, could serve as a benchmark for our results. Our more general approach can be used to go beyond the two limiting cases and explore the intermediate regime that is of interest for mesoscopic systems. At the same time, this study showed that a steady-state self-consistency solution is only possible in a limited voltage range in one-dimensional systems. The main goal of this work, however, was to study mesoscopic unconventional superconductors out of equilibrium. Firstly, we investigated an impurity-induced thermoelectric effect in a d-superconducting film and found it to be orders of magnitude larger than in conventional superconductors and experimentally accessible. Secondly, we studied the effects of a voltage-driven injection of quasiparticle current in a d-wave superconductor. Our findings indicate that corrections due to self-consistency can give substantial corrections to a simple interface-conductance model that neglects the spectral rearrangements due to current flow. The last question that this thesis addressed was how to go beyond one-dimensional models. As a step toward that goal the underlying transport equations of the quasiclassical theory of superconductivity were reformulated as a finite element method and used to study equilibrium transport.

A possible extension of the research presented in this thesis is non-equilibrium spin transport in non-diffusive superconductors. This is a field of ongoing research activity in diffusive conventional superconductors connected to superconducting spintronics[51, 126, 127]. The non-equilibrium modes used in this thesis can be generalized beyond a single spin polarization axis also in the non-diffusive case. Efficient numerical solution strategies for the case of general spin structure would allow further theoretical progress in this direction, as well as on the effects spin-orbit coupling in non-diffusive conventional and unconventional superconductors[128]. A self-consistent description of non-equilibrium situations in two-dimensional systems, either in the steady state or in (at least linear) response to a time-dependent drive is a substantial numerical challenge but would move theoretical models closer to experimental efforts on unconventional superconductors. The additional degree of freedom in higher dimensions might, similarly to the case of self-consistent equilibrium studies[118], reveal unexpected new physics in unconventional superconductors.

Appendices

A

Self-consistency & charge conservation

Charge conservation can be expressed as

$$\frac{\partial \rho(\mathbf{R},t)}{\partial t} + \nabla \cdot \mathbf{j}(\mathbf{R},t) = 0, \tag{A.1}$$

where $\rho(\mathbf{R},t)$ is the local charge density and $\mathbf{j}(\mathbf{R},t)$ the local charge current density. In the time-independent stationary state, this reduces to

$$\nabla \cdot \mathbf{j}(\mathbf{R}) = 0, \tag{A.2}$$

meaning we have local conservation of the charge current density. In the following, we will adopt the convention that the trace operation (Tr) acts on everything to right side of it, i.e., $\mathrm{Tr}\ \hat{A}(\hat{B}+\hat{C}) = \mathrm{Tr}\left[\hat{A}(\hat{B}+\hat{C})\right]$ unless explicit brackets are written out. In the following, we also assume spin degeneracy for simplicity, the generalization is straightforward. The definition of the charge current density, Eq. (2.98), reads

$$\mathbf{j}(\mathbf{R}) = e\mathcal{N}_\mathrm{F} \int_{-\infty}^{\infty} \frac{\mathrm{d}\varepsilon}{8\pi i} \left\langle \mathrm{Tr}\ \mathbf{v}_\mathrm{F}\hat{\tau}_3 \hat{g}^\mathrm{K}(\mathbf{p}_\mathrm{F},\mathbf{R},\varepsilon)\right\rangle_\mathrm{FS}. \tag{A.3}$$

Only $\hat{g}^\mathrm{K}$ depends on spatial coordinates, so after taking the divergence of both sides and small rearrangements we obtain

$$\nabla \cdot \mathbf{j}(\mathbf{R}) = -\frac{e\mathcal{N}_\mathrm{F}}{\hbar} \int_{-\infty}^{\infty} \frac{\mathrm{d}\varepsilon}{8\pi} \left\langle \mathrm{Tr}\ \hat{\tau}_3\ i\hbar\nabla \cdot \mathbf{v}_\mathrm{F}\hat{g}^\mathrm{K}(\mathbf{p}_\mathrm{F},\mathbf{R},\varepsilon)\right\rangle_\mathrm{FS}. \tag{A.4}$$

The Eilenberger equation, Eq. (2.22), for $\hat{g}^\mathrm{K}$ can be written as

$$i\hbar\nabla \cdot \mathbf{v}_\mathrm{F}\hat{g}^\mathrm{K}(\mathbf{p}_\mathrm{F},\mathbf{R},\varepsilon) = -\left[\varepsilon\hat{\tau}_3, \hat{g}^\mathrm{K}\right] + \hat{h}^\mathrm{R}\hat{g}^\mathrm{K} - \hat{g}^\mathrm{K}\hat{h}^\mathrm{A} + \hat{h}^\mathrm{K}\hat{g}^\mathrm{A} - \hat{g}^\mathrm{R}\hat{h}^\mathrm{K}. \tag{A.5}$$

In order for Eq. (A.2) to hold, we thus need to show that

$$\int_{-\infty}^{\infty} \mathrm{d}\varepsilon\ \left\langle \mathrm{Tr}\ \hat{\tau}_3 \left(-\left[\varepsilon\hat{\tau}_3, \hat{g}^\mathrm{K}\right] + \hat{h}^\mathrm{R}\hat{g}^\mathrm{K} - \hat{g}^\mathrm{K}\hat{h}^\mathrm{A} + \hat{h}^\mathrm{K}\hat{g}^\mathrm{A} - \hat{g}^\mathrm{R}\hat{h}^\mathrm{K}\right)\right\rangle_\mathrm{FS} = 0. \tag{A.6}$$

The first term vanishes trivially since the trace is cyclic under permutations, so that we find

$$\mathrm{Tr}\left(\hat{\tau}_3[\varepsilon\hat{\tau}_3,\hat{g}^{\mathrm{K}}]\right)=\varepsilon\ \mathrm{Tr}\left((\hat{\tau}_3)^2\hat{g}^{\mathrm{K}}-\hat{\tau}_3\hat{g}^{\mathrm{K}}\hat{\tau}_3\right)=\varepsilon\ \mathrm{Tr}\left((\hat{\tau}_3)^2\hat{g}^{\mathrm{K}}-\hat{g}^{\mathrm{K}}(\hat{\tau}_3)^2\right)=0. \quad \text{(A.7)}$$

Thus we only have to show that

$$\int_{-\infty}^{\infty}\mathrm{d}\varepsilon\langle\ \mathrm{Tr}\ \hat{\tau}_3\left(\hat{h}^{\mathrm{R}}\hat{g}^{\mathrm{K}}-\hat{g}^{\mathrm{K}}\hat{h}^{\mathrm{A}}+\hat{h}^{\mathrm{K}}\hat{g}^{\mathrm{A}}-\hat{g}^{\mathrm{R}}\hat{h}^{\mathrm{K}}\right)\rangle_{\mathrm{FS}}=0. \quad \text{(A.8)}$$

In this thesis we consider two contributions to the self-energy,

$$\check{h}=\check{h}_{\mathrm{MF}}+\check{h}_{\mathrm{s}}, \quad \text{(A.9)}$$

namely the mean-field order self-energy $\check{h}_{\mathrm{MF}}$ and scalar impurity scattering $\check{h}_{\mathrm{s}}$, and we will show that Eq. (A.8) holds for each of the two separately upon self-consistency.

As discussed in Sec. 2.4, for the mean-field term we have $\hat{h}^{\mathrm{K}}_{\mathrm{MF}}=0$ so the two terms that include $\hat{h}^{\mathrm{K}}$ vanish in Eq. (A.8). The retarded and advanced components are identical and given by

$$\hat{h}^{\mathrm{R,A}}_{\mathrm{MF}}=\begin{pmatrix}0&\Delta\\ \Delta^*&0\end{pmatrix}i\sigma_2=\begin{pmatrix}\Delta&0\\ 0&\Delta^*\end{pmatrix}\hat{\tau}_1 i\sigma_2, \quad \text{(A.10)}$$

where $i\sigma_2$ signals a singlet order parameter and $\Delta=\Delta_0\eta_\Gamma(\mathbf{p}_{\mathrm{F}})$ with the real basis function $\eta_\Gamma(\varphi_{\mathrm{F}})$. Using the notation of Eq. (2.35),

$$\hat{g}^{\mathrm{K}}=-2\pi i\begin{pmatrix}\mathcal{X}&\mathcal{Y}\\ \tilde{\mathcal{Y}}&\tilde{\mathcal{X}}\end{pmatrix}, \quad \text{(A.11)}$$

the cyclic properties of the trace, and relations between Pauli matrices gives

$$\begin{aligned}\mathrm{Tr}\ \hat{\tau}_3\left(\hat{h}^{\mathrm{R}}\hat{g}^{\mathrm{K}}-\hat{g}^{\mathrm{K}}\hat{h}^{\mathrm{A}}\right)&=\mathrm{Tr}\ \hat{\tau}_3\left[\begin{pmatrix}\Delta&0\\ 0&\Delta^*\end{pmatrix}\hat{\tau}_1\hat{g}^{\mathrm{K}}-\hat{g}^{\mathrm{K}}\begin{pmatrix}\Delta&0\\ 0&\Delta^*\end{pmatrix}\hat{\tau}_1\right]i\sigma_2\\ &=\mathrm{Tr}\ \left[\begin{pmatrix}\Delta&0\\ 0&\Delta^*\end{pmatrix}i\hat{\tau}_2\hat{g}^{\mathrm{K}}+i\hat{\tau}_2\hat{g}^{\mathrm{K}}\begin{pmatrix}\Delta&0\\ 0&\Delta^*\end{pmatrix}\right]i\sigma_2\\ &=2\ \mathrm{Tr}_{\mathrm{spin}}\ \left[\Delta\tilde{\mathcal{Y}}^{\mathrm{K}}i\sigma_2-\Delta^*\mathcal{Y}^{\mathrm{K}}i\sigma_2\right]\\ &=2\ \mathrm{Tr}_{\mathrm{spin}}\ \left[\Delta_0\eta_\Gamma\tilde{\mathcal{Y}}^{\mathrm{K}}i\sigma_2-\Delta_0^*\eta_\Gamma\mathcal{Y}^{\mathrm{K}}i\sigma_2\right]. \quad \text{(A.12)}\end{aligned}$$

Note that Δ_0 is a scalar quantity and can be removed from the trace. Inserting Eq. (A.12) into Eq. (A.8) thus gives

$$\begin{aligned}&\int_{-\infty}^{\infty}\mathrm{d}\varepsilon\langle\ \mathrm{Tr}\ \hat{\tau}_3\left(\hat{h}^{\mathrm{R}}\hat{g}^{\mathrm{K}}-\hat{g}^{\mathrm{K}}\hat{h}^{\mathrm{A}}\right)\rangle_{\mathrm{FS}}\\ &=2\Delta_0\int_{-\varepsilon_c}^{\varepsilon_c}d\varepsilon\left\langle\mathrm{Tr}_{\mathrm{spin}}\left[\eta_\Gamma(\mathbf{p}_{\mathrm{F}})i\sigma_2\tilde{\mathcal{Y}}^{\mathrm{K}}\right]\right\rangle_{\mathrm{FS}}-2\Delta_0^*\int_{-\varepsilon_c}^{\varepsilon_c}d\varepsilon\left\langle\mathrm{Tr}_{\mathrm{spin}}\left[\eta_\Gamma(\mathbf{p}_{\mathrm{F}})i\sigma_2\mathcal{Y}^{\mathrm{K}}\right]\right\rangle_{\mathrm{FS}}. \quad \text{(A.13)}\end{aligned}$$

We can rewrite the gap equation, Eq. (2.81), for the complex order parameter as

$$\Delta_{0,\Gamma}(\mathbf{R}) = -\mathcal{N}_\mathrm{F}\lambda_\Gamma \int_{-\varepsilon_c}^{\varepsilon_c} \frac{d\varepsilon}{4} \left\langle \mathrm{Tr}_\mathrm{spin}\left[i\sigma_2\eta_\Gamma(\mathbf{p}_\mathrm{F})\mathcal{Y}^\mathrm{K}(\mathbf{p}_\mathrm{F},\mathbf{R},\varepsilon)\right]\right\rangle_\mathrm{FS}. \tag{A.14}$$

The right-hand and left-hand sides of this equation will only agree once the self-energy Δ_0 is determined self-consistently with the solution $\mathcal{Y}^\mathrm{K}$. By the tilde symmetry, Eq. (2.29), $\tilde{\mathcal{Y}}^\mathrm{K}(\varepsilon,\mathbf{p}_\mathrm{F},\mathbf{R}) = \left(\mathcal{Y}^\mathrm{K}(-\varepsilon,-\mathbf{p}_\mathrm{F},\mathbf{R})\right)^*$. The minus sign in the energy and momentum arguments can be removed in the energy integral and FS average. Note that $\eta_{s,d}(\mathbf{p}_\mathrm{F}) = \eta_{s,d}(-\mathbf{p}_\mathrm{F})$. Comparison to Eq. (A.14) and the complex-conjugate equation then shows that Eq. (A.13) becomes

$$\left(\int_{-\infty}^{\infty} \mathrm{d}\varepsilon \mathrm{Tr}\ \hat{\tau}_3 \left\langle \hat{h}^\mathrm{R}_\mathrm{MF}\hat{g}^\mathrm{K} - \hat{g}^\mathrm{K}\hat{h}^\mathrm{A}_\mathrm{MF}\right\rangle_\mathrm{FS}\right) \propto \frac{1}{\mathcal{N}_\mathrm{F}\lambda_\Gamma}\left(\Delta\Delta^* - \Delta^*\Delta\right) = 0. \tag{A.15}$$

We now turn the to the impurity self-energy $\check{h}_\mathrm{s}$. Since it is elastic the scattering is only between different momenta at the same energy, we can thus restrict ourselves to a single energy. Since the FS average and the trace commute, we have to show

$$\mathrm{Tr}\ \hat{\tau}_3\langle \hat{h}^\mathrm{R}_\mathrm{s}\hat{g}^\mathrm{K} - \hat{g}^\mathrm{K}\hat{h}^\mathrm{A}_\mathrm{s} + \hat{h}^\mathrm{K}_\mathrm{s}\hat{g}^\mathrm{A} - \hat{g}^\mathrm{R}\hat{h}^\mathrm{K}_\mathrm{s}\rangle_\mathrm{FS} = 0, \tag{A.16}$$

is satisfied. In this thesis we solved the $\check{t}$-matrix equation for impurity scattering by using the non-crossing approximation. By combining Eq. (2.82) and Eq. (2.84), this means that upon self-consistency the self-energies satisfy the Dyson equation

$$\hat{h}^\mathrm{R,A}_\mathrm{s} = \left(\Gamma_u\hat{1} + \frac{\left\langle \hat{g}^\mathrm{R,A}\right\rangle_\mathrm{FS}\hat{h}^\mathrm{R,A}_\mathrm{s}}{\pi}\right)\tan\delta_0, \tag{A.17}$$

$$\hat{h}^\mathrm{K}_\mathrm{s} = \frac{1}{\pi\Gamma_u}\hat{h}^\mathrm{R}_\mathrm{s}\left\langle \hat{g}^\mathrm{K}\right\rangle_\mathrm{FS}\hat{h}^\mathrm{A}_\mathrm{s}. \tag{A.18}$$

Recall from Eq. (2.85) that the solution to the first equation was

$$\hat{h}^\mathrm{R,A}_\mathrm{s} = \pi\Gamma_u\frac{(\pi\cos\delta_0\ \ \sin\delta_0)\hat{1} + \sin^2\delta_0\left\langle \hat{g}^\mathrm{R,A}\right\rangle_\mathrm{FS}}{\pi^2\cos^2\delta_0 - \sin^2\delta_0\left\langle \hat{g}^\mathrm{R,A}\right\rangle^2_\mathrm{FS}}. \tag{A.19}$$

All three self-energies then do not depend on the position on the Fermi surface since they are proportional only to Fermi-surface averages (or trivial unit terms). Eq. (A.16) thus reduces to

$$\mathrm{Tr}\ \hat{\tau}_3\left(\hat{h}^\mathrm{R}_\mathrm{s}\left\langle \hat{g}^\mathrm{K}\right\rangle_\mathrm{FS} - \left\langle \hat{g}^\mathrm{K}\right\rangle_\mathrm{FS}\hat{h}^\mathrm{A}_\mathrm{s} + \hat{h}^\mathrm{K}_\mathrm{s}\left\langle \hat{g}^\mathrm{A}\right\rangle_\mathrm{FS} - \left\langle \hat{g}^\mathrm{R}\right\rangle_\mathrm{FS}\hat{h}^\mathrm{K}_\mathrm{s}\right) = 0. \tag{A.20}$$

In the Born limit, see Eq. (2.92), the self-energies are $\hat{h}^{\mathrm{R,A,K}} = (\Gamma/\pi)\left\langle \hat{g}^{\mathrm{R,A,K}} \right\rangle_{\mathrm{FS}}$, so we obtain the desired identity even without the trace,

$$\left\langle \hat{g}^{\mathrm{R}} \right\rangle_{\mathrm{FS}} \left\langle \hat{g}^{\mathrm{K}} \right\rangle_{\mathrm{FS}} - \left\langle \hat{g}^{\mathrm{K}} \right\rangle_{\mathrm{FS}} \left\langle \hat{g}^{\mathrm{A}} \right\rangle_{\mathrm{FS}} + \left\langle \hat{g}^{\mathrm{K}} \right\rangle_{\mathrm{FS}} \left\langle \hat{g}^{\mathrm{A}} \right\rangle_{\mathrm{FS}} - \left\langle \hat{g}^{\mathrm{R}} \right\rangle_{\mathrm{FS}} \left\langle \hat{g}^{\mathrm{K}} \right\rangle_{\mathrm{FS}} = 0. \tag{A.21}$$

The same holds in the unitary limit, where the self-energies read

$$\hat{h}^{\mathrm{R,A}}_{\mathrm{s,uni}} = -\pi\Gamma \frac{\left\langle \hat{g}^{\mathrm{R,A}} \right\rangle_{\mathrm{FS}}}{\left\langle \hat{g}^{\mathrm{R,A}} \right\rangle^2_{\mathrm{FS}}}, \qquad \hat{h}^{\mathrm{K}}_{\mathrm{s,uni}} = \pi\Gamma \frac{\left\langle \hat{g}^{\mathrm{R}} \right\rangle_{\mathrm{FS}} \left\langle \hat{g}^{\mathrm{K}} \right\rangle_{\mathrm{FS}} \left\langle \hat{g}^{\mathrm{A}} \right\rangle_{\mathrm{FS}}}{\left\langle \hat{g}^{\mathrm{R}} \right\rangle^2_{\mathrm{FS}} \left\langle \hat{g}^{\mathrm{A}} \right\rangle^2_{\mathrm{FS}}}. \tag{A.22}$$

Omitting the factor of $\pi\Gamma$ and the unnecessary trace, we then get by insertion into Eq. (A.20)

$$\begin{aligned}
&- \frac{\langle \hat{g}^{\mathrm{R}} \rangle_{\mathrm{FS}}}{\langle \hat{g}^{\mathrm{R}} \rangle^2_{\mathrm{FS}}} \left\langle \hat{g}^{\mathrm{K}} \right\rangle_{\mathrm{FS}} + \left\langle \hat{g}^{\mathrm{K}} \right\rangle_{\mathrm{FS}} \frac{\langle \hat{g}^{\mathrm{A}} \rangle_{\mathrm{FS}}}{\langle \hat{g}^{\mathrm{A}} \rangle^2_{\mathrm{FS}}} + \frac{\langle \hat{g}^{\mathrm{R}} \rangle_{\mathrm{FS}} \langle \hat{g}^{\mathrm{K}} \rangle_{\mathrm{FS}} \langle \hat{g}^{\mathrm{A}} \rangle_{\mathrm{FS}}}{\langle \hat{g}^{\mathrm{R}} \rangle^2_{\mathrm{FS}} \langle \hat{g}^{\mathrm{A}} \rangle^2_{\mathrm{FS}}} \left\langle \hat{g}^{\mathrm{A}} \right\rangle_{\mathrm{FS}} - \left\langle \hat{g}^{\mathrm{R}} \right\rangle_{\mathrm{FS}} \frac{\langle \hat{g}^{\mathrm{R}} \rangle_{\mathrm{FS}} \langle \hat{g}^{\mathrm{K}} \rangle_{\mathrm{FS}} \langle \hat{g}^{\mathrm{A}} \rangle_{\mathrm{FS}}}{\langle \hat{g}^{\mathrm{R}} \rangle^2_{\mathrm{FS}} \langle \hat{g}^{\mathrm{A}} \rangle^2_{\mathrm{FS}}} \\
&= - \frac{\langle \hat{g}^{\mathrm{R}} \rangle_{\mathrm{FS}}}{\langle \hat{g}^{\mathrm{R}} \rangle^2_{\mathrm{FS}}} \left\langle \hat{g}^{\mathrm{K}} \right\rangle_{\mathrm{FS}} + \left\langle \hat{g}^{\mathrm{K}} \right\rangle_{\mathrm{FS}} \frac{\langle \hat{g}^{\mathrm{A}} \rangle_{\mathrm{FS}}}{\langle \hat{g}^{\mathrm{A}} \rangle^2_{\mathrm{FS}}} + \frac{\langle \hat{g}^{\mathrm{R}} \rangle_{\mathrm{FS}}}{\langle \hat{g}^{\mathrm{R}} \rangle^2_{\mathrm{FS}}} \left\langle \hat{g}^{\mathrm{K}} \right\rangle_{\mathrm{FS}} - \left\langle \hat{g}^{\mathrm{K}} \right\rangle_{\mathrm{FS}} \frac{\langle \hat{g}^{\mathrm{A}} \rangle_{\mathrm{FS}}}{\langle \hat{g}^{\mathrm{A}} \rangle^2_{\mathrm{FS}}} \\
&= 0,
\end{aligned} \tag{A.23}$$

as wanted. Outside of the Born limit and the unitary limits, $\tan\delta_0$ and Γ_u are finite so we can rewrite Eq. (A.17) as

$$\frac{\hat{h}^{\mathrm{R,A}}}{\Gamma_u \tan\delta_0} = \hat{1} + \frac{\left\langle \hat{g}^{\mathrm{R,A}} \right\rangle_{\mathrm{FS}} \hat{h}^{\mathrm{R,A}}}{\pi\Gamma_u} = \hat{1} + \frac{\hat{h}^{\mathrm{R,A}} \left\langle \hat{g}^{\mathrm{R,A}} \right\rangle_{\mathrm{FS}}}{\pi\Gamma_u} \tag{A.24}$$

In the last identity, we have used the fact that Eq. (A.19) implies that $\hat{h}^{\mathrm{R,A}}$ and $\left\langle \hat{g}^{\mathrm{R,A}} \right\rangle_{\mathrm{FS}}$ commute. By using the cyclic properties of the trace, we then get

$$\begin{aligned}
&\mathrm{Tr}\ \hat{\tau}_3 \left(\hat{h}^{\mathrm{R}}_{\mathrm{s}} \left\langle \hat{g}^{\mathrm{K}} \right\rangle_{\mathrm{FS}} - \left\langle \hat{g}^{\mathrm{K}} \right\rangle_{\mathrm{FS}} \hat{h}^{\mathrm{A}}_{\mathrm{s}} + \frac{1}{\pi\Gamma_u} \hat{h}^{\mathrm{R}}_{\mathrm{s}} \left\langle \hat{g}^{\mathrm{K}} \right\rangle_{\mathrm{FS}} \hat{h}^{\mathrm{A}}_{\mathrm{s}} \left\langle \hat{g}^{\mathrm{A}} \right\rangle_{\mathrm{FS}} - \frac{1}{\pi\Gamma_u} \left\langle \hat{g}^{\mathrm{R}} \right\rangle_{\mathrm{FS}} \hat{h}^{\mathrm{R}}_{\mathrm{s}} \left\langle \hat{g}^{\mathrm{K}} \right\rangle_{\mathrm{FS}} \hat{h}^{\mathrm{A}}_{\mathrm{s}} \right) \\
&= \mathrm{Tr}\ \left[\left\langle \hat{g}^{\mathrm{K}} \right\rangle_{\mathrm{FS}} \left(\hat{1} + \frac{\hat{h}^{\mathrm{A}} \left\langle \hat{g}^{\mathrm{A}} \right\rangle_{\mathrm{FS}}}{\pi\Gamma_u} \right) \hat{\tau}_3 \hat{h}^{\mathrm{R}} - \left\langle \hat{g}^{\mathrm{K}} \right\rangle_{\mathrm{FS}} \hat{h}^{\mathrm{A}} \hat{\tau}_3 \left(\hat{1} + \frac{\left\langle \hat{g}^{\mathrm{R}} \right\rangle_{\mathrm{FS}} \hat{h}^{\mathrm{R}}}{\pi\Gamma_u} \right) \right] \\
&= \mathrm{Tr}\ \left[\left\langle \hat{g}^{\mathrm{K}} \right\rangle_{\mathrm{FS}} \frac{\hat{h}^{\mathrm{A}}}{\Gamma_u \tan\delta_0} \hat{\tau}_3 \hat{h}^{\mathrm{R}} - \left\langle \hat{g}^{\mathrm{K}} \right\rangle_{\mathrm{FS}} \hat{h}^{\mathrm{A}} \hat{\tau}_3 \frac{\hat{h}^{\mathrm{R}}}{\Gamma_u \tan\delta_0} \right] = 0.
\end{aligned} \tag{A.25}$$

Similarly, one shows for example that the conservation of heat current requires only self-consistency of the impurity self-energies[129].

References

[1] M. A. Schwartz, "The importance of stupidity in scientific research", J. Cell Sci. **121**, 1771 (2008) (cit. on p. v).

[2] H. K. Onnes, "The resistance of pure mercury at helium temperatures", Commun. Phys. Lab. Univ. Leiden **12** (1911) (cit. on p. 1).

[3] *The Nobel Prize in Physics 1913*, https://www.nobelprize.org/prizes/physics/1913/summary/, [Online; accessed 2022-04-25] (cit. on p. 1).

[4] W. Meissner and R. Ochsenfeld, "Ein neuer Effekt bei Eintritt der Supraleitfähigkeit", Naturwissenschaften **21**, 787–788 (1933) (cit. on p. 1).

[5] J. Bardeen, L. N. Cooper, and J. R. Schrieffer, "Microscopic Theory of Superconductivity", Phys. Rev. **106**, 162–164 (1957) (cit. on p. 1).

[6] J. Bardeen, L. N. Cooper, and J. R. Schrieffer, "Theory of Superconductivity", Phys. Rev. **108**, 1175–1204 (1957) (cit. on p. 1).

[7] M. Sigrist and K. Ueda, "Phenomenological theory of unconventional superconductivity", Rev. Mod. Phys. **63**, 239–311 (1991) (cit. on pp. 1, 2).

[8] M. Sigrist, "Introduction to Unconventional Superconductivity", AIP Conf. Proc. **789**, 165–243 (2005) (cit. on p. 2).

[9] D. D. Osheroff, R. C. Richardson, and D. M. Lee, "Evidence for a New Phase of Solid He^3", Phys. Rev. Lett. **28**, 885–888 (1972) (cit. on p. 2).

[10] D. D. Osheroff, W. J. Gully, R. C. Richardson, and D. M. Lee, "New Magnetic Phenomena in Liquid He^3 below 3 mK", Phys. Rev. Lett. **29**, 920–923 (1972) (cit. on p. 2).

[11] F. Steglich, J. Aarts, C. D. Bredl, W. Lieke, D. Meschede, W. Franz, and H. Schäfer, "Superconductivity in the Presence of Strong Pauli Paramagnetism: $CeCu_2Si_2$", Phys. Rev. Lett. **43**, 1892–1896 (1979) (cit. on p. 2).

[12] G. R. Stewart, "Heavy-fermion systems", Rev. Mod. Phys. **56**, 755–787 (1984) (cit. on p. 2).

[13] H. v. Löhneysen, T. Pietrus, G. Portisch, H. G. Schlager, A. Schröder, M. Sieck, and T. Trappmann, "Non-Fermi-liquid behavior in a heavy-fermion alloy at a magnetic instability", Phys. Rev. Lett. **72**, 3262–3265 (1994) (cit. on p. 2).

[14] D. Jérome, A. Mazaud, M. Ribault, and K. Bechgaard, "Superconductivity in a synthetic organic conductor (TMTSF)2PF 6", Journal de Physique Lettres **41**, 95–98 (1980) (cit. on p. 2).

[15] J. G. Bednorz and K. A. Müller, "Possible high-T_c superconductivity in the Ba-La-Cu-O system", Z. Phys. B: Condens. Matter **64**, 189–193 (1986) (cit. on p. 2).

[16] *The Nobel Prize in Physics 1987*, https://www.nobelprize.org/prizes/physics/1987/summary, [Online; accessed 2022-04-25] (cit. on p. 2).

[17] M. K. Wu, J. R. Ashburn, C. J. Torng, P. H. Hor, R. L. Meng, L. Gao, Z. J. Huang, Y. Q. Wang, and C. W. Chu, "Superconductivity at 93 K in a new mixed-phase Y-Ba-Cu-O compound system at ambient pressure", Phys. Rev. Lett. **58**, 908–910 (1987) (cit. on p. 2).

[18] H. Maeda, Y. Tanaka, M. Fukutomi, and T. Asano, "A New High-Tc Oxide Superconductor without a Rare Earth Element", Jpn. J. Appl. Phys. **27**, L209–L210 (1988) (cit. on p. 2).

[19] D. J. Scalapino, "The case for $d_{x^2-y^2}$ pairing in the cuprate superconductors", Phys. Rep. **250**, 329–365 (1995) (cit. on p. 2).

[20] D. J. Van Harlingen, "Phase-sensitive tests of the symmetry of the pairing state in the high-temperature superconductors—Evidence for $d_{x^2-y^2}$ symmetry", Rev. Mod. Phys. **67**, 515–535 (1995) (cit. on p. 2).

[21] C. C. Tsuei and J. R. Kirtley, "Pairing symmetry in cuprate superconductors", Rev. Mod. Phys. **72**, 969–1016 (2000) (cit. on p. 2).

[22] M. Matsumoto and H. Shiba, "Coexistence of Different Symmetry Order Parameters near a Surface in d-Wave Superconductors II", J. Phys. Soc. Jpn. **64**, 4867–4881 (1995) (cit. on pp. 2, 46, 63).

[23] A. Shurakov, Y. Lobanov, and G. Goltsman, "Superconducting hot-electron bolometer: from the discovery of hot-electron phenomena to practical applications", Supercond. Sci. Technol. **29**, 023001 (2015) (cit. on p. 3).

[24] A. Fornieri and F. Giazotto, "Towards phase-coherent caloritronics in superconducting circuits", Nat. Nanotechnol. **12**, 944–952 (2017) (cit. on p. 3).

[25] M. Marín-Suárez, J. T. Peltonen, and J. P. Pekola, "Active Quasiparticle Suppression in a Non-Equilibrium Superconductor", Nano Lett. **20**, 5065–5071 (2020) (cit. on p. 3).

[26] G. Catelani and J. P. Pekola, "Using materials for quasiparticle engineering", Mater. Quantum Technol. **2**, 013001 (2022) (cit. on p. 3).

[27] A. Schmid and G. Schön, "Linearized kinetic equations and relaxation processes of a superconductor near T_c", J. Low Temp. Phys. **20**, 207–227 (1975) (cit. on pp. 3, 13, 55).

[28] W. Belzig, F. K. Wilhelm, C. Bruder, G. Schön, and A. D. Zaikin, "Quasiclassical Green's function approach to mesoscopic superconductivity", Superlattices Microstruct. **25**, 1251–1288 (1999) (cit. on pp. 3, 55).

[29] Y. V. Nazarov, "Novel circuit theory of Andreev reflection", Superlattices Microstruct. **25**, 1221–1231 (1999) (cit. on p. 3).

[30] K. Y. Arutyunov, S. A. Chernyaev, T. Karabassov, D. S. Lvov, V. S. Stolyarov, and A. S. Vasenko, "Relaxation of nonequilibrium quasiparticles in mesoscopic size superconductors", J. Phys.: Condens. Matter **30**, 343001 (2018) (cit. on p. 3).

[31] S. N. Artemenko and A. F. Volkov, "Electric fields and collective oscillations in superconductors", Sov. Phys. Usp. **22**, 295–310 (1979) (cit. on p. 4).

[32] S. Datta, *Electronic Transport in Mesoscopic Systems* (Cambridge University Press, Cambridge, England, UK, Sept. 1995) (cit. on p. 3).

[33] S. Datta, *Lessons from Nanoelectronics | Lessons from Nanoscience: A Lecture Notes Series*, Vol. 1 (World Scientific Publishing Company, Singapore, Nov. 2011) (cit. on p. 50).

[34] C. Timm, *Vielteilchentheorie kondensierter Materie (lecture notes)* (2014) (cit. on p. 5).

[35] L.V.Keldysh, "Diagram Technique for Nonequilibrium Processes", Zh. Eksp. i Teor. Fiz. **47**, 1515 (1964) (cit. on p. 5).

[36] J. Rammer and H. Smith, "Quantum field-theoretical methods in transport theory of metals", Rev. Mod. Phys. **58**, 323–359 (1986) (cit. on pp. 5, 6).

[37] Henrik Bruus and Karsten Flensberg, *Many-Body Quantum Theory in Condensed Matter Physics - An Introduction* (Oxford Graduate Texts, Jan. 14, 2016) (cit. on p. 5).

[38] L. Gorkov, "On the Energy Spectrum of Superconductors", Sov. Phys. JETP **34**, 505–508 (1958) (cit. on pp. 6, 7).

[39] G. Eilenberger, "Transformation of Gorkov's equation for type II superconductors into transport-like equations", Z. Physik **214**, 195–213 (1968) (cit. on p. 8).

[40] A. Larkin and Y. N. Ovchinnikov, "Quasiclassical Method in the Theory of Superconductivity", Zh. Eksp. i Teor. Fiz. **55**, 2262 (1968) (cit. on pp. 8, 13).

[41] J. A. Sauls, "Andreev bound states and their signatures", Philos. Trans. Royal Soc. A **376**, 20180140 (2018) (cit. on p. 9).

[42] J. W. Serene and D. Rainer, "The quasiclassical approach to superfluid 3He", Phys. Rep. **101**, 221–311 (1983) (cit. on pp. 9, 20, 21).

[43] G. Eliashberg, "Inelastic Electron Collisions and Nonequilibrium Stationary States in Superconductors", Zh. Eksp. i Teor. Fiz. **61**, 1254–1272 (1971) (cit. on p. 9).

[44] A. I. Larkin and Yu. N. Ovchinnikov, "Nonlinear conductivity of superconductors in the mixed state", Soviet Journal of Experimental and Theoretical Physics **41**, 960 (1975) (cit. on p. 9).

[45] M. Eschrig, "Scattering problem in nonequilibrium quasiclassical theory of metals and superconductors: General boundary conditions and applications", Phys. Rev. B **80**, 134511 (2009) (cit. on pp. 9, 14–17, 19, 26).

[46] T. Champel and M. Eschrig, "Effect of an inhomogeneous exchange field on the proximity effect in disordered superconductor-ferromagnet hybrid structures", Phys. Rev. B **72**, 054523 (2005) (cit. on p. 10).

[47] Y. Nagato, K. Nagai, and J. Hara, "Theory of the Andreev reflection and the density of states in proximity contact normal-superconducting infinite double-layer", J. Low Temp. Phys. **93**, 33–56 (1993) (cit. on p. 10).

[48] N. Schopohl and K. Maki, "Quasiparticle spectrum around a vortex line in a d-wave superconductor", Phys. Rev. B **52**, 490–493 (1995) (cit. on p. 10).

[49] N. Schopohl, "Transformation of the Eilenberger Equations of Superconductivity to a Scalar Riccati Equation", arXiv (1998), eprint: `cond-mat/9804064` (cit. on p. 10).

[50] A. Shelankov and M. Ozana, "Quasiclassical theory of superconductivity: A multiple-interface geometry", Phys. Rev. B **61**, 7077–7100 (2000) (cit. on pp. 10, 13).

[51] F. S. Bergeret, M. Silaev, P. Virtanen, and T. T. Heikkilä, "Colloquium: Nonequilibrium effects in superconductors with a spin-splitting field", Rev. Mod. Phys. **90**, 041001 (2018) (cit. on pp. 14, 76).

[52] M. Eschrig, "Distribution functions in nonequilibrium theory of superconductivity and Andreev spectroscopy in unconventional superconductors", Phys. Rev. B **61**, 9061–9076 (2000) (cit. on p. 17).

[53] E. Zhao, T. Löfwander, and J. A. Sauls, "Nonequilibrium superconductivity near spin-active interfaces", Phys. Rev. B **70**, 134510 (2004) (cit. on p. 17).

[54] J. C. Cuevas and M. Fogelström, "Quasiclassical description of transport through superconducting contacts", Phys. Rev. B **64**, 104502 (2001) (cit. on p. 17).

[55] M. J. Graf, S.-K. Yip, J. A. Sauls, and D. Rainer, "Electronic thermal conductivity and the Wiedemann-Franz law for unconventional superconductors", Phys. Rev. B **53**, 15147–15161 (1996) (cit. on p. 20).

[56] M. Eschrig and J. A. Sauls, "Charge dynamics of vortex cores in layered chiral triplet superconductors", New J. Phys. **11**, 075009 (2009) (cit. on pp. 22, 68).

[57] D. G. Anderson, "Iterative Procedures for Nonlinear Integral Equations", J. ACM **12**, 547–560 (1965) (cit. on p. 25).

[58] R. Grein, T. Löfwander, and M. Eschrig, "Inverse proximity effect and influence of disorder on triplet supercurrents in strongly spin-polarized ferromagnets", Phys. Rev. B **88**, 054502 (2013) (cit. on p. 26).

[59] W. T. Reid, *Riccati differential equations* (Academic Press, 1972) (cit. on pp. 11, 27).

[60] C. Johnson, *Numerical Solution of Partial Differential Equations by the Finite Element Method* (Dover Publications, 2009) (cit. on pp. 29, 32).

[61] B. Cockburn, G. E. Karniadakis, and C.-W. Shu, "The Development of Discontinuous Galerkin Methods", in *Discontinuous Galerkin Methods* (Springer, Berlin, Germany, 2000), pp. 3–50 (cit. on p. 32).

[62] B. Cockburn, "Discontinuous Galerkin methods", Z. angew. Math. Mech. **83**, 731–754 (2003) (cit. on pp. 32, 33).

[63] H. G. Kaper, G. K. Leaf, and A. J. Lindeman, "Applications of Finite Element Methods in reactor mathematics. Numerical solution of the neutron transport equation", Argonne National Lab Report **ANL-8126** (1974) (cit. on p. 32).

[64] P. Lasaint and P. A. Raviart, "On a Finite Element Method for Solving the Neutron Transport Equation", in *Mathematical Aspects of Finite Elements in Partial Differential Equations* (Academic Press, Cambridge, MA, USA, 1974), pp. 89–123 (cit. on p. 32).

[65] D. N. Arnold, F. Brezzi, B. Cockburn, and L. D. Marini, "Unified Analysis of Discontinuous Galerkin Methods for Elliptic Problems", SIAM J. Numer. Anal. **39**, 1749â€"1779 (2002) (cit. on p. 34).

[66] F. Brezzi, L. D. Marini, and E. Süli, "Discontinuous Galerkin Methods for First-Order Hyperbolic Problems", Math. Models Methods Appl. Sci. **14**, 1893–1903 (2004) (cit. on p. 35).

[67] D. Xu, S. K. Yip, and J. A. Sauls, "Nonlinear Meissner effect in unconventional superconductors", Phys. Rev. B **51**, 16233–16253 (1995) (cit. on p. 41).

[68] P. W. Anderson, "Theory of dirty superconductors", J. Phys. Chem. Solids **11**, 26–30 (1959) (cit. on p. 40).

[69] W. J. Tomasch, "Geometrical Resonance in the Tunneling Characteristics of Superconducting Pb", Phys. Rev. Lett. **15**, 672–675 (1965) (cit. on p. 40).

[70] W. J. Tomasch and T. Wolfram, "Energy Spacing of Geometrical Resonance Structure in Very Thick Films of Superconducting In", Phys. Rev. Lett. **16**, 352–354 (1966) (cit. on p. 40).

[71] L. J. Buchholtz and G. Zwicknagl, "Identification of p-wave superconductors", Phys. Rev. B **23**, 5788–5796 (1981) (cit. on p. 41).

[72] T. Löfwander and M. Fogelström, "Large thermoelectric effects in unconventional superconductors", Phys. Rev. B **70**, 024515 (2004) (cit. on p. 42).

[73] A. V. Balatsky, I. Vekhter, and J.-X. Zhu, "Impurity-induced states in conventional and unconventional superconductors", Rev. Mod. Phys. **78**, 373–433 (2006) (cit. on p. 42).

[74] T. Löfwander, V. S. Shumeiko, and G. Wendin, "Andreev bound states in high-Tc superconducting junctions", Supercond. Sci. Technol. **14**, R53–R77 (2001) (cit. on p. 43).

[75] C.-R. Hu, "Midgap surface states as a novel signature for d^2_{xa}-x^2_b-wave superconductivity", Phys. Rev. Lett. **72**, 1526–1529 (1994) (cit. on p. 43).

[76] A. Poenicke, Y. S. Barash, C. Bruder, and V. Istyukov, "Broadening of Andreev bound states in $d_{x^2-y^2}$ superconductors", Phys. Rev. B **59**, 7102–7107 (1999) (cit. on p. 44).

[77] M. Fogelström, D. Rainer, and J. A. Sauls, "Tunneling into Current-Carrying Surface States of High-T_c Superconductors", Phys. Rev. Lett. **79**, 281–284 (1997) (cit. on pp. 45, 62, 63).

[78] L. J. Buchholtz, M. Palumbo, D. Rainer, and J. A. Sauls, "Thermodynamics of ad-wave superconductor near a surface", J. Low Temp. Phys. **101**, 1079–1098 (1995) (cit. on p. 45).

[79] Y. V. Sharvin, "A Possible Method for Studying Fermi Surfaces", Journal of Experimental and Theoretical Physics **48**, 984 (1964) (cit. on p. 51).

[80] T. Löfwander, M. Fogelström, and J. A. Sauls, "Shot noise in normal metal–d-wave superconducting junctions", Phys. Rev. B **68**, 054504 (2003) (cit. on p. 52).

[81] K. M. Seja, *Transport in mesoscopic superconducting devices (Licenciate thesis)* (Chalmers Research, 2019), eprint: 514396 (cit. on p. 52).

[82] I. Giaever, "Energy Gap in Superconductors Measured by Electron Tunneling", Phys. Rev. Lett. **5**, 147–148 (1960) (cit. on p. 53).

[83] J. R. Schrieffer, *Theory Of Superconductivity* (Perseus Books, New York, NY, USA, 1999) (cit. on p. 53).

[84] G. E. Blonder, M. Tinkham, and T. M. Klapwijk, "Transition from metallic to tunneling regimes in superconducting microconstrictions: Excess current, charge imbalance, and supercurrent conversion", Phys. Rev. B **25**, 4515–4532 (1982) (cit. on pp. 53, 55).

[85] T. Löfwander, R. Grein, and M. Eschrig, "Is CrO_2 Fully Spin Polarized? Analysis of Andreev Spectra and Excess Current", Phys. Rev. Lett. **105**, 207001 (2010) (cit. on p. 53).

[86] G. R. Boogaard, A. H. Verbruggen, W. Belzig, and T. M. Klapwijk, "Resistance of superconducting nanowires connected to normal-metal leads", Phys. Rev. B **69**, 220503 (2004) (cit. on p. 55).

[87] J. Sánchez-Cañizares and F. Sols, "Self-consistent current-voltage characteristics of normal-superconductor interfaces", J. Phys.: Condens. Matter **7**, L317–L323 (1995) (cit. on p. 55).

[88] Sánchez-Cañizares, J. and Sols, F., "Self-Consistent Theory of Transport in Quasi-One-Dimensional Superconducting Wires", J. Low Temp. Phys. **122**, 11–35 (2001) (cit. on p. 55).

[89] J. Clarke, "Experimental Observation of Pair-Quasiparticle Potential Difference in Nonequilibrium Superconductors", Phys. Rev. Lett. **28**, 1363–1366 (1972) (cit. on p. 58).

[90] M. Tinkham and J. Clarke, "Theory of Pair-Quasiparticle Potential Difference in Nonequilibrium Superconductors", Phys. Rev. Lett. **28**, 1366–1369 (1972) (cit. on p. 58).

[91] M. Tinkham, "Tunneling Generation, Relaxation, and Tunneling Detection of Hole-Electron Imbalance in Superconductors", Phys. Rev. B **6**, 1747–1756 (1972) (cit. on p. 58).

[92] R. S. Keizer, M. G. Flokstra, J. Aarts, and T. M. Klapwijk, "Critical Voltage of a Mesoscopic Superconductor", Phys. Rev. Lett. **96**, 147002 (2006) (cit. on p. 59).

[93] N. Vercruyssen, T. G. A. Verhagen, M. G. Flokstra, J. P. Pekola, and T. M. Klapwijk, "Evanescent states and nonequilibrium in driven superconducting nanowires", Phys. Rev. B **85**, 224503 (2012) (cit. on p. 59).

[94] J. Geerk, X. X. Xi, and G. Linker, "Electron tunneling into thin films of $Y_1Ba_2Cu_3O_7$", Z. Phys. B: Condens. Matter **73**, 329–336 (1988) (cit. on p. 59).

[95] J. Lesueur, L. H. Greene, W. L. Feldmann, and A. Inam, "Zero bias anomalies in $YBa_2Cu_3O_7$ tunnel junctions", Physica C **191**, 325–332 (1992) (cit. on p. 59).

[96] S. Kashiwaya, M. Koyanagi, M. Matsuda, and K. Kajimura, "Study of zero-bias conductance peaks in YBCO films by LT-STM", Physica B **194-196**, 2119–2120 (1994) (cit. on p. 59).

[97] Y. Tanaka and S. Kashiwaya, "Theory of Tunneling Spectroscopy of d-Wave Superconductors", Phys. Rev. Lett. **74**, 3451–3454 (1995) (cit. on p. 59).

[98] S. Kashiwaya, Y. Tanaka, M. Koyanagi, and K. Kajimura, "Theory for tunneling spectroscopy of anisotropic superconductors", Phys. Rev. B **53**, 2667–2676 (1996) (cit. on p. 59).

[99] S. K. Yip and J. A. Sauls, "Nonlinear Meissner effect in CuO superconductors", Phys. Rev. Lett. **69**, 2264–2267 (1992) (cit. on p. 62).

[100] M. Covington, M. Aprili, E. Paraoanu, L. H. Greene, F. Xu, J. Zhu, and C. A. Mirkin, "Observation of Surface-Induced Broken Time-Reversal Symmetry in $YBa_2Cu_3O_7$ Tunnel Junctions", Phys. Rev. Lett. **79**, 277–280 (1997) (cit. on p. 62).

[101] J. Y. T. Wei, N.-C. Yeh, D. F. Garrigus, and M. Strasik, "Directional Tunneling and Andreev Reflection on $YBa_2Cu_3O_{7-\delta}$ Single Crystals: Predominance of *d*-Wave Pairing Symmetry Verified with the Generalized Blonder, Tinkham, and Klapwijk Theory", Phys. Rev. Lett. **81**, 2542–2545 (1998) (cit. on p. 62).

[102] Y. Dagan and G. Deutscher, "Doping and Magnetic Field Dependence of In-Plane Tunneling into $YBa_2Cu_3O_{7-x}$: Possible Evidence for the Existence of a Quantum Critical Point", Phys. Rev. Lett. **87**, 177004 (2001) (cit. on p. 62).

[103] A. Andreev, "The Thermal Conductivity of the Intermediate State in Superconductors", Sov. Phys. JETP **19**, 1228–1231 (1964) (cit. on p. 65).

[104] W. Meissner, "Das elektrische Verhalten der Metalle im Temperaturgebiet des flüssigen Heliums", Zeitschrift für die gesamte Kälte-Industrie, 197 (1927) (cit. on p. 65).

[105] J. G. Daunt and K. Mendelssohn, "Thomson Effect of Supraconductive Lead", Nature **141**, 116 (1938) (cit. on p. 65).

[106] V. L. Ginzburg, "On thermoelectric phenomena in superconductors", Zh. Eksp. Teor. Fiz. **14**, engl.: Journ. Phys. USSR 8 148 (1944), 177 (1944) (cit. on p. 65).

[107] V. L. Ginzburg, "Nobel Lecture: On superconductivity and superfluidity (what I have and have not managed to do) as well as on the 'physical minimum' at the beginning of the XXI century", Rev. Mod. Phys. **76**, 981–998 (2004) (cit. on p. 65).

[108] S. Artemenko and A. Volkov, "The thermoelectric field in superconductors", Sov. Phys. JETP **43**, 548 (1976) (cit. on p. 65).

[109] D. J. Van Harlingen, "Thermoelectric generation of charge imbalance at a superconductor-normal metal interface", J. Low Temp. Phys. **44**, 163–176 (1981) (cit. on pp. 65, 67).

[110] C. M. Falco, "Observation of Thermally Induced Potential in a Superconductor", Phys. Rev. Lett. **39**, 660–663 (1977) (cit. on pp. 65, 67).

[111] G. Schön, "Thermoelectric effects in superconductors", in *Festkörperprobleme 21* (Springer, Berlin, Germany, July 1981), pp. 341–362 (cit. on p. 65).

[112] F. Giazotto, T. T. Heikkilä, A. Luukanen, A. M. Savin, and J. P. Pekola, "Opportunities for mesoscopics in thermometry and refrigeration: Physics and applications", Rev. Mod. Phys. **78**, 217–274 (2006) (cit. on p. 65).

[113] T. T. Heikkilä, T. Vänskä, and F. K. Wilhelm, "Supercurrent-induced Peltier-like effect in superconductor/normal-metal weak links", Phys. Rev. B **67**, 100502 (2003) (cit. on p. 66).

[114] J. C. Cuevas and F. S. Bergeret, "Magnetic Interference Patterns and Vortices in Diffusive SNS Junctions", Phys. Rev. Lett. **99**, 217002 (2007) (cit. on p. 68).

[115] F. S. Bergeret and J. C. Cuevas, "The Vortex State and Josephson Critical Current of a Diffusive SNS Junction", J. Low Temp. Phys. **153**, 304–324 (2008) (cit. on p. 68).

[116] M. Amundsen and J. Linder, "General solution of 2D and 3D superconducting quasiclassical systems: coalescing vortices and nanoisland geometries", Sci. Rep. **6**, 1–13 (2016) (cit. on p. 68).

[117] K. D. Usadel, "Generalized Diffusion Equation for Superconducting Alloys", Phys. Rev. Lett. **25**, 507–509 (1970) (cit. on p. 68).

[118] M. Håkansson, T. Löfwander, and M. Fogelström, "Spontaneously broken time-reversal symmetry in high-temperature superconductors", Nat. Phys. **11**, 755–760 (2015) (cit. on pp. 68, 76).

[119] M. Håkansson, *Mesoscopic thin film superconductors - A computational framework (Licenciate thesis)* (Chalmers Research, 2015), eprint: 211094 (cit. on p. 68).

[120] P. Holmvall, M. Fogelström, T. Löfwander, and A. B. Vorontsov, "Phase crystals", Phys. Rev. Res. **2**, 013104 (2020) (cit. on p. 68).

[121] P. Holmvall, "Crystallization of the superconducting phase in unconventional superconductors", PhD thesis (Chalmers University of Technology, Sweden, 2019), eprint: 513562 (cit. on p. 68).

[122] N. W. Wennerdal, A. Ask, P. Holmvall, T. Löfwander, and M. Fogelström, "Breaking time-reversal and translational symmetry at edges of *d*-wave superconductors: Microscopic theory and comparison with quasiclassical theory", Phys. Rev. Res. **2**, 043198 (2020) (cit. on p. 69).

[123] D. Chakraborty, T. Löfwander, M. Fogelström, and A. M. Black-Schaffer, "Disorder-robust phase crystal in high-temperature superconductors from topology and strong correlations", arXiv (2021) 10.48550/arXiv.2103.12756, eprint: 2103.12756 (cit. on p. 69).

[124] E. Trabaldo, S. Ruffieux, E. Andersson, R. Arpaia, D. Montemurro, J. F. Schneiderman, A. Kalaboukhov, D. Winkler, F. Lombardi, and T. Bauch, "Properties of grooved Dayem bridge based YBa2Cu3 O 7 - δ superconducting quantum interference devices and magnetometers", Appl. Phys. Lett. **116**, 132601 (2020) (cit. on p. 69).

[125] E. Trabaldo, C. Pfeiffer, E. Andersson, M. Chukharkin, R. Arpaia, D. Montemurro, A. Kalaboukhov, D. Winkler, F. Lombardi, and T. Bauch, "SQUID Magnetometer Based on Grooved Dayem Nanobridges and a Flux Transformer", IEEE Trans. Appl. Supercond. **30**, 1–4 (2020) (cit. on p. 69).

[126] M. Eschrig, "Spin-polarized supercurrents for spintronics", Phys. Today **64**, 43 (2010) (cit. on p. 76).

[127] D. Beckmann, "Spin manipulation in nanoscale superconductors", J. Phys.: Condens. Matter **28**, 163001 (2016) (cit. on p. 76).

[128] I. V. Bobkova and A. M. Bobkov, "Quasiclassical theory of magnetoelectric effects in superconducting heterostructures in the presence of spin-orbit coupling", Phys. Rev. B **95**, 184518 (2017) (cit. on p. 76).

[129] C. Richard and A. B. Vorontsov, "Heat transport in nonuniform superconductors", Phys. Rev. B **94**, 064502 (2016) (cit. on p. 82).